UDK 621.3:(53+54+621+66)(05)(497.1)=00 ISSN 0352-9045

INFORMACIJE MIDEM 1 ◦1994

Strokovno društvo za mikroelektroniko elektronske sestavne dele in materiale

Časopis za mikroelektroniko, elektronske sestavne dele in materiale
Časopis za mikroelektroniku, elektronske sastavne dijelove i materijale
Journal of Microelectronics, Electronic Components and Materials

INFORMACIJE MIDEM, LETNIK 24, ŠT. 1(69), LJUBLJANA, MAREC 1994

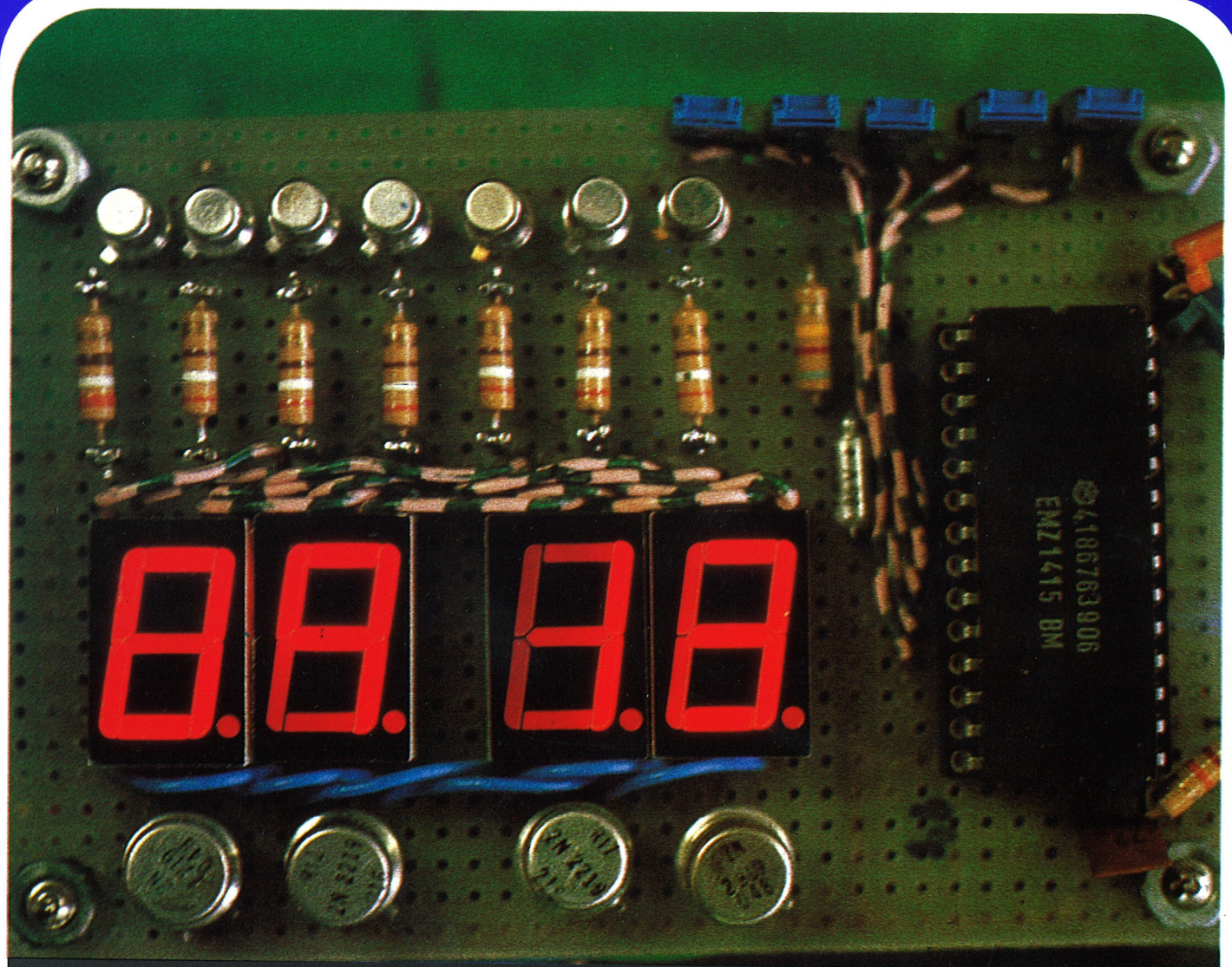

Qmil

INFORMACIJE MIDEM 1 ° 1994

INFORMACIJE MIDEM	LETNIK 24, ŠT. 1(69), LJUBLJANA,	MAREC 1994
INFORMACIJE MIDEM	GODINA 24, BR. 1(69), LJUBLJANA,	MART 1994
INFORMACIJE MIDEM	VOLUME 24, NO. 1(69), LJUBLJANA,	MARCH 1994

Izdaja trimesečno (marec, junij, september, december) Strokovno društvo za mikroelektroniko, elektronske sestavne dele in materiale.
Izdaja tromjesečno (mart, jun, septembar, decembar) Stručno društvo za mikroelektroniku, elektronske sastavne dijelove i materiale.
Published quarterly (march, june, september, december) by Society for Microelectronics, Electronic Components and Materials - MIDEM.

Naslov uredništva
Adresa redakcije
Headquarters
Uredništvo Informacije MIDEM
Elektrotehniška zveza Slovenije
Dunajska 10, 61000 Ljubljana, Slovenija
(0)61 - 316 886

Letna naročnina znaša 7000,00 SIT, cena posamezne številke je 1750,00 SIT. Člani in sponzorji MIDEM prejemajo Informacije MIDEM brezplačno.
Godišnja pretplata iznosi 7000,00 SIT, cijena pojedinog broja je 1750,00 SIT. Članovi i sponzori MIDEM primaju Informacije MIDEM besplatno.
Annual subscription rate is DEM 100, separate issue is DEM 25. MIDEM members and Society sponsors receive Informacije MIDEM for free.

Znanstveni svet za tehnične vede I je podal pozitivno mnenje o časopisu kot znanstveno strokovni reviji za mikroelektroniko, elektronske sestavne dele in materiale. Izdajo revije sofinanci rajo Ministrstvo za znanost in tehnologijo in sponzorji društva.
Scientific Council for Technical Sciences of Slovene Ministry of Science and Technology has recognized Informacije MIDEM as scientific Journal for microelectronics, electronic components and materials.
Publishing of the Journal is financed by Slovene Ministry of Science and Technology and by Society sponsors.

Znanstveno strokovne prispevke objavljene v Informacijah MIDEM zajemamo v:
* domačo bazo podatkov ISKRA SAIDC-el, kakor tudi
* v tujo bazo podatkov INSPEC
Scientific and professional papers published in Informacije MIDEM are assessed into:
* domestic data base ISKRA SAIDC-el and
* foreign data base INSPEC

Po mnenju Ministrstva za informiranje št.23/300-92 šteje glasilo Informacije MIDEM med proizvode informativnega značaja, za katere se plačuje davek od prometa proizvodov po stopnji 5 %.

Grafična priprava in tisk
Grafička priprema i štampa
Printed by
BIRO M, Ljubljana

Naklada
Tiraž
Circulation
1000 izvodov
1000 primjeraka
1000 issues

UDK621.3:(53+54+621+66),ISSN0352-9045 Informacije MIDEM 24(1994)1,Ljubljana

VSEBINA CONTENT

STORY ON SUCCESS

More than 10 years ago I worked for the-then ambitious company Iskra Microelectronics and collaborated with another microelectronics company that was just being created at Unterpremstatten near Graz, Austria. At that time both companies had the same license partner that was American Microsystems Incorporation - AMI, Santa Clara, USA. Both companies started their work on the basis of similar technology, with only slight difference in their approach.

Couple of years before the production actually started in Iskra Microelectronics, its technologists were trained in the AMI factory - Pocatello, Idaho, USA. As well, Iskra continued to have connection technologist working with the license partner even in the time it started its production with own staff.

On the contrary, the factory in Austria that was also connected to Americans financially through capital began to work with American experts who were training their Austrian colleagues on the spot.

Collegial and business relationship between Iskra and Austrian Microelectronics were established during many-year-long fruitful and pleasant collaboration that was interrupted only by Iskra Microelectronic's ruin.

However, there has always been basic difference between the "Slovene" and the "Austrian" microelectronics approach. On one side, Iskra Microelectronics had support of the-then relatively strong electronics industry materialized in the company of ISKRA employing 36 000 people at that time, as well as support of the Yugoslav civil and military electronics on the other side. At first sight those were outstanding conditions to begin with !

The Austrian Microelectronics - AMS, was built by Austrian iron industry. At that time Austrian electronics industry development stage was far beyond the Yugoslav one. However, building the new microelectronics factory the Austrians already took into account the fact of rapid development in microelectronics. It was built bigger to what they needed initially and also later they continued to invest into new installations, equipment and technologies.

What a contrast to our impoverished and short-term orientation !

As distinguished from ISKRA that did not construct and invest into microelectronics in order to be exploited by outside users (an argument that I have often heard from "old true" members of ISKRA) the Austrians have quickly oriented their production onto world markets.

Despite my personal disappointment at the Slovene microelectronics production disintegration, I am nevertheless very happy to see AMS company, Austria, succeeding and becoming a great, prosperous and famous "forge" of application specific integrated circuits. Despite its relatively small size, it is among the greatest silicon foundaries in Europe.

And what about the financial aspect ? Their stocks list on the stock Exchange. 10% dividends were distributed for the year 1994.

They have so many orders that their responding time extends even to some months.

Every "true" microelectronics-ist should share his joy with them.

MIDEM Society President
Dr. Rudolf Ročak

UDK 621.3:(53+54+621+66), ISSN0352-9045 Informacije MIDEM 24(1994)1, Ljubljana

REACTIVE COATING TECHNOLOGIES FOR DIELECTRIC LAYERS

Hans K. Pulker
BALZERS AG, FL-9496 Balzers, Liechtenstein

Keywords: reactive coating, RPVD reactive physical vapour deposition, coating technologies, thin films, dielectric layers, planar waveguides, optoelectronic sensors, telecommunication systems, optical interference, reactive gases, discharge plasma, stoichiometry, PVD physical vapour deposition, film properties, film stability, gas discharge, IBS, Ion beam sputtering, IAD ion assisted deposition

Abstract: High quality dielectric films are required today for planar optical wave quides used in opto-electronic sensors and telecommunications. Many inorganic chemical compounds which were difficult to deposit by conventional techniques in form of well adherent, dense, hard and stable low-loss films are now routinly synthesized by reactive gas discharge plasma and energetic ion and/or coating material atom processes. The plasma provides an in-situ source of increased ionization and energetic deposition species. This is suitably used to enhance various chemical and physical processes that influence stoichiometry and growth properties of deposited films. A survey over such PVD coating technologies and on the resulting film properties is given. Among others Ta_2O_5, ZrO_2, TiO_2, SiO_2 and Si_3N_4 single films and multilayers were deposited in the new reactive low-voltage ion plating system Balzers BAP 800. The properties of the individual films and spectral filter characteristics of multilayers were investigated particularly with respect to time, humidity and temperature. The observed stability is correlated with film density, water vapour content and intrinsic film material properties.

Reaktivne tehnologije nanašanja dielektričnih tankih plasti

Ključne besede: nanašanje reaktivno, RPVD naparjevanje reaktivno fizično, tehnologije nanašanja, plasti tanke, plasti dielektrične, valovodi planarni, senzorji optoelektronski, sistemi telekomunikacijski, interferenca optična, plini reaktivni, plazma razelektrilna, stihiometrija, PVD nanašanje, lastnosti plasti, stabilnost plasti, razelektritev plinska, IBS naprševanje ionsko, IAD nanašanje

Povzetek: Tehnologija izdelave optičnih valovodov v optoelektronskih senzorjih in telekomunikacijskih sistemih, kakor tudi druge uporabe v interferenčni optiki zahtevajo nanašanje zelo kvalitetnih dielektričnih plasti. Mnoge anorganske kemične sestavine smo včasih s konvencionalnimi metodami nanašanja zelo tekčo nanašali v obliki trdih, gostih, stabilnih filmov brez izgub in z dobro adhezijo na podlago. Danes uspemo z uporabo nekaterih novih tehnik, kot so reaktivno plazemsko nanašanje in energijsko ionsko nanašanje atomov tarče, pospešiti razline kemične in fizikalne procese, ki vplivajo na rast, stohiometrijo in lastnosti tankih plasti.
V prispevku podajam pregled zgoraj omenjenih PVD tehnik nanosa, kakor tudi lastnosti tako dobljenih tankih plasti. Enojne in večplastne strukture Ta_2O_5, ZrO_2, TiO_2, SiO_2 in Si_3N_4 smo nanesli v novem sistemu za reaktivno nanašanje plasti Balzers BA 800. Zanimale so nas lastnosti posameznih plasti ter spektralne karakteristike večslojnih struktur zlasti časovna stabilnost ter občutljivost na temperaturo in relativno vlago. Stabilnost plasti smo korelirali z njihovimi notranjimi lastnostmi, vsebnostjo vlage in gostoto.

1. Introduction

The properties of thin oxide films deposited on glass substrates by evaporation and subsequent condensation or by sputtering under vacuum were generally found to be different from those of the bulk materials. Dissociation is a problem with many compound films. Even in evaporation, which is the gentlest physical vapour deposition process, chemical compounds are dissociated to a certain extent. Due to their low sticking coefficient, gaseous components can be pumped off, resulting in substoichiometric composition of the deposit. Optical films produced in processes without ion bombardment show properties associated with low mobility of the condensing atoms and molecules as consequence of their low energies of about 0,2eV. Most films evaporated conventionally have a columnar microstructure with large void volume. Silica films have a less dense spongy microstructure. This leads to deviations of the optical and mechanical properties from those of the bulk materials. The voids enlarge the internal surface of the coatings and encourage gas, particularly moisture adsorption. Anything filling the voids increases their refractive index so that the film index and consequently the optical thickness increase. Thus, whenever the environmental conditions change the films exhibit a shift in their properties. In view of the importance of dielectric films in optical coatings, it is not surprising that considerable work has been devoted to these materials. Attention has been paid how to make stoichiometric, low absorbing, stable and hard oxide, nitride and oxynitride films for various filter and mirror applications and for optical wave guides. Special reactive higher energetic deposition techniques have been developed to improve optical and mechanical properties of compound films. Among them, processes that retain as much of the traditional techiques as possible seem the most attractive ones. Work along these lines showed exciting results. The important reactions in plasma supported PVD processes are ionization, dissociation, radical formation, electron impact excitations and the ion energies involved. In this review most of these powerful ion or plasma supported techiques, particularly the new reactive low-voltage ion plating, will be discussed.

2. Reactive Evaporation Techniques

The loss of oxygen and nitrogen that usually occurs during evaporation or sputtering of transparent metal oxides and nitrides may cause optical absorption in the films. The effect could be appreciably corrected particularly in the case of oxides in the reactive deposition process /1,2/ by adding oxygen to the residual gas: **$MeO + 1/2O_2 \dashrightarrow MeO_2$ I, $Me + O_2 \dashrightarrow MeO_2$ II**

The partial pressure of the reactive gas component is usually few 10^{-4} mbar. Reactive evaporation is applied in all cases where direct evaporation of a chemical compound is not possible because of degradation. In practice, oxide films are produced using suboxides as starting materials. Basically it is also possible to produce other compounds in this manner. The low reactivity of nitrogen (N_2), however, prevents the applicability of conventional reactive evaporation for metal nitride film synthesis.

When evaporating under reactive conditions, care must be taken that the gas components consumed during the chemical reaction are continuously replenished. This is frequently carried out through a pressure controlled gas inlet valve. The average mean free path at 10^{-4} mbar is still only 50 cm, which is somewhat less than the distance from boat to substrate. Reactions from collision in the gas space between gas molecules and metal atoms are only possible to a small percentage, althought the collision probability is often more than 50 %. The reaction takes place to a far greater extent on the substrate surface.

Formation of a metal-oxide film by reactive evaporation takes place in the following stages:

1) The substrate surface is exposed to the coating material vapour atoms and gas molecules which impinge at a certain rate.

2) A portion of these atoms and molecules is adsorbed on the substrate surface, and another portion is either reflected or, after a short dwell on the surface, again desorbed. The ratio of the actually adsorbed quantity to the number of incident particles is given by the condensation coefficient. The condensation coefficients of metal vapours are frequently near to unity; large rates of incidence are chosen in the vacuum evaporation, so that they correspond to pressures which are much larger than the equilibrium pressures at the usual substrate temperatures.

3) In the adsorbed phase, in which the particles are mobile because of surface diffusion, the chemical reaction of the metal- oxide formation takes place via dissociative chemisorption of the oxygen. This means that, since the reaction takes place in the adsorption phase and the various reaction partners can have different condensation coefficients, the ratio of the rates of incidence is a necessary but not adequate criterion. It is assumed /3/, that the chemisorption rate of oxygen is the critical step for the completion of the reaction.

The need thus arises to select all parameters for the relevant process so that the film obtained fulfills the demand upon in the best possible way. For all that, however, oxide coatings produced in this way are often still slightly understoichiometric and slightly absorbing. Compound films approach asymptotically to stoichiometry and it should be considered that, for example, the composition of silica films correspond to SiO_{2-x} whereby x is between 10^{-3} and 10^{-6}.

Concerning structure, evaporated films are disordered polycrystalline, amorphous or polymeric. They show rough surfaces and have columnar or spongy microstructures with large void volume and great internal surface area /4/. Their adhesion to the substrate is poor and their abrasion resistance and hardness are low. As a consequence of the low density the film refractive indices are considerably lower than the values for the bulk oxides. They absorb water vapour on wet atmosphere and other gases which change their refractive index and other physical properties.

Heating the substrates to about 250 to 350°C during reactive evaporation improved a number of film properties including stoichiometry, purity, density, refractive index and adhesion. Therefore substrate heating became the standard procedure in this process, although it favours generally undesirable coarser film microstructure and surface roughness. Because of the high reactivity of oxygen and the low reactivity of nitrogen only oxide films have been successfully produced industrially by reactive evaporation.

3. Activated Reactive Deposition

Films for highly sophisticated optical applications, such as for special laser mirrors, should have extremly low absorption losses because these obviously decrease the reflectivity and lower the damage threshold for high power radiation. It is very important in the deposition of such films to achieve more complete oxidation, since traces of metal atoms or substoichiomietric species cause absorption. It has been found by various researchers that better stoichiometric films can be achieved with activated and ionized reactive gas. The process is shown schematically in the left branche of Fig.1.

Reactive evaporations performed under the above mentioned standard conditions, but with additional activation of the reactive gas, further improved film quality /5/. Better stoichiometry and rather low absorption values have been obtained when films were prepared by activated reactive evaporation (ARE) /8/. These coating experiments with ions and excited molecules clearly

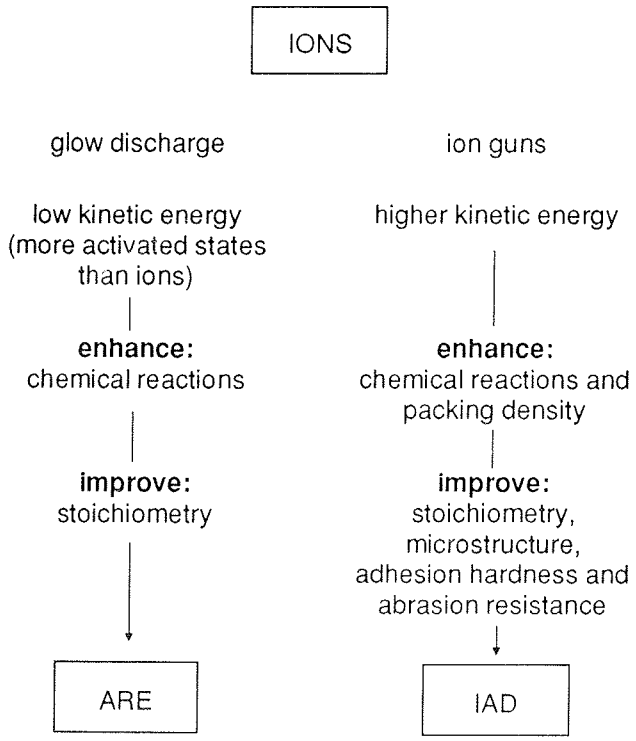

Fig. 1: Schematic of plasma and ion supported reactive evaporations

showed that chemical reactivity is enhanced in the presence of a gas-discharge plasma. To generate oxygen ions for activated reactive evaporation cold gas discharge ion sources with a hollow cathode inside a quartz tube are used /6/. With this technique it became possible also to deposit metal oxynitride films.

In the case of TiO_2 films, the partial ionization of oxygen reduces the absorption by a factor of 10 for TiO starting material, or by factor of 100 for Ti_2O_3 or Ti_3O_5 starting materials compared with the values of films obtained with ordinary oxygen /7/. It was found that negative oxigene ions produced the best oxidizing effect /7/. They were therefore used to produce all the films.

4. Ion Assisted Deposition

Most properties of evaporated films are highly determined by the lack of mobility of the condensing atoms and molecules due to their low thermal energies between 0.1 and 0.2 eV. The activation energy necessary for physical and chemical processes is supplied by energetic ions, which replaces the requirement of elevated substrate temperature as discussed further above. This is shown schematically in the right branche of Fig.1. Controlled bombardment of a growing film by argon or/and oxygen ions with energies up to several hundred electron volts has been shown to improve density and stoichiometry and therefore optical properties of oxide coatings /8,9/. To make sure stoichiometry energy values below 100 eV are to prefere. Adding energy to the film growth process also appears to improve adhesion /10/ and to modify stress /11/. Similar effects are observed when the ad- atoms of thin film materials have increased energy as is the case in sputtering. Ion beam techniques can be applied, however also before and after film deposition. Substrates can be ion beam cleaned with inert or reactive gas ions, depending upon substrate materials involved and freshly deposited films can be bombarded to further improve their properties.

Hot-cathode Kaufman-type /12/ ion guns are used usually in ion assisted deposition processes (IAD), but also other installations have been applied. It is impossible to discuss and compare here all the variants of this technique. Considerable efforts have been directed to the analysis of plasma conditions and their correlation with deposited film properties. The mechanism responsible for densification seems to be momentum transfer as was shown recently by molecular-dynamics calculation /13/.

5. Gas Discharge and Ion Beam Sputtering

In sputtering atoms or molecules from a target are ejected by momentum transfer processes caused by noble gas ion bombardment. Various possibilities are shown schematically in Fig.2. The initially relatively high energetic coating material atoms with energies between 1 and 40 eV pass through a more or less dense gas phase lose energy by collisions and condense at substrates which, in case of gas discharge sputtering, are arranged oposit the target at a small distance.

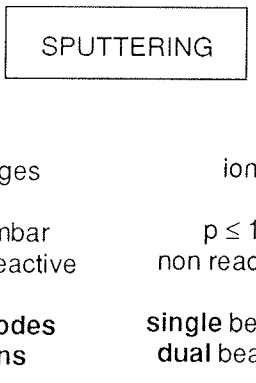

Fig. 2: Schematic of sputtering

Ions stem from a dc of rf gas discharge or from special ion guns. In the first case the typical working gas pressure is in the 10^{-2} to 10^{-3} mbar range whereas with ion beam sputtering lower background pressures and there-

fore a larger distance target to substrate can be applied. Many variants of sputtering processes are known /14/. With all of them reactive gas processes can be performed. Conventional gas discharge sputtering is a rather slow process. The speed of deposition is increased, however, by magnetrons where, in addition to the electric field, a magnetic field enables, by keeping the electrons in trajectories close to the target surface, to increase the number of ionizing collisions in the bombardment-ion generation. Such devices are used for the deposition of large flat substrates, e.g. architectural glass and plastic foils /15,16/.

With reactive sputtering, one has to distinguish between a compound film synthesis under the actions of a diluted reactive gas atmosphere starting from pure metal, alloy or multi-element targets on the one hand, and the making up for the lost constituent when using compound targets on the other. The main difference is found in the dependence of the deposition rate on the partial pressure of the reactive gas. Generally the reactive gas component, which can be for example O_2, H_2O for the formation of oxides, N_2, NH_3 for nitrides, $O_2 + N_2$ for oxynitrides, H_2S for sulfides, C_2H_2, CH_4 or other hydrocarbons for carbides and CF_4 or HF for fluorides, is added to the sputtergas - mainly Ar^4 - in small amounts, between 10^{-5} and 10^{-4} mbar. In all gas discharge sputter arrangements, the added gas is in an activated state and therefore highly reactive.

Reactions in the gas phase, ignored in reactive evaporation, are here also generally negligible; the heat of reaction liberated cannot be dissipated in a two-body collision. Conservation of momentum and energy lead to heterogeneous reactions on the substrate surface but are unfortunately also possible on less eroding areas of the target surface. Reactions of the target surface are often called target poisoning when the reaction product, a chemical compound, is dielectric and leads to charging of the target surface. The compounds also frequently have a lower sputter rate. To overcome this disadvantage an interesting technical solution exists by alternating dc-magnetron sputtering of 2-3 monolayers metal film and subsequent oxidation in a separate reactive plasma zone /17/. A highly intense reactive plasma is present in a long narrow zone, isolated physically from the metal deposition zone by a region of relatively low pressure. A reactive ion source with a high intensity ion flux generates an intense reactive plasma of highly energetic oxygen adjacent to the periphery of the substrate, keeping the time required for the reaction very short. As a further advantage of this technique, compounds can be formed using a less reactive gas than oxygen, such as nitrogen and other, to form metal nitrides, or other compound films. The cyclic depostion/oxidation sputtering process seems to overcome all disadvantages of the prior art in reactive sputtering. The use of multiple stations affords a further advantage with a considerable increase of deposition speed. The possible film deposition rates are comparable with those in reactive evaporation. The elimination of the prior requirement of tight baffling allows for the coating of curved substrates. It is, however, impossible to coat lager flat surfaces.

In ion beam sputtering (IBS) the target erosion is produced by a mono-energetic argon ion beam usualy from a Kaufman-type ion gun, but also high frequency ion sources should be considered /18/. In dual ion beam sputtering a second ion gun is used with the beam directed at the growing film similar to ion assisted deposition e.g. /19/. With the IB-sputtering techniques dense, well adherent and stoichiometric films of low optical absorption and with stable properties can be obtained. In all variants care must be taken to avoid unwanted sputtering of plant installations by high energetic neutral atoms what could cause film contamination. Unfortunately, the process has several practical limitations. It is relatively slow, and to deposit a thin film of one quarterwave optical thickness (visible range) takes 15 to 20 min. The area to be uniformly coated rarely exceeds a diameter of about 10 cm.

6. Reactive Ion Plating

In a conventional ion plating process /20/ evaporation is performed in the presence of an argon gas discharge. In collisions and electron impact reactions, coating material ions are formed and accelerated in the electric field of biased substrates so that condensation and film formation take place under the influence of ion bombardment. It can involve ions of the working gas, of the film-material vapour or of a mixture of both. In addition, the higher energetic neutral atoms of vapour and gas are also very important for the deposition process. This complex action is typically for ion plating. A large number of process variants is possible and different components can be combined to more complex triode and tetrode ion plating systems. It is furthermore remarkable that also high-speed sputtering cathodes are used as vapour sources in special ion plating arrangements. Bias sputtering and some types of plasma CVD also fall under the definition of ion plating. In conventional ion plating the degree of ionization is low and so the accelerating voltage must be rather high, generally between 3 and 5 kV, to supply the necessary energy for the formation of well adherent and dense films. The small number of ions, however, is also disadvantageous for a reactive gas process. Therefore, to overcome this problems a new form of reactive ion plating, shown schematically in Fig.3, has been developed in our laboratory /21/.

6.1. Reactive Low-Voltage Ion Plating

The new reactive ion plating process (RLVIP) /22/ performed in the specially designed automatic box type plating system BALZERS BAP 800, shown in Fig.4a and 4b, can be used for the deposition of single layer and multilayer oxide coatings onto unheated glass and other substrates. All evaporations are made by two special 270°-type electron beam evaporators.

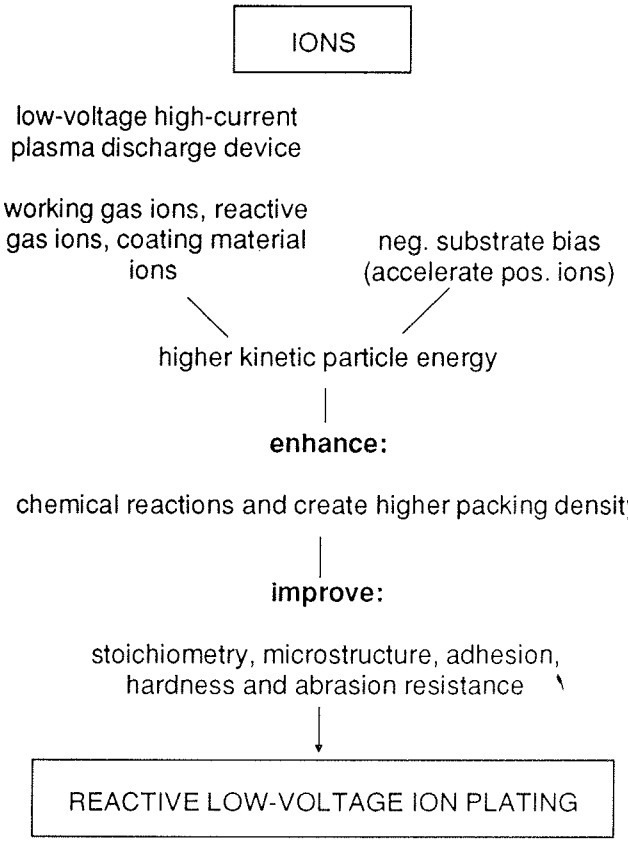

Fig. 3: Schematic of reactive low-voltage ion plating

The starting materials, metals or suboxides, form electrically conducting melts. Very effective ionisation and activation of the evaporating coating material atoms and the admitted reactive gas molecules occur by a low-voltage high-current argon plasma beam (hot cathode type) directed to the crucibles (anode). The substrate holder is electrically insulated. In contact with the formed plasma cloud the substrates receive a relatively high negative self-biasing potential of 15-20 V with respect to the plasma, which acts as accelerating voltage for positive ions. The repulsive force of the anode, gas phase collisions and the negative substrate bias determine the kinetic energy of the impinging positive ions. The total pressure in the plant is in the low 10^{-3} mbar range. Film deposition is started and stopped by opening or closing a moveable shutters in front of the electron beam evaporators. Film thickness and deposition rate are controlled by an oscillating quartz crystal monitor /23/. Optical thickness monitoring can be used too. Quarter-wave films in the visible are deposited within 3 to 4 minutes. Uniformity in thickness distribution of ± 1 % over the whole substrate holder of 800 mm diameter can be achived by the use of a static correction shield. The BAP 800 can be tooled for both reactive ion plating and conventional reactive evaporation allowing alternating processes without requiring any changes in the plant.

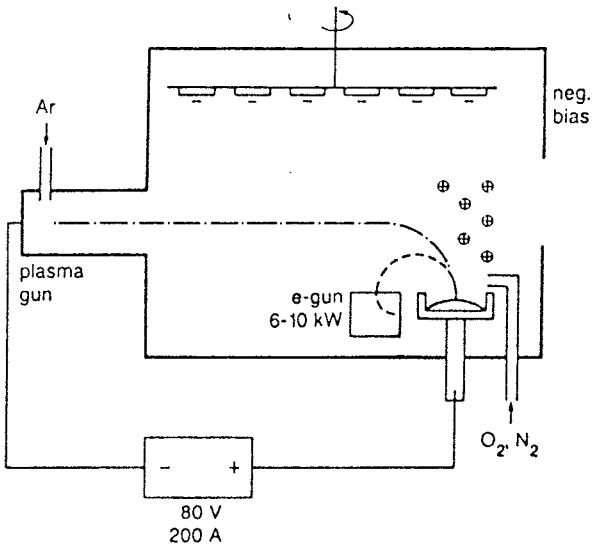

Fig. 4a: Schematic of the reactive low voltage high-current dc ion plating system Balzers BAP 800

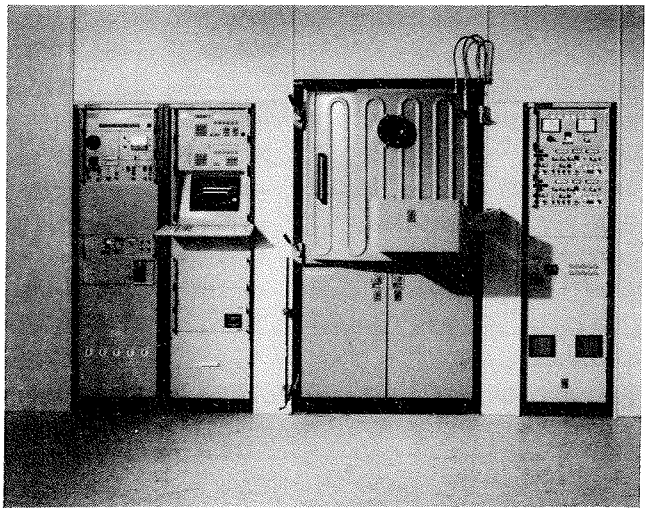

Fig. 4b: Front view of the BAP 800

6.2. Structure, Microstructure, Non-Optical Properties

Electron optical investigations of plated oxide films onto unheated substrates showed amorphous and fine grained polycrystalline structures. Substrate temperatures of about 200° C seem not develope a coarser structure. All the films are very dense and generally without columnar microstructure. The surfaces were found to be very smooth compared with films deposited by conventional evaporation /24/.

Infrared, ultraviolet and Rutherford backscattering measurements of plated deposits showed stoichiometry and absence of incorporated water. The high density prevented water vapour sorption at humid atmosphere. The films are therefore also interesting as protective layers /25/.

Excellent adherence of single films and film systems on glass substrates was found in scratch adhesion test. And with the exception of TiO_2, film indentation hardness (Knoop) and abrasion resistance values (eraser test) of all other coatings were found to be very high. Ion plated films are generally under compressive intrinsic stress /26/. Their environmental stability according to US MIL-specifications shows a remarkable degree of quality. Some data are listed in Tab.1.

6.3. Optical Properties

Ion plated oxide films are very good oxidized. No absorption could be measured in the high transmittance range of well prepared single films with simple photometric intensity methods. Photothermal deflection spectroscopy /27/ and loss measurments in optical waveguides /28/, showed very low values of k between 10^{-4} and 10^{-6}.

Film refractive index determinations from photometric and ellipsometric measurments showed values close to the bulk materials. In all cases measured indices were much higher than those of evaporated films. For comparision the various values are listed in Tab.2. The index values of single films could be reproduced within an accuracy of better than 1 %.

Homogeneity of the refractive index was good for films up to thicknesses of 7 λ/4 (λ=550 nm). Thicker films were found to be slightly inhomogeneous. As a consequence of the intrinsic compressive stress the films showed

Film (deposited on unheated glass)	Structure (electr. diffr.)	Microstructure (SEM, TEM)	Water Vapour Sorption	Adhesion to Glass (Scratch Test)	Indentation Hardness / Abrasion Resistance	Intrinsic Mechan. Stress
TiO_2	amorphous	dense, homogeneous	in all films no measurable H_2O-sorption.	in all cases excellent, between 2.4 and 2.5 kgf (that is onset of strong glass substrate damage).	higher Knoop microhardness than glass / excellent abrasion resistance according to US MIL-C-675 C.	for all nd = λ/4 oxide films compressive in the 10^9 dyn.cm^{-2} range. No increase in thicker films and multilayers ---> stress relaxation.
Nb_2O_5	amorphous	dense, homogeneous				
Ta_2O_5	amorphous	dense, homogeneous				
ZrO_2	finest grained polycrystalline	dense, spheroidal				
HfO_2	amorphous	dense, homogeneous				
Y_2O_3	amorphous	dense, homogeneous				
Al_2O_3	amorphous	dense, homogeneous				
SiO_2	amorphous	dense, homogeneous				
SiO_xN_y	amorphous	dense, homogeneous				

Table 1: **Non-Optical Properties of Ion Plated Oxide and Oxynitride Films**

Film/(Starting Material) Glass Substrates $T_s \approx 50^0C$	Refractive Index n_{550}	Homogeneity of n	Absorption Coefficient k_{546} PTDS (a) Photometric (b)	Stability on Wet Atmosphere	Stability at High Temperature
TiO_2 (Ti)	2.55	excellent up to nd = 7 λ/4	1.77 $\cdot 10^{-4}$ (a)	no measurable changes on wet atmosphere	no degradation by baking up to and higher to 400°C
TiO_2 (TiO)	2.55	excellent up to nd = 7 λ/4	7.0 $\cdot 10^{-5}$ (a)		
Nb_2O_5 (NbO_x)	2.40	excellent up to nd = 7 λ/4	> 5 $\cdot 10^{-4}$ (b)		
Ta_2O_5 (TaO_x)	2.26	excellent up to nd = 7 λ/4	4.0 $\cdot 10^{-6}$ (a)		
ZrO_2 (ZrO_x)	2.19	excellent up to nd = 4 λ/4	2.3 $\cdot 10^{-5}$ (a)		
HfO_2 (Hf)	2.17	-	< 10^{-4} (b)		
Y_2O_3 (Y)	1.95	-	< 10^{-4} (b)		
Al_2O_3 (Al)	1.66	excellent up to nd = 7 λ/4	< 10^{-4} (b)		
SiO_2 (Si)	1.485	excellent up to nd = 7 λ/4	< 10^{-4} (b)		
SiO_xN_y (Si)	1.5 - 2.0	-	< 10^{-4} (b)		

Table 2: **Optical Properties of Ion Plated Oxide and Oxynitride Films**

slight birefringence. Avoidance of water vapour sorption and desorption phenomena by the dense microstructure resulted in very stable film refractive indices. This is important for firm spectral system characteristics. The effect could be demonstrated with ion plated all-dielectric multilayer long-pass edge filters. Examples are shown in figures 5a and 5b. During controlled heating of such filters in a photometer to at least 130°C there occured either no measurable or only an extremly small shift in the position of the edge or of the transmittance band. The optical characteristics remained constant even during repeated heat treatment cycles. The marginal shift of 0.1 to 0.2 nm is not caused by water desorption/sorption phenomena but by the intrinsic material properties i.e. the change in refractive index with temperature dn/dT and the change in thickness by the expansion of the material with temperature dt/dT. Baking ZrO_2/SiO_2 and Ta_2O_5/SiO_2 multilayers on glass during a few hours at 400°C and subsequent storage tests in liquid water for three days produced no failure in optical and mechanical properties.

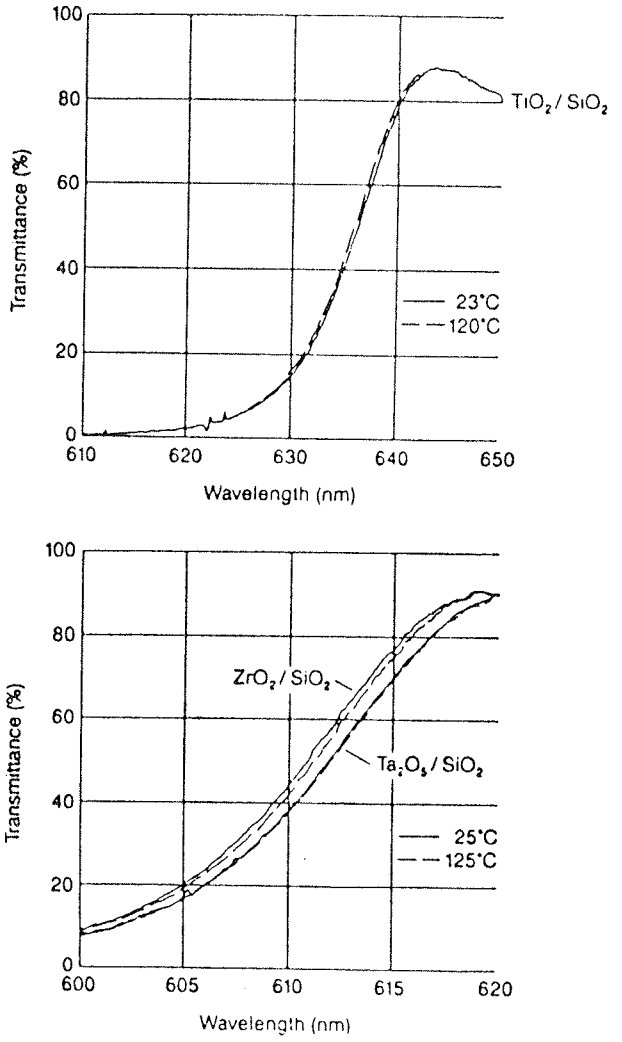

Figs. 5a and 5b: Transmittance versus wavelenght curve of the edge of ion plated long pass edge filters, each consisting of 23 layers of TiO_2/SiO_2, Ta_2O_5/SiO_2 or ZrO_2/SiO_2 including two matching layers. The dashed lines indicate the extremly small spectral edge shifts during heating to 125°C inside a photometer.

7. Discussion and Conclusion

The possibility to improve film performance in conventional reactive and even in activated reactive evaporation is rather limited. It is very effective, however, with the more recent developed higher energetic ion processes such as ion assisted deposition, sputtering, particularly ion beam sputtering and low- voltage reactive ion plating. Important features of coatings made by these techniques are: dense homogeneous microstructure resulting in relatively high refractive indices, low optical losses, insensitivity to changes in humid environment, high hardness and abrasion resistance and stability at high temperatures. A comparison of optical data is given in Tab.3.

Film	Conventional Reactive Evaporation	Reactive IAD	Reactive Sputtering	Reactive Ion Plating
SiO_2	1.46	1.485	1.48	1.485
Si_3N_4		1.93	1.95	2.05
Al_2O_3	1.63	1.68	1.67	1.66
ZrO_2	2.08	2.15	2.15	2.18
Ta_2O_5	2.10	2.30	2.15	2.26
TiO_2	2.30	2.43	2.51	2.52

Table 3 Refractive indices (λ=633 nm) of various compound films ($k << 10^{-4}$) obtained with different coating techniques

Bombardment of growing films with noble or reactive gas ions in ion assisted deposition and generation of energetic coating- material atoms in ion beam sputtering are powerful tools for basic parameter investigations in high energetic ion process developments and optimization studies.

The techniques are very effective for the deposition of low-loss oxide films on few small to medium size substrates.

Upscaling of directed ion beam processes for production purposes, however, is difficult and requires for IAD and IBS large size ion guns and highly efficient pumping systems. In film production the deposition time is important. Particularly with ion beam sputtering the low deposition rate of 15-20 minutes for a quarterwave thick film (visible range) is extremly time consuming in multilayer depositions. The new reactive low-voltage ion plating technology in the BAP 800 is an optimized and fast process for high volume production. Energetic conditions in the film formation are similar to those in IBS. The resulting film properties are similar with those obtained by ion assisted deposition. For comparison the typical energetic conditions of the mentioned processes are listed in Tab. 4. A slight deficit of the oxygen content in single films can occur /29,30/ depending on preparation conditions. The kinetic energy transferred to the atoms of the growing deposit should never exceed the

Technology	Gases Vapour Ions	Ion Current Density (Substrate)	Film Properties	Known Since	
Reactive Evaporation (RE)	O_2-neutral coating material		Columnar microstructure, close to stoichiometry	Aufwärter	1952
Activated Reactive Evaporation (ARE)	O_2-ions and activated states coating mat. atoms	$3 \cdot 10^{-4}$ mA/cm^2 < 100 eV	Reduction in opt. losses, improved stoichiometry	Heitmann Bunshah Ebert	1971 1972 1982
Ion Assisted Deposition (IAD)	Ar-and O_2-ions coating mat. atoms	$3 \cdot 10^{-1}$ mA/cm^2 50-500 eV	Densification by ion bombardment, good adhesion	McNeil Macleod	1982 1983
Reactive Gas Discharge Sputtering (RGS)	Energetic activated neutral	Power density on target 2-15 W/cm^2	Dense microstructure, good stoichiometry and adhesion	Coleman Pawlewicz	1974 1978
Reactive Ion Beam Sputtering (RIBS)	Energetic atoms and ions	Target: ≈ 4 mA/cm^2 Substr.: 0.5-1 mA/cm^2 Beam energy: 500-2000 V		Wei	1979
Ion Plating (IP)	Coating material and Ar-ions	≈ $1\text{-}5 \cdot 10^{-2}$ mA/cm^2 ≥ 1000 eV	Very dense microstruct. improved, adhesion	Berghaus Mattox	1937 1964
Reactive Low-Voltage Ion Plating (RLVIP)	Coating material Ar-, O_2- and N_2-ions	≈ 1 mA/cm^2 5-50 eV	Very dense microstruct. smooth surface, improved stoichiometry and adhesion	Pulker Moll	1985

Table 4 Reactive PVD Coating Technologies

displacement energy to avoid chemical damage that produces optical absorption in the films. This effect is even more critical in multilayers. To lower particle energy of the condensing and bombarding species seems to be an important requirement /31/. RLVIP is not a cold technology. In multilayer production processes the substrate temperature rises from ambient values to approximately 200 ° mainly due to heat radiating from the large evaporation sources. There is, however, no influence on the film microstructure. It seems that RLVIP in the BAP 800 will become an extremly useful production technique for high quality optical coatings with many applications.

It is impossible to discuss and compare all the ion and plasma techniques currently used for optical film deposition. Plasma assisted CVD, plasma polymerization, plasma etching and the non- reactive energetic PVD techniques have been omitted intentionally. For the moment there is also little experience available about reactive ion beam deposited films produced by filtered arc evaporation /32/. Because of their importance, however, it should be mentioned here that some fluorides, particularly AlF_3,CeF_3 and LaF_3, have also been successfully deposited by ion assisted deposition and low-voltage ion plating. Many rare earth metal fluorides as those of Sm, Gd, Tb, Ho, Er and Y have been successfully processed by IAD /33/. MgF_2 is more critical because of slight impact dissociation. Only few results are available on plated sulfide films. ZnS-films on Ge substrates deposited by dc ion plating /34,35/ improved considerably humidity resistance and adhesion compared to films obtained by conventional evaporation. Clearly further work is required on this topic. Extensive literature on modern reactive and energetic coating technologies using gas discharge plasma or ions has been published in form of review papers by Holland /36/, Bunshah /37/, Macleod /38/, Moll at al. /39/ and Martin /40/.

References

/1/ M. Auwärter, Balzers AG, Austrian Pat. No. 192 650 (1952) USA Pat. No. 2.920.002 (1960), FRG Pat. No. 1.104.283 (1968), and in many other countries

/2/ D.S. Brinsmaid et al. Kodak, USA Pat. No. 2.784.115 (1957), Application made on May 4, 1953

/3/ E. Ritter, J.Vac.Sci.Technol., 3 (1966) 225

/4/ H.K. Pulker, K.H. Guenther, Vak. Technik, 21 (1972) 201, B.A. Movchan,

A.V. Demchishin, Fiz. Metal Metalloved, Vol. 28 (1969) 653, and H.A. Macleod, Proc. SPIE, Vol. 325 (1982) 21

/5/ W. Heitmann, Appl. Optics, 10 (1971) 2414, and H.K. Pulker, Coatings on Glass, Chapter 6, p 262, Elsevier, Amsterdam 1984, 1985 and 1987

/6/ J. Ebert, Proc. SPIE, Vol. 325 (1982) 29

/7/ H. Küster, J. Ebert, Thin Solid Films, 70 (1980) 43

/8/ P.J. Martin, H.A. Macleod, R.P. Netterfield, C.G. Pacey, W.G. Sainty, Appl. Optics, 22 (1983) 178

/9/ T.H. Allen, Proc. Internat. Ion Engineering Congress, ISIAT 83 and IPAT 83, Kyoto, Japan, Vol. 2 (1983) 1305, and P.J. Martin, R.P. Netterfield, Progress in Optics, 23 (1986) 115

/10/ E.H. Hirsch, I.K. Varga, Thin Solid Films, 52 (1978) 445

/11/ W.C. Herrmann, J.R. McNeil, Proc. SPIE, Vol. 325 (1982) 101

/12/ H.R. Kaufman, J.J. Cuomo, J.M.E. Harper, J.Vac.Sci.Technol., 21 (1982) 725, H.R. Kaufman, Fundamentals of Ion Source Operation, Commonwealth Scientific Corp., Virginia, 1984, and H.R. Kaufman, J.Vac.Sci.Technol., A4 (1986) 764

/13/ K.H. Müller, J.Vac.Sci.Technol., A4 (1986) 461 and Physical Rev. B, Vol. 35, No. 15 (1987-II) 7906

/14/ J.L. Vossen, W. Kern, Thin Film Processes, Academic Press, NY, 1978, W.T. Pawlewicz, P.M. Martin, D.D. Hays, I.B. Mann, Proc. SPIE, Vol. 35 (1982) 105, and H.K. Pulker, Coatings on

Glass, Chapter 6, p. 268, Elsevier, Amsterdam 1984, 1985 and 1987

/15/ J.A. Thornton, V.L. Hedgcoth, J.Vac.Sci.Technol., 13 (1976) 117, A.D. Grubb, T.S. Mosakowski, W.G. Overacker, Proc. SPIE, Vol. 325 (1982) 74, S.Manniv, C.J. Miner, W.D. Westwood, J.Vac.Sci.Technol., A1 (1983) 1370, and H. Frey, G. Kienel, Dünnschicht Technologie, VDI Verlag, Düsseldorf 1987, Chapter 9

/16/ M.I. Ridge, Proc. SPIE, Vol. 325 (1982) 46 and M.I. Ridge, R.P. Howson, I. Ten Have, Proc SPIE, Vol. 401 (1983) 301

/17/ M.A. Scobey, R.I. Seddon, J.W. Seeser, R.R. Austin, P.M. Le-Febvre, US Pat. No. 4,851,095 (1989)

/18/ J.M.E. Harper, Ion Beam Deposition in Thin Film Processes, J.L. Vossen, W. Kern (Ed) Academic Press, NY 1987, and H. Oechsner, Plasma Physics, 16 (1974) 835

/19/ S. Scaglione, G. Emiliani, Proc. IPAT 85, Munich, 1985 p.399, CEP Consultants Ltd., Edinburgh, 1985, and J.Vac.Sci. Technol., A3 (6) (1985) 2702

/20/ D.M. Mattox, Electro Chem. Techn., Vol. 2 (1964) 295, and Proc. IPAT 79, London, 1979, p. 1, CEP Consultants Ltd., Edinburgh, 1979

/21/ H.K. Pulker, W. Haag, E. Moll, Balzers AG, Swiss Pat. applied, 00928/85-05 (1.3.1985), USA Pat. No. 4.619.748 (1986), and other countries

/22/ H.K. Pulker, W. Haag, M. Buehler, E. Moll, Proc. IPAT 85, Munich, 1985, p. 299, CEP Consultants Ltd., Edinburgh, 1985

/23/ J. Edlinger, M. Buehler, H.K. Pulker, Proc. Internat. Sympos. on Trends and New Applications in Thin Films, Strasbourg (F), March 1987, Vol. II, p. 735, Supplém. à la Revue: Le Vide, les Couches Minces, No. 235 (Janv./Fév. 1987)

/24/ H.K. Pulker, W. Haag, M. Buehler, E. Moll, J.Vac.Sci.Technol., A3 (6) (1985) 2700

/25/ H.K. Pulker, M. Buehler, R. Hora, Proc. SPIE, Vol. 678 (1986) 110, H.K. Pulker, J. Edlinger, M. Buehler, Proc. Internat. Sympos. on Trends and New Applications in Thin Films, Strasbourg (F), March 1987, Vol. II, p. 741, Supplém. à la Revue: Le Vide, les Couches Minces, No. 235 (Janv./Fév. 1987), H.K. Pulker, J. Edlinger, M. Buehler, Proc. IPAT 87, Brighton, UK, May 1987, p. 371, CEP Consultants Ltd., Edinburgh, 1987, M. Buehler, J. Edlinger, H.K. Pulker, M. Reinhold, B. Bendow, O. El Bayoumi, Proc. Halide Glass Sympos., Hyatt Regency, Monterey, CA, Jan. 1987

/26/ H.K. Pulker, M. Lardon, R. Buhl, E. Moll, J.Vac.Sci.Technol., A4 (6) (1986) 2922

/27/ A. Saxer, ENEA/Casaccia, Roma (I), Thin Film Lab., private communication, 1987; published in Vuoto 17 (3) (1987)

/28/ K. Tiefenthaler, Institute of Optoelectronic, Swiss Federal Institute of Technology, Zürich, private communication, 1987

/29/ K. Gürtler, K. Bange, W. Wagner, F. Rauch, H. Hantsche, Thin Solid Films, 175 (1989) 185

/30/ K. Bange, C.R. Ottermann, O. Anderson, U. Jechkowski, M. Laube, R. Feile, Thin Solid Films, 197 (1991) 279

/31/ J. Edlinger, H.K. Pulker, Proc. SPIE, Vol. 1323 (1990)

/32/ P.J. Martin, R.P. Netterfield, T.J. Kinder, Proc. 8. internat. Conf. Thin Films, ICTF-8, April 1-6, 1990, San Diego, CA, USA

/33/ M.J. Messerly, J.D. Targove, Proc. SPIE, Vol. 652 (1986) 222, and /37/

/34/ E. Henderson, Proc. IPAT 77, Edinburgh, 1977, p. 122, CEP Consultants Ltd., Edinburgh, 1977

/35/ I.M. Reid, H.A. Macleod, E. Henderson, M.J. Carter, Proc. IPAT 79, London, 1979, p. 114, CEP Consultants Ltd., Edinburgh, 1979

/36/ L. Holland, Design and Operating Characteristics of Low Pressure Plasma Systems, Vacuum, 28 (1978) 437, and J.Vac.Sci.Technol., 14 (1977) 5

/37/ R.F. Bunshah, C.V. Deshpandey, Plasma Assisted Physical Vapour Deposition Processes: A review, J.Vac.Sci.Technol., A3 (3) (1985) 553

/38/ H.A. Macleod, Ion Assisted Deposition of Thin Films, Proc. Internat. Sympos. on Trends and New Applications in Thin Films, Strasbourg (F), March 1987, Vol. I, p. 43, Supplém. à la Revue: Le Vide, les Couches Minces, No. 235 (Janv./Fév. 1987)

/39/ E. Moll, R. Buhl, H.K. Pulker, E. Bergmann, Surf. Coat. Technol., 39/40 (1989) 475

/40/ P. Martin, IEEE Transactions on Plasma Science, Vol. 18 (1990) 855

Prispelo (Arrived): 16.11.93 *Sprejeto (Accepted): 10.03.94*

Dr. Hans K. Pulker
BALZERS AG
FL - 9496 Balzers
Liechtenstein
tel. + 41-(0)75-44111

INHOMOGENITY OF LASER-DRIVEN TECHNOLOGICAL PROCESSES I. BEAM RELATED INHOMOGENITIES

S. Lugomer
Ruđer Bošković Institute, Zagreb, Croatia

Keywords: laser-driven technological processes, process inhomogenity, laser beam inhomogenity, inhomogene tempreatures, pressure fields, material surfaces, laser material deposition, laser chemical reactions, metal surfaces, semiconductor surface, laser treatments, laser glazing, beam-plasma

Abstract: Inhomogenity of laser-driven technological processes caused by inhomogenity of the laser beam is considered. Inhomogeneous beam induces the inhomogeneous temperature and the pressure fields on the material surface, thus dividing it into domains of the solid response, liquid response, and of the vapor/liquid response regime. The set of the gradient pairs $\Delta T^{\prime}_{\perp,\parallel}$ $\Delta P^{\prime}_{\perp,\parallel}$ give rise of 16 possible subdomains (basins) everyone of which is origin of characteristic dynamics. Depending on a dominant gradient pair combination, a number of physical phenomena is derived. They may simultaneously appear in various basins of the interaction space, generated in the single shot.

Inhomogenost laserski-iniciranih tehnoloških procesa

Ključne besede: procesi tehnološki laserski, nehomogenost procesov, nehomogenost žarkov laserskih, temperature nehomogene, polja tlakov, površine materialov, nanašanje materialov lasersko, reakcije kemične laserske, površine kovin, površine polprevodnikov, postopki laserski, loščenje lasersko, žarki plazemski

Sažetak: Razmatrana je nehomogenost laserski iniciranih tehnoloških procesa, uzrokovana nehomogenošću laserskog snopa. Nehomogenost snopa indicira nehomogeno polje, pritiska i tamperature na površini materiala i tako generira bazene različitih responsa režima: režim solida, tekućina i režim karakterističan za prijelaz tekućina/para. Skup gradijentnih parova $\Delta T^{\prime}_{\perp,\parallel}$ $\Delta P^{\prime}_{\perp,\parallel}$ daje 16 mogućih subdomena (bazena) od kojih svaki ima drukčiju dinamiku. Ovisno o dominantnoj kombinaciji gradijentnih parova, moguće je dobiti niz fizikalnih fenomena. Oni se mogu simultano pojavljivati u različitim bazenima interakcijskog prostora, generirani jednim jedinim laserskim pulsom.

Introduction

This paper deals with very common phenomena appearing in many (if not all) laser-driven technological processes, i.e. the process inhomogenities. They have been observed in:

- laser material deposition
- laser chemical reactions on the surface of metals and semiconductors
- laser treatment of metal surfaces
- laser glazing,

on both, thin films and plates. They are important for the surface processing technology on the microscale but in the engineering of the surface properties, surface protection, alloying and cladding on the macro- scale as well. These inhomogenities originate from laser-material (L-M) interaction, depending on the wavelength-scale (λ-scale), on the power- scale (P-scale), and the pulse duration (τ-scale), i.e. on the "beam related scales". Besides, they depend on the experimental conditions like the beam size, and the scan velocity, but also on the type of the material. Inhomogenities may be characterized with respect to "regime" of the surface response, determined by the maximal temperature reached in the L-M interaction.[1]

For the L-M interaction with $T_S < T_{melting}$, i.e. for the "solid response regime", the inhomogenity may appear in the form of plastic and superplastic deformations sometimes accompanied with various kinds of cracks.[1]

For the L-M interaction with $T \geq T_{melting}$, i.e. for the "liquid response regime", the inhomogenities may appear as 2D turbulent flow, vortices, viscous fingering, 1D and/or 2D supersonic jets, the convection phenomena etc..

For the L-M interactions exceeding T_B, i.e. in the presence of the surface ablation, or in the "vapor/liquid response regime", the inhomogenities may appear in the form of Rayleigh-Taylor R-T instabilities, various kinds of craters, transition from planar to nonplanar ablation etc.[1]

Here we should mention a very complex case of the high-power laser-metal interactions in the gaseous atmospheres when (in addition to the above types of response), one finds the surface chemical reactions. The inhomogenity appears in the form of different reaction rates, different types of reaction and consequently

of different composition on various places of the interaction space. In the high-power pulsed L-M interactions, the inhomogenity is observed as a fingerprint of the surface dynamics frozen in the interaction space. The pattern is of the complex nature, consisting of individual separated basins of the surface response dynamics.

Inhomogenities in the high-power L-M interactions have been mentioned in the literature many times. Their origins have been very seldom discussed, and in general, they are not well understood. Interest for these interactions was recently well increased because of their importance in the laser-driven technological processes on one side, and because of purely fundamental reasons on the other side. Up to now there is no systematic overview of inhomogeneous L-M interactions, and of physical phenomena simultaneously taking place in the interaction space.

This paper, on the phenomenological basis, and in a scatchy way, connects a number of these phenomena with their source in the laser beam.

Origins of inhomogeneity in the L-M interactions

Inhomogeneity in the L-M interaction may be caused by two type of sources: those (i) beam related, and those (ii) material related.

The beam-related sources are:

(i) laser beam inhomogenity [2, 3, 4]

(ii) inhomogeneous beam-plasma interaction above the material surface, while the material -related sources are:

(i) ablation instability[5]

(iv) structural /compositional surface disorder.

In this paper we consider the beam-related-sources.

(i) Laser beam inhomogeneity

Laser beam inhomogenity appears in the surface multimode processing (laser transformation hardening, laser glazing, laser alloying...). Multimode processing is strongly recommended because of the "top hat" profile and optimal surface covering.[6] In such a case the first few modes are dominant, and the beam structure (in the transversal cross-section) is approximately homogeneous and constant in time.

However, in the multimode, high repetition pulsing, the laser operation may become unstable. Multimode oscillations change the beam structure and cause the intensity space-time oscillations. These phenomena belong to the class of nonlinear optics and bring the analogy with the nonequilibrium phase transitions.[2,3,4]

Spontaneous mode-mode transitions are common in nonlinear optical systems (variously called self-focusing, fillamentation or profile instability) and lead to the formation of complex spatial structures, whenever the Fresnel number F, $F = \frac{\rho_0^2}{\lambda L}$, is small, ($\rho_0$ = mirror radius, L = laser cavity length, λ = wavelength). It may be understood as the ratio between the geometric angle ρ_0/L of view of one mirror from the other, and the difractive angle λ/ρ_0.[2]

The new features leading to increasing complexity of multimode spatial patterns appear when nonaxially symmetric modes are present. They can be described as a number (and dynamical motion) of defects in the patterns (where the intensity is zero, about which the electric field phasors[7] circulate and through which the electric field changes sign.(3) Defect in the optical field can appear for only a two modes present (for example with the combination of two Hermitte-Gaussian modes of indices n, m and m, n with a phase shift of $\pi/2$). Complex patterns can appear when the number of active modes is as many as five.[3]

The study of these problems was recently intensified from a few standpoints. Theoretically, one can look for the numerical solutions of the full set of Maxwell-Bloch equations describing the multimode laser operation and analyze the results in terms of the appearance and motion of defects in the intensity patterns.[3]

Alternatively, one can start from defects in the intensity field, and make the analogy with defect-mediated turbulence, by the study of influence of the singularities on the correlation of intensity fluctuations at spatially separated points and on the existence of different temporal and length scales in the system.[3] Here we concentrate on the time scales of fluctuations equal or larger than the pulse duration, so that the instantaneous mode pattern is the actual (pulse) pattern structure.

D'Angelo at al.[3] have shown that for small values of gain, C, and small Fresnel numbers (C = 1.1, a= 0.1) the intensity patterns are radially symmetric and the total intensity is time independent.

(Parameter a is related to the Fresnel number through: $a = \frac{8}{T}\tan^{-1}\left(\frac{L\lambda F}{4\pi\rho_0^2}\right)$, where T = oscillation period and ρ_0 = mirror radius)

More than 1 mode are present in the cavity, but the intensity is stationary in time - representing the cooperative frequency looking.

Upon increasing C(C = 1.2, a = 0.1) periodic pulsations in the laser intensity appear.[3]

Further increase of C leads to the appearance of complex spatio-temporal structures, each bifurcation involves the simultaneous appearance of a new frequency in

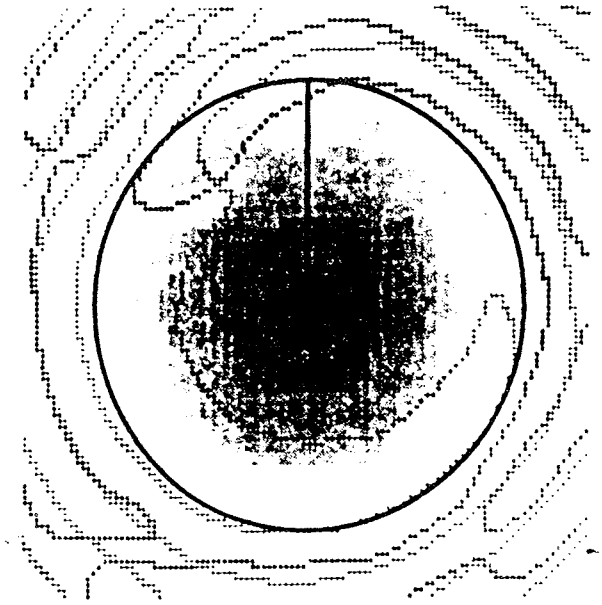

Fig. 1: Pattern a single defect of periodically pulsating intensity with for C = 2.5 and a = 0.1. Isophase and brightness plot the instantaneous intensity distribution. Darker shading corresponds to higher intensity. In this graph crossed (dotted) lines in the x-y space are the locus where the real (imaginary) part of the field vanishes. The point marked in the fixture is a topological defect. The solid circle marks the nominal boundary of the laser. $\rho = \rho_0$ (where the losses rapidly increase) while the solid line is an aid to identifying the center of the pattern $\rho = 0$. From ref. 3.

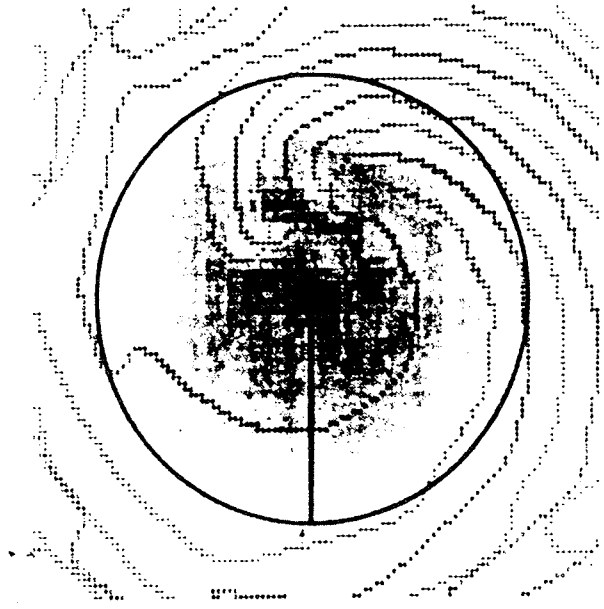

Fig. 2: Pattern of quasiperiodically pulsating intensity with two defects for C = 3.5 and a = 0.1. From ref. 3.

the intensity power spectrum and a spontaneous symmetry breaking of the spatial structure.[3]

Increasing the gain (C = 2.5, a = 0.1) the intensity becomes time dependent but the pattern at any particular time has an asymmetric profile. Oscillations of the intensity in time at each point of the pattern are periodic and are locked to the ratio 1;19.[3] The equiphase lines corresponding to this pattern show the existence of a point near the center where both real and imaginary parts of the field are zero simultaneously. This point is called "defect" in the beam structure.[3] Fig. 1. This defect can also be viewed as a phase vortex as the electric field phases have a net circulation around this point which when measured in mitts of 2π is called its topological charge. In this case the defect has a topological charge +1. Analysis of equiphase lines shows that the location of the defect is rotating around the center of the beam. This motion is in the form of a traveling wave of the type $\cos(l\phi - \omega t)$.[3]

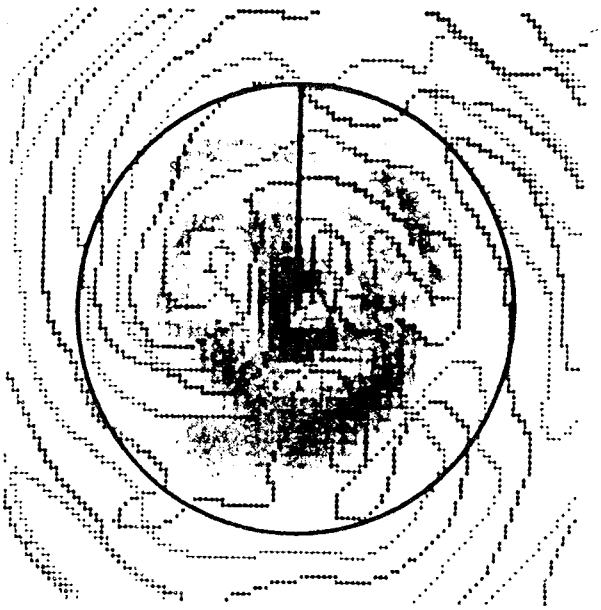

Fig. 3: Pattern with on average of 9 moving defects. Instantaneous equiphase lines showing the presence of mine defects. From ref. 3.

Increasing the gain further on (C = 3.5, a = 0.1) a more complex pattern appears. It contains two "defects" present in the beam, rotating around the center of the beam at different speeds.[3] Fig. 2.

Even more complicated patterns are obtained for C = 3.5, a = 0.4, in which many "defects" are present. In fact we get locally chaotic behaviour of intensity. Fig. 3. This pattern has (in average) nine defects of various topological charge. The number of defects is not constant, as pairs of opposite topological charge can annihilate and pairs can be also created.[3] These phenomena were recently discussed by Arecchi[2]. The transverse (x, y) intensity pattern and its autocorrelation function (right) are shown. Fig. 4a. For low F (F = 5) one single mode at the time oscillates and the wavefront is wholly correlated, and the correlation length ξ is of the some order or the cross lie D of the beam.(2) Fig. 4b. For high F (F = 70) many modes oscillates simultaneously yielding a speckle-like pattern (C), whose correlation length ξ is very small. Fig. 4c.

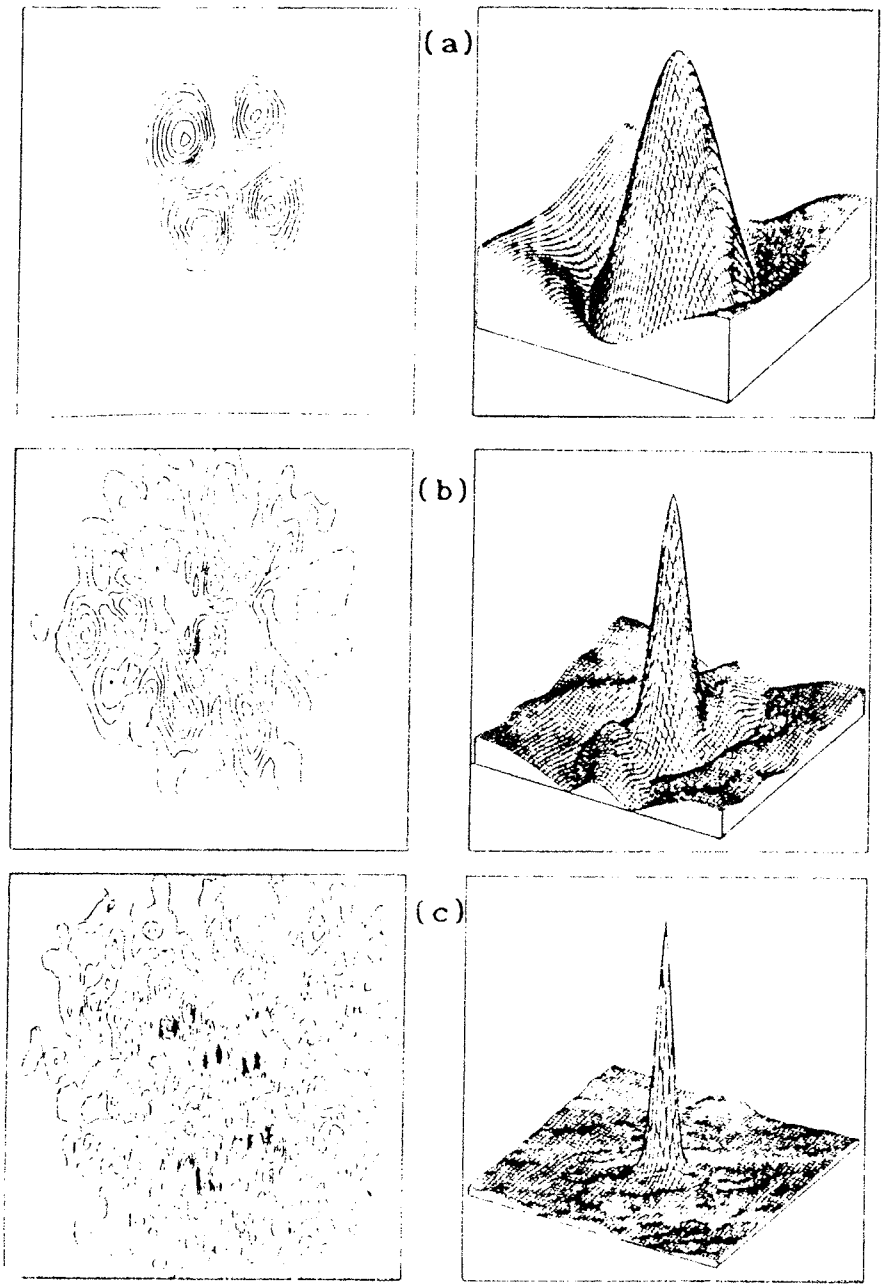

Fig. 4: *Intensity distribution on the wavefront (left) and space autocorrelation function (right) for increasing Fresnel number. (a) F = 5, one single mode at a time is present, ratio between coherence length ξ and frame size D is ξ/D = 1. (b) F = 20, ξ/D = 0.25. (c) F = 70, ξ/D = 0.1. From ref. 2.*

The low-limit F, corresponds to a periodic alternation of a few modes of the diffraction limit propagation followed by a dark period.[2] Technically, transition to the unstable multimode laser operation is sensitive on a number of operating parameters and conditions. It is sensitive on the variation of the laser pump profile (which adds spontaneous emission noise) and affects the beam intensity structure.

It is sensitive on the variation on the cavity loses (which may be important for the larger cavity radius). It is sensitive on the environmental influence on laser operation through the temperature oscillations, vibrations etc. which may influence the resonator parameters.

It is sensitive on the gain variation, which may appear if the processing conditions put the requirement for the high power at high pulse representation rate, etc.

Finally, it is sensitive on the back reflection of the beam from the metal surface. Radiation traveling in opposite direction enters resonator under small angle - and changes population emission. (The effect is equivalent to the

variation of the Fresnel number F and appearance of the asymmetric gain in the cavity.)

Whenever we have multimode laser operation every mode is a Hermitte- Gaussian (HG) or Laguerr-Gaussian (LG) function. The set of all these functions represent the topological, multidimensional space X, i.e.

$$x_i = A_{m,n} \qquad m,n = 0,1,2$$

$$\text{and } X \supseteq \{x_1, x_2, x_i \ldots\}, \qquad (1)$$

where $A_{m,n}$ stays for the HG or LG functions. Projection of the space X into the physical space, represents the optical intensity field I(x,y), for which we can simply write

$$I(x, y) \propto \sum_{m,n} A_{m,n}(x,y) \qquad (2)$$

(ii) Inhomogeneous beam-plasma interaction

At the high laser-power densities exceeding 10^8 W/cm^2 applied for the laser shock hardening or similar processes, generation of the vapor/plasma cloud above the material surface is the basic phenomenon. The plasma cloud is created by the leading edge of the pulse, while the rest of the pulse is partially absorbed in the cloud, and partially transmitted to the metal surface. Plasma density oscillations (as observed for the high power Nd:YAG and CO_2 lasers) are the common processes. In addition, arise of the plasma turbulence, inhomogeneous pair recombination etc., may cause the inhomogeneous beam scattering, absorption, or other complex photonic phenomena. Consequently, the surface will be (inhomogeneously) irradiated as to be stochastically screened. It receives less energy below the highly absorption regions of the plasma cloud, and more energy below the nonabsorptive regions.

In short, the homogeneous single mode laser beam, passing through the inhomogeneous material (plasma) cloud becomes inhomogeneous, just before it reaches the material surface. In this case the scattering functions $\alpha_{m,n}$ also give rise of multidimensional space X, whose projection into the real space gives the beam intensity I(x,y).

Generation of the Stochastic fields

The L-M interaction represents the mapping of the vector space X (beam related space) into the vector spaces Y and Z (material related spaces):

$$I_1 : X \dashrightarrow Y$$
$$I_2 : X \dashrightarrow Z. \qquad (3)$$

Supposing that the L-M interaction occurs in very short time so that dissipation processes are not significant, both imaging processes I_1 and I_2 represent nearly isomorphous mapping of X into Y and Z spaces. It means that the vector fields may be expressed by the

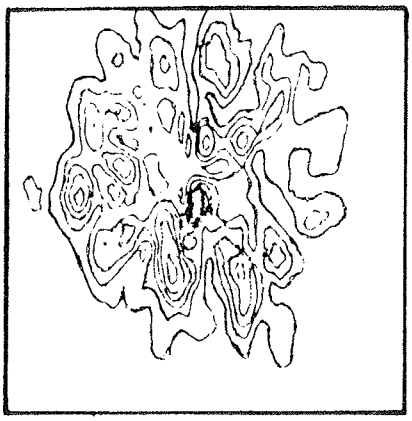

A

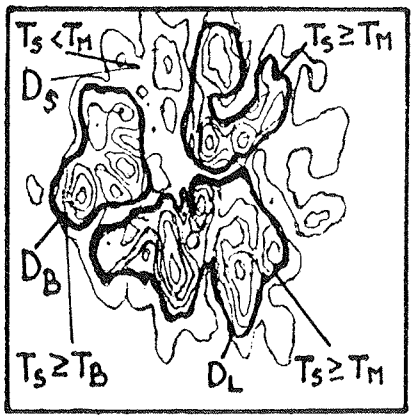

B

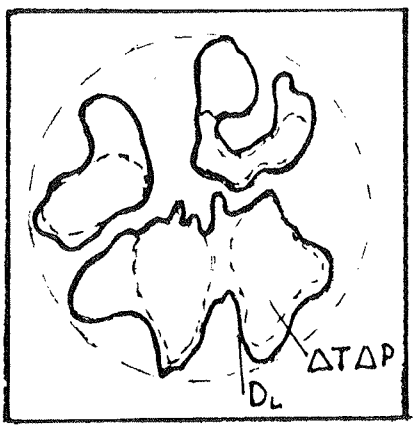

C

Fig. 5: Mapping process which transforms the stochastic optical intensity field into the stochastic temperature intensity field. (Schematically).
a) inhomogeneous optical intensity
b) inhomogeneous temperature intensity on the surface Dark lines are convolutes of the domains $D(T < T_M)$, $D_L(T > T_M)$ and $D_B(T > T_B)$
c) Definition of subdomains (dashed lines) inside domains D_S, D_S and D_B.

representing solution of diffussion equation (Bessel functions). Projection of the X space into the physical space represents the optical intensity, while the projections of Y and Z spaces, represent the temperature intensity and the pressure intensity, respectively (induced by the laser on the material surface). In this interaction the maps of the temperature and the pressure fields are similar to map of the optical field. (This, in fact, is well known for the lowest order mode TEM_{00}). For the long pulses, and for the significant role of thermal diffusivity, convection, etc. the mapps in Y and Z are very different from the mapps in X becouse of dissipation processes. The mapping process representing the L-M interaction is schematically given in Fig. 5. The stochastic optical intensity field is given in Fig. 5a. Nearly isomorphous mapp of the temperature field is given in Fig. 5b. The temperature field is obviously the stochastic field in which contours (Fig. 5b) represent the isotherms.

Further analysis of L-M interaction requires some characterization of this field to be introduced.

In the next step one can make the convolution of the isothermal curves by taking the convolute equal to T_M (melting temperature of the system), and T_B (boiling temperature). Thus, all these isothermal curves will be convoluted into 3 groups; one, which convolutes all isothermal curves $T_S \geq T_B$, one which convolutes all the curves $T_M \leq T_S < T_B$, and the third one in which stay all the isotherms outside the above two, i.e. those for which $T_S < T_M$. Fig. 5b.

Therefore, comparing the temperature intensity with the system transformation temperatures the three response regimes can be identified: the solid one ($T_S < T_M$), the liquid one ($T_S > T_M$) and the boiling one ($T_S < T_B$) or the vapor/liquid. The region inside any of the above convolutes is called a domain **D**. The interaction space therefore, consists of domains which may be of the solid, liquid or the vapor/liquid type. Further characterization of domains is based on the directional first-derivative operators. The directional operation yield a good localization of the intensity changes.

Following this idea we concentrate on the first-directional derivatives of stochastic temperature and pressure fields, ΔT and ΔP, inside the domain **D**. A part of domain in which ΔT and ΔP change only slightly from a given value (in module and direction), is called a subdomain D. A domain space D is supposed to consists of subdomains represented by the pair of ΔT, ΔP gradients. Assuming that subdomain has the coordinate R, the local gradients will be denoted by $\Delta T(R)$, $\Delta P(R)$. Fig. 5d. Therefore, any point in the interaction space satisfies: $(x,y) \in D \subseteq \mathbf{D}$, with

$$[\Delta t\,(R), \Delta P(R)] \in D. \qquad (4)$$

Local gradient field classification

Representation of subdomains can be made more precise by decomposing the thermal gradient field with respect to the surface, into two components:

$$\Delta T(R) = \Delta T_{\perp}(R) + \Delta T_{\parallel}(R) \qquad (5)$$

as well as the pressure gradient field:

$$\Delta P(R) = \Delta P_{\perp}(R) + \Delta P_{\parallel}(R). \qquad (6)$$

Considering the subdomain with the solid surface response, all the possible cases characterizing any subdomain may be represented by the combination of gradient pairs: $\Delta T_{\perp}(R)\ \Delta P_{\perp}(R)$; $\Delta T_{\parallel}(R)\ \Delta P_{\parallel}(R)$; $\Delta T_{\perp}(R)\ \Delta P_{\parallel}(R)$ and $\Delta T_{\parallel}(R)\ \Delta P_{\perp}(R)$.

The situation is more complex for the subdomain with the liquid response regime. However, the most complex and most general case occurs for the subdomain with the surface ablation, i.e. for the vapor/liquid interface dynamics. In the case of ablative interaction, one should take into account the fact that vertical temperature and pressure gradients $\Delta T_{\perp}(R)$ and $\Delta P_{\perp}(R)$, have either (+) or (-) sign.

The (+) sign will be attributed to the case when the temperature is the highest on the surface and decreases toward the metal interior. The negative (-) sign will be attributed to the case when the highest temperature is below the surface and the lowest on the surface.

The negative vertical temperature gradients $\Delta T_{\perp}^{-}(R)$ may appear because of subsurface superheating in the evaporation of the target. The surface is being cooled by the latent heat of evaporation, while the finite amount of laser energy is deposited within a certain depth from the surface of the target. This depth is characterized by the inverse of the absorption coefficient of the target for the incident laser beam. In contrast to the surface latent heat cooling mechanism, the only cooling mechanism inside the target is the conduction of heat into the bulk.(8) This results in internal temperatures being higher than the evaporating surface temperature, thus generating negative temperature gradient, $\Delta T_{\perp}^{-}(R)$.

The degree of superheating or $|\Delta T_{\perp}^{-}|$ module is dependent on the pulse duration τ and was observed on the nanosec. time scale. As a pulse duration is decreased to about 10 ns, the degree of superheating shows almost linear increase[8]. As the pulse duration increase for example above 120 ns, the superheating effects **vanish, thus meaning that** $\Delta T_{\perp}^{-}$ is transferred into the positive one, i.e. $\Delta T_{\perp}^{+}$. This is a direct influence of the beam parameters (P, τ) on the structure of the thermal gradient fields.

The pressure field in the above case especially $\Delta P_{\perp}(R)$ component is also reversed. Namely, the inverse thermal gradient $\Delta T_{\perp}^{-}(R)$ causes (because of the subsurface

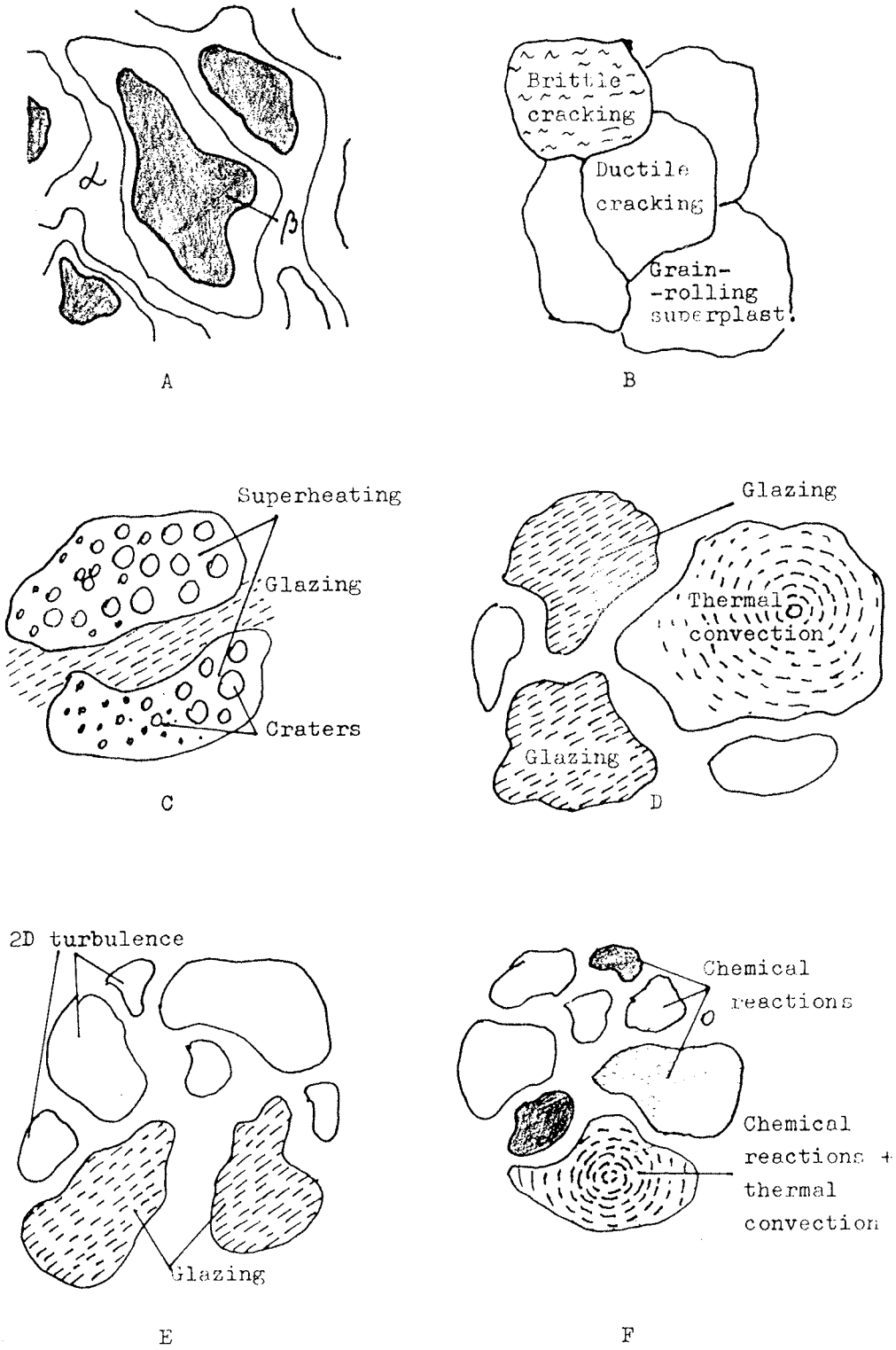

Fig. 6: *Schematic illustration of the inhomogeneous L-M interaction:*
a) in the case of inhomogeneous solid-solid phase transformation on the surface of composite materials (alloys).
b) in the case of inhomogeneous appearance of plastic and superplastic basins, accompanied by different types of cracks
c) in the case of inhomogeneous appearance of subsurface superheating and glazing
d) in the case of inhomogeneous appearance of glazing and thermal convection
e) in the case of inhomogeneous appearance of 2D turbulence and glazing
f) in the case of inhomogeneous surface chemical reaction (in alloying/cladding) accompanied by thermal convection and glazing. (See text.)

gas phase nucleation) a strong, inverse $\Delta P_{\perp}^{-}(R)$ gradient component.

Thus, both gradients $\Delta T_{\perp}(R)$ and $\Delta P_{\perp}(R)$ may, in general, have (+) or (-) sign. For the reason of completeness one should allow (+) and (-) signs for the horizontal gradients of $\Delta T_{||}(R)$ and $\Delta P_{||}(R)$, too. (As a matter of fact the two neighbour subdomains with either $\Delta T_{\perp}^{+}(R)$ or $\Delta T_{\perp}^{-}(R)$ of different modules automatically induce the horizontal $\Delta T_{||}^{-}(R)$ or $\Delta T_{||}^{+}(R)$ gradients). The reference point for the (+) or (-) ort orientation of horizontal components is the center of the particular subdomain. In this respect (+) sign of $\Delta P_{||}(R)$and $\Delta T_{||}(R)$ will relate to the ort orientation from the center of the subdomain toward its periphery, and vice versa for the (-) components sign.

On the basis of the above gradient field notation one can realize the mathematical construction as a representation of all possible cases of the local gradient field(s) configuration, given in the TAB. I.

This representation gives a 16 subdomains with specific configuration of the process-driving fields capable to generate a number of physical phenomena in the interaction space and in the single shot.

Local field characteristics and arise of physical phenomena

Dominant components of the local gradient field initiate a specific kind of phenomena in the particular subdomain.

Since the term subdomain is more familiar with mathematical consideration, we shall use the term "basin" which is more familiar with the physical description of dynamical processes. The list of physical phenomena (which is not complete) characteristic for various basins is given in TAB. II.

In the complex pattern of inhomogeneous L-M interaction, various basins are, first identified in the micrograph. Then, they are classified according to physical phenomena on the basis of TAB. II. Finally, local field configuration is identified. This procedure should be repeated for every basin in the micrograph.

A few characteristic examples appearing on refractory metals (Ti, Ta, Mo, W), are described below, and schematically illustrated in Fig. 6.

The "solid type response" represents the case appearing in the laser- transformation hardening of composite materials. These materials may have a complex phase diagrams with transitions of solid-solid type. The L-M interaction which establishes the inhomogeneous temperature distribution may cause inhomogeneous transformation, or appearance of the small zones of phase β (or γ) inside the matrix of the α phase. Schematically, this phenomena is illustrated in Fig. 6a.

Another example of the "solid type response" was observed in the Q-switched Nd:YAG high power multipulse treatment of refractory metals, (Ti, Ta, Mo, W...) with the high degree of beam focusing (2ω = 90 μm).[9] Fig. 6b. All the basins are of the solid type response. Different types of the surface breakdown (cracking) appearing above the critical power density - were obtained in every basin. Different crack growth mechanisms and the crack organization are obtained by the specific stress field configuration and by the symmetry of defects which

TAB. I: Representation of th local gradient fields

Symbolic notation	Local field configuration
1. $\Delta T_{\perp}^{+}(R)\,\Delta P_{\perp}^{+}(R)$	↓↓
2. $\Delta T_{\perp}^{+}(R)\,\Delta P_{\perp}^{-}(R)$	↓↑
3. $\Delta T_{\perp}^{-}(R)\,\Delta P_{\perp}^{+}(R)$	↑↓
4. $\Delta T_{\perp}^{-}(R)\,\Delta P_{\perp}^{-}(R)$	↑↑
5. $\Delta T_{\perp}^{-}(R)\,\Delta P_{||}^{+}(R)$	↓→
6. $\Delta T_{\perp}^{+}(R)\,\Delta P_{||}^{-}(R)$	↓←
7. $\Delta T_{\perp}^{-}(R)\,\Delta P_{||}^{+}(R)$	↑→
8. $\Delta T_{\perp}^{-}(R)\,\Delta P_{||}^{-}(R)$	↑←
9. $\Delta T_{||}^{+}(R)\,\Delta P_{\perp}^{+}(R)$	←↓
10. $\Delta T_{||}^{+}(R)\,\Delta P_{\perp}^{-}(R)$	←↑
11. $\Delta T_{||}^{-}(R)\,\Delta P_{\perp}^{+}(R)$	→↓
12. $\Delta T_{||}^{-}(R)\,\Delta P_{\perp}^{-}(R)$	→↑
13. $\Delta T_{||}^{+}(R)\,\Delta P_{||}^{+}(R)$	←→
14. $\Delta T_{||}^{+}(R)\,\Delta P_{||}^{-}(R)$	←←
15. $\Delta T_{||}^{-}(R)\,\Delta P_{||}^{+}(R)$	→→
16. $\Delta T_{||}^{-}(R)\,\Delta P_{||}^{-}(R)$	→←

Table II: Local field representation and arrise of physical phenomena

	local field represent.	The set of material parameters taking place in physical phenomena:
	$\Delta P_{\perp}^{+-}(R)$	$\mathcal{M}_p \in \{ \varepsilon, \dot{\varepsilon}, E, k, D..\}$
		ε = strain amplitude, $\dot{\varepsilon}$ = strain rate, E = Young module, k = thermal conductivity, D = vacancy diffussion coef.
	$\Delta P_{\perp}^{+-}$	– Spallation of metal grain
	$\Delta T_{\perp}^{+}(R)\,\Delta P_{||}^{+-}(R)$	– plastic behaviour controlled by $\dot{\varepsilon} < 2$; $\Delta P_{\perp}^{+-}$ component is origin of the strong shear waves which travel in all directions because of reverberations from the sample boundaries.
		– generation of vacancies and cavitation at grain boundaries (GB); [9,10]

		– cavity aggregation at GB junctions of "triple junction" type (Y-type) generating the "wedge crack" equilateral triangular crack and "isoscales triangular" crack.(10) The other cavity aggregation centers are "twin boundary", "ledge" and the "cusp", every one generating different type of crack.
	?	– "the bull eye" structure, osberved on the surface of Cu, Al and Ta[11], not well understand.
	$\Delta T_{\perp}^{+}(R)\ \Delta P_{\parallel}^{+-}(R)$	– Superplastic behaviour controlled by $\dot{\varepsilon} < 2\ \Delta P_{\perp}^{+-}$ components generate the shear waves which deposite the stress σ on the Y-sites (triple junction sites). Assymetric loading of 3 GB of the Y-site - one compressive, one tensile and one sliding-leads to the grain rotation with cleavage appearing on the tensile GB.[12] (Paidar and Takeuchi model) symmetric loading of 3 GB of the Y-site leads to the grain rotation with uncompensed tension at the center of the Y-site, thus generating the triangular crack in the center.[12] (The model of Beere). The other types of the grain rotation seems to be also present.

TAB. II: (continued)

LIQUID RESPONSE REGIME		
	local field represent.	The set of material parameters taking place in physical phenomena:
	$\Delta P_{\perp}^{+}(R)$	$\mathcal{M}_p \in \{\nu, \gamma, k, Ra, P, N..\}$ ν = kinematic viscosity, γ= surface tension, k = thermal difussivity, Ra = Raynolds number, P = Prandtl number, N = Nusselt number.
	$\Delta T_{\perp}^{+}(R)\Delta P_{\parallel}^{+}(R)$	– hydrodynamic 2D flow
	$\Delta T_{\perp}^{+}(R)$ $\Delta P_{\parallel}^{+-}(R)$	– shear flow in the micron size regions or larger. Appearance of regular structures (regular solutions), and very irregular ones (transition to turbulence). In the high power laser-metal intreractions turbulent structures are dominant.
	$\Delta T_{\perp}^{+}(R)\ (\Delta P_{\parallel}^{+-})$	– viscous fingering (equivalent to directional solidification), caused by the horizontal thermal gradient.
	$\Delta T_{\perp}^{+}(R)$	– convection instability appearing for $R_a = \frac{v_{\perp} d}{\nu} \geq 10^3$. ($v_{\perp}$ is temperature induced vertical fluid motion, d = layer thickness). They appear as: a) regular roll structures (Benard structures for steady conditions) of circular symmetry taking form of rings. b) irregular, disturbed rings, and c) chaotic, or turbulent patterns. In many cases, especially on Ta, the convection waves were observed.[13,14] The other (mixed type, structures found on Ti seems to indicate the nonvariational principle i.e. the non- potential nature of the problem.[15]
		– Benard-Marangoni convection in the presence of surface tension γ.
	$\Delta T_{\perp}^{+}(R)\Delta P_{\parallel}^{+}(R)$	– 1D and/or 2D supersonic jets of liquid metal traversing one or more liquid basins. ($\Delta P_{\parallel}^{+}$ induces the strong $v_{\parallel}$ component).
	$\Delta T_{\perp}^{+}(R)\Delta P_{\parallel}^{+}(R)$	

TAB. II: (continued)

VAPOR/LIQUID RESPONSE REGIME		
	local field represent.	The set of material parameters taking place in physical phenomena:
		$\mathcal{M}_p \in \{\nu, \gamma, Ra, P, N, \rho, A...\}$ ν, γ, Ra, P, N = as defined before, A = Atwood number, ρ = density.
	$\Delta P_{\parallel}^{+}(R)$	– viscous fingering
	$\Delta T_{\perp}^{+}(R)\Delta P_{\perp}^{+}(R)$	– Rayleigh-Taylor instability: vertical temperature gradient $\Delta T_{\perp}^{+}$ induces strong $\Delta\rho_{\perp}^{+}$ density gradient, this generating the two layer structure with ρ_{HIGH} and ρ_{LOW}. For the laser-induced R-T instability, the ratio $A = \frac{\rho_H - \rho_L}{\rho_L + \rho_H}$, called the Atwood number ≈ 1. The two types of bubles, appearing in (+) and (-) pairs as small 2D structures, or large 3D ones were found. These structures are the scale selected.[16]
	$\Delta T_{\perp}^{-}(R)\Delta P_{\perp}^{-}(R)$	– subsurface superheating: vertical temperature gradient causes subsurface boilling, and the buble generation on the surface. The exploded bubbles leave the craters on the surface. (Gas phase expelled). In some cases, the hot liquid metal comes to the surface, where $\Delta P_{\parallel}$ causes its 2D flow. This flow is irregular, organized into the structure of "dragon" (spiral) type, which can only be obtained by mathematical construction called the Barnsley collage. (Liquid phase expelled). For the subsurface superheating which ocurs in time shorter than time for the void formation, the small metal grains or their parts are expelled from the metal interior. Very irregular craters sometimes accompanied by melting are generated. (solid phase expelled).

play the role of the organizing centers. Surface breakdown structures were separately treated and their systematization was given with respect to the level of their topological complexity.[1]

In another case relating to the "liquid type response" obtained by the Q- switched Nd-YAP laser (P = Perovskite) again on the surface of refractory metals (especially on Ta plates), a different kind of inhomogeneous response was observed. The interaction

space consists of basins showing the superheating effects in the form of craters (regular), or of hillocks (still unexploded), and of basins showing pure glazed zones.[17] Fig. 6c.

Examples of inhomogeneous "liquid type response" may appear in the laser solidification hardening based either on the

- grain size strengthened alloys
- dispersion strengthened alloys
- metastable substitutional alloys
- amorphous, or glassy alloys,

where different new phases may appear inside the matrix of the old one, in the form of localized basins.

Another class of effects appear in the pulsed CO_2 laser treatment of Ti and Ta plates in the gaseous atmospheres of N_2 or O_2 under pressure. By changing the number of pulses, power density ... various kinds of phenomena appear in the basins of the inhomogeneous response.[14] Fig. 6d, e, f. Inhomogeneous interaction on the above figures contains two or three types of physical phenomena, located in separate basins. Every of these phenomena is established under specific conditions, or the field gradient representation which can be identified on the basis of TAB. II.

Plastic behaviour with cavitation cracking is established in the basin with $T_S < T_M$ in particular with $T_S < 0.3\ T_M - 0.4\ T_M$, and $\dot{\varepsilon} < 2$. The component $\Delta T_\perp{}^+$ establishes the layer of the above temperature of the thickness d (≈ to the grain size), while $\Delta T_{||}{}^{+-}$ defines the size of the basin on the surface in which the effects take place. The driving field represent the $\Delta P_{||}{}^{+-}$ components which establish the "shear waves" and cause the cavitation based "plasticity". The cavities aggregate on the point defects like triple junctions (Y-sites) giving rise of the wedge crack, isosceles triangular and equilateral triangular crack, depending on the aggregation symmetry.[10]

Superplastic behaviour is established in the basin with $T_S < T_M$, in particular with $0.7\ T_M < T_S - 0.9\ T_M$, and with $\dot{\varepsilon} \geq 2$. The component $\Delta T_\perp{}^+$ establishes the layer of the above temperature, and $\Delta T_{||}{}^{+-}$ establishes the (surface size) of the basin. The components $\Delta P_{||}{}^{+-}$ induce the shear waves, which on the Y-sites generate the superplastic behaviour of the grain- rolling type.[12]

Subsurface superheating is established in the basin with dominant $\Delta T_\perp{}^-$ in the presence of ablation, as mentioned previously. Various kinds of craters, bubbles or irregular flow which is combination of $v_\perp$ motion of subsurface liquid to the surface, and $v_{||}$ i.e. flow on the surface may also be observed.[8]

Surface glazing is established in the basins in which maximal temperature $T_S > T_M$. A very fast quenching to the room temperature, associated with the strong surface tension γ, makes the frozen surface smooth, and of the amorphous structure.

2D turbulent flow is established in the basins $T_S > T_M$ with dominant $\Delta T_{||}$ and $\Delta P_{||}$ components, which induce the $v_{||}$ shear flow, with the Rayleigh number $Ra = \frac{v_{||}\, d}{\nu}$ (d = basin size, ν = kinematic viscosity) which can take a large scale of the Ra values. Various kinds of turbulent patterns are generated on 10 ns τ-scale on Ta surface with Nd:YAP laser-spanning the range of purely periodic vortex-type patterns, to the merged-vortex pairs of ∞ type, elongated and finally purely chaotic ones. At the basin boundaries they show tenderadency to stratification.[17]

Thermal convection instability is established in the basin with $T_S > T_M$. Dominant role has the thermal gradient component $\Delta T_\perp{}^+$ which generates vertical convection velocity $v_\perp$. The convection appears for the Rayleigh number $Ra = \frac{v_{||}\, d}{\nu}$ (d = surface layer thickness) equal or higher than 10^3.

Rayleigh-Taylor instability is established in the basin with $T_S > T_B$. Dominant role has the thermal gradient component $\Delta T_\perp{}^+$ which induces a vertical gradient density $\Delta\rho_\perp$. It is responsible for appearance of two layer system of low density ρ_L and the high density ρ_H. Vertical pressure gradient component $\Delta P_\perp{}^+$ pushes the low density layer into the lower high density one, thus generating the R-T instability, which appears for the Atwood number $A = \frac{\rho_H - \rho_L}{\rho_L + \rho_H} \approx 1$.[16]

The arise of various phenomena is derived from various configurations of the first-directional derivation of the T and P stochastic fields. In the second approximation every basin may be distinguished with respect to the dominant component of the material parameters, and consequently with respect to the symmetry of related kinetic coefficients. This would lead to the basin division into subbasins. Obviously, this division would not give a new classes of phenomena, but the pattern structure (geometric and topological characteristic) as a different subclasses of the same phenomena (different pattern symmetries).

This is a necessary step to study of dynamics on the basis of various models (linear and nonlinear) in the particular basin.

Conclusion

We considered inhomogeneity in the L-M interaction which manifests as a number of localized physical processes (phenomena), simultaneously taking place in the interaction space. The concept of inhomogeneity discussed here is based on the beam related reasons.

The stochastic optical field establishes the stochastic field in the interaction space, which initiate various kinds of (stochastic) processes. The interaction space is devided in to the isolated domains and subdomains (basins) of the characteristic, localized response. Various classes of dissipative, dynamics processes may simultaneously appear in these basins existing in the close vicinity.

This problem is of a complex nature; it has a few complexity levels represented by the hierarchical tree introduced previously.[1] The concept of domains and subdomains (basins) represented by different combinations of ΔT and ΔP gradient components is a valuable one, since it includes a great deal of phenomena really observed in the experiments or in the technological processes. On this basis a number of inhomogeneous patterns observed in laser technological applications may be understood, classified, or possibly modified according to the requirements. Further development of the concept requires a more basic treatment and the exact mathematical approach, which to our knowledge was not yet done.

References

1. S. Lugomer; Vacuum; 43 (1992) 1217.

2. F.T. Arecchi; Physica; D51 (1991) 450.

3. E.J. D'Angelo, C. Green, J.R. Fredicce, N.B. Abraham, S. Balle, Z. Chen and G.L. Oppo; Physica; D61 (1992) 6.

4. F.T. Arecchi, S. Boccaletti, G. Giacomelli, G.P. Pucioni, P.L. Kamazza and S. Residori; Physica; D61 (1992) 25.

5. B. Luk'yanchuk; Modeling of Pulsed-laser Ablation and Surface Instabilities; ISLOE'93, Singapore, 11-13, Nov 1993.

6. M.E. Ashby and K.E. Earterling; Acta Metall., 32 (1984) 1935.

7. Phasor; A rotating line used to represent a sinusoidally varying quantity. The length of the line represents the magnitude of the quantity, and its angle with the x-axis at any instant represents the phase.

8. D. Bhattacharya, R.K. Singh and P.H. Holloway; J. Appl. Phys., 70 (1991) 5433.

9. S. Lugomer, M. Stipančić and M. Kerenović; Vacuum; (in press).

10. S. Lugomer; Vacuum; 44 (1993) 1053.

11. C.T. Walters and A.H. Clauer; Appl. Phys. Lett., 36 (1978) 713.

12. S. Lugomer, K. Furić, M. Stipančić and R. Ročak; "Grain-Rolling Superplasticity Induced by Q-Switched Nd:YAG Laser on Tungsten Surface; ISLOE'93, Singapore, 11-13 Nov. 1993.

13. S. Lugomer, G. Bitelli and M. Stipančić; "Laser-Hardening of Tantalum in the Nitrogen Atmosphere", ISLOE'93, Singapore, 11-13 Nov. 1993.

14. S. Lugomer, G. Bitelli and M. Stipančić; "The CO2 Laser Effects on Metal Surface", Technical Report on Cooperation between "Ruđer Bošković" Institute and ENEA INN. SVIL. Frascatii, to be published by Frascati Center, Roma, Italy (1993).

15. E. Bodenschatz, D.S. Connell, J.R. de Brugu, R. Ecke, Y.C. Hu, K. Lerman and G. Ahlers; Physica; D61 (1992) 77.

16. S. Lugomer and M. Stubičar; Vacuum (in press).

17. S. Lugomer, M. Stipančić and J. Kvapil; (Results of Cooperation between "Ruđer Bošković" Institute Zagreb and "Monokrystali" Laser Factory, Turnov, The Czech Republic) unpublished.

Prispelo (Arrived): 09.12.93 *Sprejeto (Accepted): 10.03.94*

Dr. S. Lugomer, dipl. ing.
Institut Ruđer Bošković
Bijenička 54
41000 Zagreb
tel. +85-41-45 111
fax. +385-41-425 497

UDK 621.3:(53+54+621+66), ISSN0352-9045 Informacije MIDEM 24(1994)1, Ljubljana

TEORIJSKE OSNOVE FOTOELEKTRIČNOG TENZOMETRA

Zvonimir Ogorelec
Fizički odjel Prirodoslovno-matematičkog fakulteta Zagreb, Hrvatska

Ključne besede: osnove teoretične, trak raztezni merilni, senzorji raztezka, deformacije mehanske, deformacije male, merjenje deformacij, tenzometrija, merjenje električno, merjenje fotoelektrično, napetosti mehanske, polprevodniki, pretvorniki

Sažetak: U radu je opisana nova vrsta senzora za električno mjerenje malih mehaničkih deformacija. Senzor se sastoji od prozirne plastične pločice te poluvodičkog izvora i dvaju detektora svjetlosti. Geometrijski odnosi odabrani su tako da jedna od svjetlosnih zraka, koju emitira izvor, pada na površinu nedeformirane pločice pod kutem vrlo bliskim kutu totalne refleksije. U tim uvjetima reflektancija granice dvaju optičkih sredstava jako ovisi o upadnom kutu, a posredno i o deformaciji senzora. To ujedno znači da tok reflektiranog zračenja, odnosno električni signal detektora postaje mjerom te deformacije. Račun na osnovi izvedenih jednadžbi ukazuje na vrlo visoku osjetljivost novog senzora (mnogo višu, na primjer, od osjetljivosti široko rasprostranjenih otpornih tenzometara), ali u relativno uskom mjernom intervalu. Stoga bi (po predviđanju kompliciranа) eksperimentalna istraživanja imala smisla poglavito u slučaju ako se žele razviti novi i ekstremno osjetljivi *detektori* mehaničkih naprezanja.

Theory of a Photoelectrical Strain Gauge

Keywords: theoretical foundations, strain gauge, strain sensors, mechanical deformations, small deformations, deformation measurements, tensometry, electrical measurements, photoelectrical measurements, mechanical stresses, semiconductors, converters

Abstract: A new type of strain gauge is described. It is composed of a transparent plastic plate, a light emitting diode (LED) and two photodiodes. These components are placed in such a mutual position that the incident angle of a light ray from the LED is nearly equal to the angle of total internal reflection. Under this condition the reflectance of the surface between two optical media is strongly dependent upon the incident angle, and, in turn, upon the sensor's deformation. Thus the flux of reflected light, i.e. the signal of the detectors, becomes a measure of this deformation. Calculations according to derived equations point at a very high sensitivity of the new sensor (much higher than the sensitivity of, e.g. the resistance strain gauges), but in relative narrow measuring intervals. Therefore, complicated exsperimental investigations would be of interest especially if extremely sensitive *strain detectors* are to be developed.

1. UVOD

Pod izrazom *tenzometrija* krije se skup metoda za mjerenje dinamičkih i statičkih naprezanja ili deformacija koje se javljaju u različitim mehaničkim konstrukcijama. Mjerenja te vrste vrlo su česta i smatraju se nezaobilaznim prilikom testiranja strojevnih dijelova, elisa, mostova, spremnika, kotlova i drugih sličnih tvorevina. Svede li se mnoštvo po detaljima različitih postupaka na najjednostavniji primjer, zadatak tenzometrije jest mjerenje sitnih produljenja, recimo, mjerenje elastičnog produljenja neke grede koje se pri opterećenju opaža na njenoj konveksnoj strani. U posredne zadatke tenzometrije spadaju još i mjerenja sile, tlaka, akceleracije, brzine i tako dalje, sve na osnovi mjerenja upravo spomenutih sitnih deformacija.

Iz razumljivih razloga najveću pozornost već odavna privlače električna mjerenja mehaničkih deformacija, pa su do danas razvijeni podjednako i različiti senzori (tenzometri, strain gauges) i sklopovi za mjerenje njihovih električnih signala /1,2/. To, naravno, ne znači da traganje za novim, možda boljim i osjetljivijim senzorima naprezanja ne traje i dalje. Ovaj preliminarni rad, na primjer, ukazuje na to da se jedan od takvih senzora može zasnivati i na do sada neiskorištenim fotoelektričnim mjerenjima. On, inače, pripada mnogo široj porodici senzora kojoj je autor pridijelio zajednički naziv "Fresnelovski senzori" /3/.

2. GEOMETRIJA SENZORA

Novi senzor prikazan je na Sl.1A, a sastoji se iz prozirne kvadratične plastične pločice debljine D i indeksa loma N. Plohe su joj visoko polirane i u dodiru su s drugim optičkim sredstvom (zrakom) indeksa loma n. Na lijevoj strani učvršćena je poluvodička emisijska dioda ED čije zračenje nakon višestrukih refleksija osvjetljava dvije fotodiode FD1 i FD2. One su postavljene simetrično pod pravim kutem i nalaze se na jednakim udaljenostima L od diode ED. Pogledajmo najprije situaciju u nenapregnutom senzoru (SL.1B). Iz slike se vidi da na FD1 padaju samo one zrake svjetlosti (1, 2, 3.... k) koje ED emitira pod ovim nizom kuteva: α_{1i} = arctg (L/2D), α_{2i} = arctg (L/4D), α_{3i} = arctg (L/8D) ..... Taj niz izražava se općenitom formulom

$$\alpha_{ki} = \text{arctg}\,\frac{L}{2^k D} \qquad (1)$$

Lako je uočiti da je broj refleksija na površinama senzora to veći što je α_{ki} manji. Za k = 1 imamo jednu refleksiju

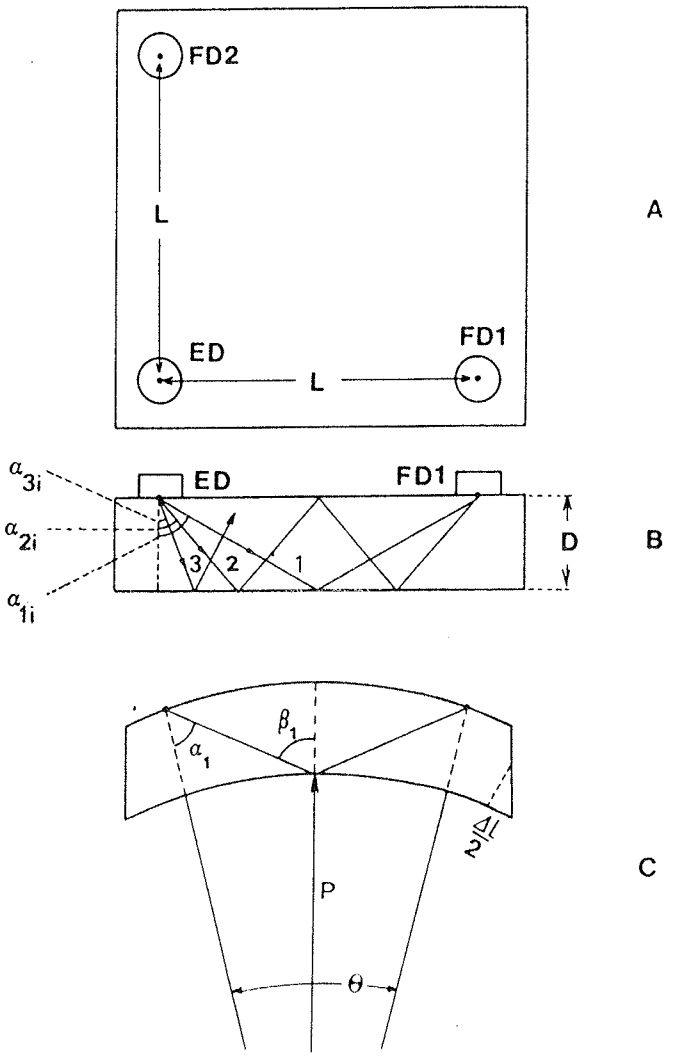

Slika 1: Nedeformirani i deformirani senzor naprezanja. Radi jednostavnosti izvor svjetlosti i njeni detektori prikazani su kao točke.

(r = 1), za k = 2 tri refleksije (r = 3) i tako redom. Općenit broj refleksija iznosi r = 2^k -1. Treba još pripomenuti da u nenapregnutom senzoru potpuno isti odnosi vrijede i za fotodiodu FD2 te da su kutevi refleksije u tom slučaju egzaktno jednaki kutevima emisije. Ta jednakost, međutim, gubi se u napregnutom senzoru (SL.1C).

Predpostavljeno je da je senzor priljepljen na gredu i da se ona zajedno sa senzorom deformira cirkularno. Zbog jednostavnosti nacrtana je samo zraka 1. Dok za diodu FD2 kutevi (1) ostaju nepromijenjeni, za diodu FD1 oni se mijenjaju. Na nju više ne pada zraka svjetlosti inicijalno emitirana pod kutem α_{1i}, već zraka emitirana pod manjim kutem α_1. Ona se reflektira pod kutem β_1 većim od α_{1i} te pada na FD1 ponovno pod kutem α_1. Za neku k-tu zraku vrijede, dakle, ovi općeniti odnosi: zraka k emitira se pod kutem α_k, reflektira se ukupno r = 2^k -1 puta, od čega p = 2^{k-1} puta pod kutem β_k i q = 2^{k-1} -1 puta pod kutem α_k.

Daljnji zadatak jest pronaći međuovisnost kuteva α_k i β_k te ih izraziti uz pomoć veličine, kojom se najčešće karakterizira deformacija senzora, a to je relativna promjena duljine X = $\Delta L/L$. Pritom će pripomoći poopćena SL.1C iz koje je vidljivo da vrijede ove zakonitosti: sinusov poučak, P/sin α_k = (P+D)/sin β_k , poučak o sumi kuteva, $\alpha_k + 2\Pi - \beta_k + \Theta/2^k = 2\Pi$ te formula koja regulira duljine lukova, $(L-\Delta L)/L$ = P/(P+D/2). Jednostavnom transformacijom ovih izraza dobivaju se četiri relacije neophodne za analizu signala senzora. To su relacije za polumjer zakrivljenosti P, za središnji kut Q te za kuteve α_k i β_k :

$$P = \frac{D}{2}\frac{1-X}{X} \qquad \Theta = \frac{2L}{D}\frac{X}{1-X} \qquad (2)$$

$$\alpha_k = \operatorname{arctg}\frac{L}{2^k D}\frac{1-X}{1+X} \qquad \beta_k = \alpha_k + \frac{\Theta}{2^k}$$

Tijekom izvoda iskorištena je još i činjenica da je centralni kut čak i kod maksimalne deformacije (obično se uzima X = ± 0.001, ili 1 milistrain) toliko malen da su dozvoljene aproksimacije sin $\Theta \cong \Theta$ i cos $\Theta \cong 1$. Na kraju, ako se senzor deformira u suprotnom smjeru (zakrivljenost na SL.1B prema gore), X prelazi u (-X), predznaci u formulama za P i Q se mijenjaju, a kutevi α_k i $\beta\kappa$ jednostavno zamjenjuju uloge.

3. SIGNAL SENZORA

Za analizu signala senzora potrebno je najprije izračunati tokove svjetlosti koja nakon niza refleksija pada na obje fotodiode. To posljedično znači da treba u prvom redu poznavati kutnu raspodjelu toka upotrebljene emisijske diode $\phi_E = \phi_{E0} F_E(\xi)$ te kutne raspodjele toka obiju fotodioda: $\phi_1 = \phi_{10} F_1(\xi)$ i $\phi_2 = \phi_{20} F_2(\xi)$, pri čemu je s ξ označen neki općenit kut. Pored toga nužno je poznavati i reflektanciju $R(\xi)$ granice dvaju optičkih sredstava u svim točkama refleksije. U njima se, naime, u senzor vraća samo dio $R(\xi)$ svjetlosnog toka. Drugi dio (nakon loma) izlazi iz senzora i nepovratno se gubi. Traženu reflektanciju određuju Fresnelova relacija /4/ koja za naravnu (nepolariziranu) svjetlost, kakvu emitiraju poluvodičke emisijske diode, daje:

$$R(\xi) = \frac{1}{2}\left[\left(\frac{A^2C - \sqrt{A^2 - B^2}}{A^2C + \sqrt{A^2 - B^2}}\right)^2 + \left(\frac{C - \sqrt{A^2 - B^2}}{C + \sqrt{A^2 - B^2}}\right)^2\right] \qquad (3)$$

U ovoj formuli iskorištene su kratice A = n/N (omjer indeksa loma), B = sin ξ i C = cos ξ. Ako poznajemo sve te veličine tok svjetlosti ϕ_{D1} koja pri napregnutom senzoru pada na diodu FD1 dobiva se sumacijom tokova pojedinih zraka:

$$\phi_{D1} = \phi_{E0} F_E(\alpha_1) R(\beta_1) \phi_{10} F_1(\alpha_1) + \phi_{E0} F_E(\alpha_2) R^2(\beta_2) R(\alpha_2) \phi_{10} F_1(\alpha_2) + \phi_{E0} F_E(\alpha_3) R^4(\beta_3) R^3(\alpha_3) \phi_{10} F_1(\alpha_3) + \ldots$$

ili potpunije:

$$\phi_{D1} = \phi_{E0} \phi_{10} \sum_k F_E(\alpha_k) F_1(\alpha_k) R^p(\beta_k) R^q(\alpha_k) \qquad (4)$$

Podsjetimo se da su eksponenti p i q dani relacijama: $p = 2^{k-1}$ i $q = 2^{k-1} - 1$. Izraz za tok svjetlosti koja pada na diodu FD2 nešto je jednostavniji, jer se u poprečnom smjeru senzor ne deformira, pa vrijedi $\alpha_k = \beta_k = \alpha_{ki}$. Umjesto relacije (4) dobivamo:

$$\phi_{D2} = \phi_{E0} \phi_{20} \sum_k F_E(\alpha_{ki}) F_2(\alpha_{ki}) R^r(\alpha_{ki}) \qquad (5)$$

U obje posljednje relacije nisu uračunati eventualni interferencijski efekti. No, na njih ni ne treba računati, jer pojedine zrake svjetlosti sasvim sigurno ne zadovoljavaju uvjet vremenske koherencije: $D < \lambda^2/\Delta\lambda$, u kojem je λ valna duljina upotrebljene svjetlosti, a $\Delta\lambda$ odstupanje od njene monokromatičnosti /5/. Budući da je kod General Electricove /6/ GaAs emisijske diode, na primjer, $\lambda \cong 950$ nm, a $\Delta\lambda \cong 50$ nm, $\lambda^2/\Delta\lambda$ iznosi oko 0.02 mm. Pločice pak senzora moraju biti otprilike za dva reda veličine deblje od te vrijednosti. To znači da pojavu interferencije zaista ne treba razmatrati.

Kao signal senzora može u najjednostavnijem slučaju poslužiti napon V_{D1} koji se uslijed toka svjetlosti ϕ_{D1} generira na diodi FD1. No, radi kompenzacije eventualnih fluktuacija toka emisijske diode bolje je mjeriti razliku napona $\Delta V = V_{D2} - V_{D1}$ od kojih V_{D2} odgovara signalu nedeformiranog senzora. Radi li se nadalje o linearnim diodama, naponi su proporcionalni tokovima, pa je njihova razlika $\Delta V = C_1 \phi_{D2} - C_2 \phi_{D1}$, gdje su C_1 i C_2 konstante. Kao što je uobičajeno u tenzometriji, signal ćemo u daljnjim relacijama izražavati u relativnim jedinicama, to jest, kao omjer $\Delta V/V_{D2}$. U stvari, prikazat ćemo ga za idealni slučaj kad su diode FD1 i FD2 identične ("uparene"). Tada vrijedi $C_1 = C_2$, $\phi_{10} = \phi_{20}$ i $F1 = F_2 = F$, što daje konačnu relaciju

$$\frac{\Delta V}{V_{D2}} = \frac{\sum_k \left[F_E(\alpha_{ki}) F(\alpha_{ki}) R^r(\alpha_{ki}) - F_E(\alpha_k) F(\alpha_k) R^p(\beta_k) R^q(\alpha_k) \right]}{\sum_k F_E(\alpha_{ki}) F(\alpha_{ki}) R^r(\alpha_{ki})} \qquad (6)$$

S obzirom na činjenicu da su prema formulama (2) kutevi α i β određeni relativnom promjenom duljine, $X = \Delta L/L$, upravo ispisan izraz daje ovisnost relativne promjene napona o relativnoj promjeni duljine, pa predstavlja karakteristiku novog senzora naprezanja.

4. RAČUN

Račun je proveden za senzor načinjen iz prozirne plastične pločice indeksa loma N = 1.5, što otprilike odgovara polimetil metakrilatu (pleksi staklu). Senzor je po pretpostavci u dodiru sa zrakom indeksa loma n = 1, pa je parametar A = n/N, koji se javlja u izrazu (3), jednak 0.6667. Pretpostavljeno je nadalje da i emisijska dioda i obje fotodiode imaju kuglastu raspodjelu toka $F_E(\xi) = F(\xi) = \cos\xi$. Za račun je odabrana pločica takve duljine L i takve debljine D da omjer L/D iznosi 14.3108. To je, naime, vrijednost za koji je kut refleksije četvrte zraka α_{41} upravo jednak kutu totalne refleksije $\alpha_t = \arcsin(n/N)$. U tom se slučaju pokazuje da su refleksivnosti $R(\xi)$ za zrake petog i višeg reda mnogo manje od jedinice, što zbog relativno velikih eksponenata p i q u relaciji (6) znači da je tok tih zraka na mjestu obje fotodiode zanemarivo malen. Pokazuje se pored toga, da je tok treće i nižih zraka ugrubo konstantan s obzirom na deformaciju. Pod tim uvjetima račun karakteristike (6) senzora daje krivulju prikazanu na SL.2. Vidi se da je to krivulja sastavljena od dvije grane centrirane oko

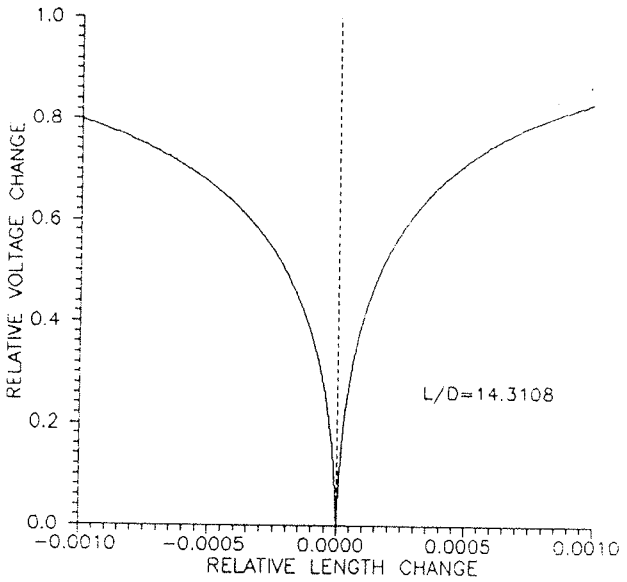

Slika 2: Relativna promjena napona senzora u ovisnosti o relativnoj promjeni duljine za slučaj kad je zraka 4 sa Sl.1 emitirana iz izvora pod kutem totalne reflaksije.

ishodišta deformacije $\Delta L/L = 0$. Njihov analitički oblik vrlo je kompliciran, no za daljnju analizu dobro će poslužiti i približni izrazi dobiveni nelinearnom regresijom. Ona za pozitivnu (desnu) granu daje izraz:

$$\frac{\Delta V}{V_{D2}} = (2.13 \pm 0.01) + (0.187 \pm 0.002) \ln \frac{\Delta L}{L} \qquad (7)$$

a za negativnu (ljevu) granu izraz:

$$\frac{\Delta V}{V_{D2}} = (2.10 \pm 0.01) + (0.189 \pm 0.001) \ln\left(-\frac{\Delta L}{L}\right) \qquad (8)$$

Senzor je, dakle, nelinearan, što - općenito rečeno - nije njegova odlika. Odlika mu je, međutim, izrazito visoka osjetljivost S. Ta važna veličina definira se kao derivacija signala (7) i (8) po relativnoj promjeni duljine, što za obje grane daje približno $S = 0.19/(\Delta L/L)$. Osjetljivost je, dakle, hiperbolički ovisna o relativnoj deformaciji, što znači primjerice da S neograničeno raste u blizini ishodišta, da kod ekstremno sitne deformacije $\Delta L/L = \pm 0.00001$ ima vrijednost oko 2.10^4, a kod maksimalne deformaci- je $\Delta L/L = \pm 0.001$ vrijednost 2.10^2. Premda te vrijednosti nisu do kraja vjerodostojne (zbog toga što su formule (7) i (8) samo približne) riječ je svakako o vrlo velikim brojkama. Kompletan račun osjetljivosti prikazan je na Sl.3.

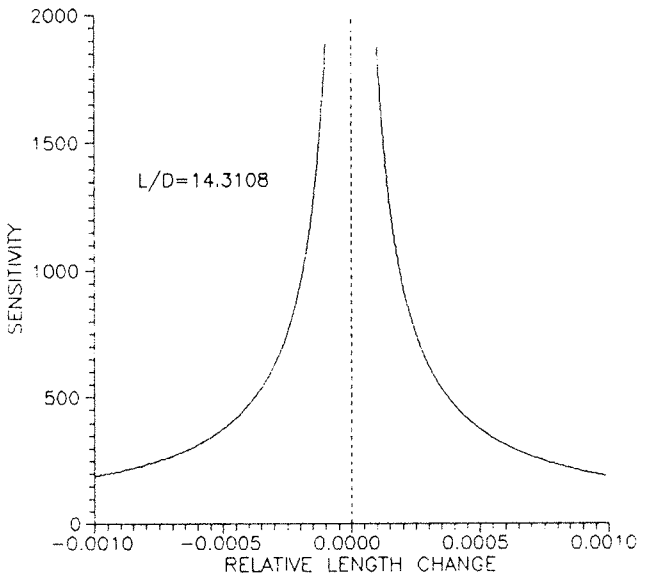

Slika 3: Osjetljivost senzora za slučaj prikazan na Sl.2.

Kao primjer za usporedbu može se uzeti široko rasprostranjeni piezootporni tenzometar koji na relativnu promjenu duljine reagira promjenom otpora ρ. Njegova karakteristika je linearna i glasi $\Delta\rho/\rho = \gamma\, \Delta L/L$. Mjeri li se otpor V-I metodom uz konstantnu struju, ta se karakteristika pretvara u $\Delta V/V = \gamma\, \Delta L/L$ što omogućuje usporedbu s relacijama (7) i (8). Osjetljivost piezootpornog tenzometra dana je, dakle, konstantnim faktorom γ koji za Philipsove senzore /7/ iznosi oko 2. To je za nekoliko redova veličine manje od osjetljivosti fotoelektričnog senzora u blizini ishodišta i barem za dva reda veličine manje od njegove osjetljivosti pri maksimalnoj deformaciji $\Delta L/L = \pm 0.001$.

Na žalost, tako visoku osjetljivost u blizini ishodišta moguće je postići samo uz veliku preciznost izrade senzora. Račun, naime, pokazuje da već mala odstupanja od vrijednosti omjera L/D = 14.3108 (koja je kao jedna od bezbroj mogućnosti korištena u računu) uzrokuje dramatične promjene u karakteristici senzora (Sl.4). Posebno su nezgodna odstupanja prema većim vrijednostima L/D, jer ona u blizini ishodišta potpuno "umrtvljuju" senzor. Već za odstupanje u drugoj decimali (L/D = 14.3200) "mrtva zona" prostire se od $\Delta L/L = -0.0004$ do $\Delta L/L = +0.0003$. Još veće odstupanje moglo bi senzor učiniti neaktivnim u čitavom području razmatranih deformacija.

Na sreću, odstupanja prema nižim vrijednostima od zadane nisu tako fatalna. Dapače, ona senzoru daju sasvim nove karakteristike (donji dio Sl.4). Doduše, osjetljivost u blizini ishodišta ima i u tom slučaju male vrijednosti, ali ona vrlo brzo raste te poprima maksimalne vrijednosti pri nekim kritičnim pozitivnim i negativnim deformacijama, koje se omjerom L/D mogu unaprijed odrediti. S lijeve i desne strane ishodišta, dakle, karakteristika senzora ima oblik sličan onom koji je prikazan na Sl.2. Jedna dvogranska krivulja, centrirana oko ishodišta, rascijepila se na dvije, centrirane oko nekih kritičnih, pozitivnih i negativnih deformacija.

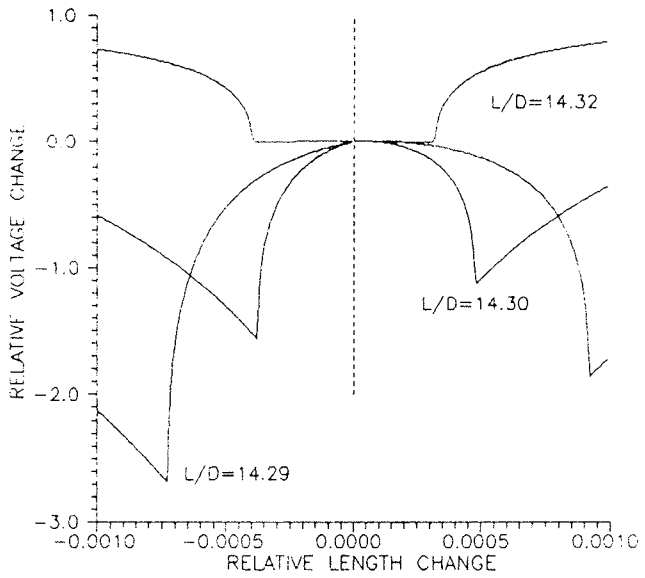

Slika 4: Utjecaj odstupanja omjera L/D od unaprijed zadane veličine na signal senzora.

ZAKLJUČAK

Ovaj preliminarni, boljereći eksplorativni rad pokazuje da se na osnovi jednostavnih optičkih zakonitosti te uz korištenje komercijalno dostupnog fotoelektričkog pribora može konstruirati nova vrsta senzora mehaničkih deformacija. Izvedena teorija ukazuje na njihovu izrazito visoku osjetljivost, makar uz evidentnu nelinearnost signala. Iako se na njegov oblik može utjecati upotrebom emisijske diode te obiju fotodioda

različitih kutnih raspodjela toka $F_E(\xi)$ i $F(\xi)$, nelinearnost se zacijelo ne bi mogla izbjeći. To sugerira, dakako, da bi u eventualnom eksperimentalnom razvoju ovog senzora valjalo misliti na elektroničku linearizaciju signala. No evidentno je da se senzor i bez ikakvog kondicioniranja signala može upotrijebiti ili kao vrlo osjetljivi detektor početka deformacije (Sl.2) ili kao jednako osjetljivi detektor neke kritičke deformacije (Sl.4).

Među dobra svojstva novog senzora treba svakako ubrojiti i njegovu neosjetljivost na temperaturne promjene. Budući da se u svim relacijama dimenzije L i D javljaju kao omjer, toplinska dilatacija ili kontrakcija senzora ne utječe na iznos njegova signala. Eksperimentalna istraživanja, međutim, trebala bi ustvrditi kakav utjecaj na signal ima toplinsko širenje predmeta na koji je senzor tijekom mjerenja učvršćen. U eksperimentu, nadalje, valjalo bi ispitati kako na signal utječe svjetlost reflektirana na bočnim stranama senzora koju račun u ovom radu nije uzimao u obzir. Eksperimentalni senzor, na kraju, morao bi se prekrivanjem nekom neprozirnom folijom zaštititi i od vanjske, parazitne svjetlosti. Tada bi se možda pokazalo da je konstrukcija troslojnog senzora sastavljenog od različitih optičkih sredstava mnogo pogodnija od konstrukcije jednoslojnog senzora u dodiru sa zrakom. Sve u svemu, rezultati teorije izložene u ovom preliminarnom radu sugeriraju eksperimantalna istraživanja barem u slučaju potrebe za vrlo osjetljivim detektorima mehaničkih naprezanja.

LITERATURA

/1/. Tehnička enciklopedija, Vol.12, p.685, Leksikografski zavod "Miroslav Krleža", Zagreb 1992.

/2/. D.M.Considine (Ed), Handbook of Applied Instrumentation, McGraw-Hill, New York 1974.

/3/. Z.Ogorelec, Microelectronics J. 19 (1988) 25.

/4/. J.D.Jackson, Classical Electrodynamics 2 Edition, p.281, John Wiley, New York 1975.

/5/. I.V.Savelyev, Physics, a General Course, p.358, MIR Publishers, Moscow 1980.

/6/. W.H.Sahm, General Electric Optoelectronic Manual, p.12, Syracuse 1978.

/7/. Directions for Use of Philips Strain Gauges, N.V.Philips' Gloeilampenfabrieken, Eindhoven 1970.

Prispelo (Arrived): 11.11.93 ***Sprejeto (Accepted): 10.02.94***

Prof.dr.Zvonimir Ogorelec,
Fizički odjel Prirodoslovno-matematičkog fakulteta,
41000 Zagreb, Bijenička 32, P.P.162.
tel. +85-41-43 24 82
fax. +385-41-4 25 25

MICROSTRUCTURAL ENGINEERING OF POWER FERRITES

Miha Drofenik
Jožef Stefan Institute Ljubljana, Slovenia

KEYWORDS: magnetic materials, Mn-Zn ferrites, power losses, eddy currents, material microstructures, grain size, ferrite powders, ferrite powder synthesis

ABSTRACT: The correlation between the high frequency power loss of MnZn ferrites and microstructure was considered. It was shown that when the grain boundaries in MnZn ferrites are permeable to eddy currents during the ferrite core operation in the MHz range, the power loss is proportional to the average grain size. From this interpretation it follows that the most effective way to decrease the power loss of MnZn ferrites is to reduce the average grain size during sintering. A nanosized MnZn ferrite powder would be promising for the preparation of dense and fine grained ferrite cores.

Krmiljenje mikrostrukture močnostnih feritov

KLJUČNE BESEDE: materiali magnetni, Mn-Zn feriti, izgube močnostne, tok vrtinčni, mikrostrukture materialov, velikost zrn, prahovi feritni, sinteza prahov feritnih

POVZETEK: Proučevali smo odvisnost močnostnih izgub v MnZn feritih v odvisnosti od mikrostrukture. V primeru, ko so meje med zrni ferita propustne za električne tokove pri frekvencah okoli 1 MHz, je možno pokazati, da so močnostne izgube sorazmerne povprečni zrnavosti MnZn ferita.

Introduction

The use of MnZn ferrites in power electronics is constantly increasing. Particularly the growth of the commercial market for Switch Mode Power Supplies (SMPS) places demands on the ferrite industry to produce high performance ferrite cores capable of operating at increasingly higher frequencies[1]. In SMPS the switching frequency is related to power output, making it possible for smaller core volumes to transform the same amount of power as a larger core would at lower frequencies. This is a direct challenge for the miniaturisation of SMPS[2] and related power devices.

MnZn ferrites exhibit a relatively high electrical resistivity in comparison to alloys, and a saturation magnetisation which is the highest among ferrites. These properties make MnZn ferrite very suitable for use in power applications[3].

Power loss and intrinsic properties

The main core characteristics are core losses which contribute the major part of the total electrical loss. In general the core loss can be divided into residual loss, hysteresis loss and eddy current loss. The residual loss is important only at low induction levels and can be ignored in power application of MnZn ferrites. The hysteresis loss $P_H = W_H f$, where $W_H = \int HdB$ is the energy represented by the area of the hysteresis loop measured under the maximum flux density, depends on many parameters; however, the hindernice to the domain wall displacements[4], which takes part at high induction levels[5], play the major role.

The factors governing the hysteresis loss are the magnetocrystalline anisotropy K_1, magnetostriction λ, stress σ, porosity p and saturation magnetisation M_S. For low hysteresis loss K_1, λ, σ, and p should be low. These parameters are composition dependent and can be controlled by the chemical formulation; however, the porosity (p) and mechanical stress (σ) are controlled mostly by the microstructure and impurities. The ferrous content, which is essential in MnZn ferrites for achieving low magnetocrystalline anisotropy and magnetostriction and thus low hysteresis loss, give rise to a high electrical conductivity due to the thermally activated hopping mechanism between Fe^{2+} and Fe^{3+} in spinel ferrites. The relatively low electrical resistivity, ρ_{bulk}, influences the eddy current loss, $P_E = d^2 B_{m2f2} / \rho_{bulk}$ where d^2 is the core cross section, B_m is the maximal flux density, and f is the frequency. In the case of very pure MnZn ferrites where the grain boundary resistivity is low, the resistivity of the bulk ρ_{bulk} is roughly equal to the grain resistivity. The most effective way to suppress electron hopping and thus the electric conductivity inside the ferrite grains, is by the substitution of Ti^{4+}, which occupies the B site adjacent to Fe^{2+} [6].

At higher operating frequencies the contribution of the eddy current loss to the total loss strongly increases and above 500 kHz it dominates all other losses. Therefore in order to increase the performance of MnZn ferrites for power applications at high frequencies, the eddy current

losses must be suppressed to the greatest possible extent.

However, in considering the eddy current loss, the extent of the eddy current in the magnetic core must be considered and correlated to the microstructure.

In general, two extreme cases regarding the eddy current in the magnetic core can be considered. In the first case, when the magnetic grains are isolated and the eddy current in this hypothetical case is localized inside the grains, Fig. 1, the core behaves as an assembly of individual magnetic grains in which each grain contributes to the eddy current loss.

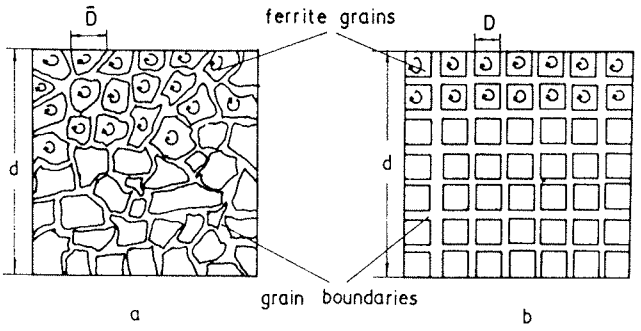

Fig. 1: Schematic picture of a real (a) and an ideal (b) microstructure of a material with isolated magnetic grains exposed to micro eddy currents.

In this case the parameter d loses its original meaning of the core dimension, and stands rather for the "size" of the micro eddy current in individual grains, representing their average diameter D̄. Thus, using these arguments the core cross section, d^2 in the Eq. for P_E, becomes the average grain cross section of an individual grain and written $\bar{D}^2$. In the limiting case when the grain boundaries are thick enough to substantially decrease the electric capacity of the grain boundaries and eliminate the frequency dispersion of the electrical resistivity, the bulk electrical resistivity ρ_{bulk} becomes the pure ohmic resistivity and does not depend on the material's microstructure, i.e. $\rho_{bulk} = \rho_{grain}$. In this case the total power loss at higher frequencies is proportional to the square of the average grain size;

$$P \approx P_E = \bar{D}^2 f^2 B^2_m / \rho_{grain}.$$

Such a dependence was indeed observed when Fe-based soft magnetic particles were separated by insulating layers of metal oxides[7].

A different dependence between the total loss and the microstructure holds when the grain boundaries are permeable to the eddy current.

In MnZn ferrites the grain boundary shows different chemical and physical properties from the ferrite grains. The segregation of impurities and partial reoxidation of Fe^{2+} during cooling on the grain boundaries makes the MnZn ferrite grain boundaries highly insulating in comparison to the grain interior. These insulating layers are in practice very thin and therefore exhibit a relatively high electrical capacity (C).

For such a ferrite core the equivalent electrical circuit of the semiconducting grain and the insulating grain boundaries are a parallelly connected resistance and capacitance whose impedance is proportional to $1/\Omega C$. This property causes a dispersion of the electrical resistivity with respect to the frequency[8].

In order to elucidate the dependence of power loss (P) on the average grain size D̄, we will divide the ferrite material into small cubes. In this hypothetical model the grain boundaries will lie in directions perpendicular and parallel to the principal axis, i.e. to the electric field direction. The grain boundaries which are parallel to the principal axis will be electrically bypassed by the bulk material. Therefore the small cubes can be approximated by bulk material separated by high ohmic layers - the grain boundaries - which are perpendicular to the principal axis. Each layer can be represented by a resistance-capacitance (r - c) lumped circuit of high ohmic layers. When the resistivity of the bulk is much lower in comparison to the grain boundary layers, the equivalent circuit of the ferrite can be represented by a series of lumped r - c circuits of the grain boundary layers. The resistivity of the ferrite material is in this simplified approach proportional to the number of grain boundaries per unit length. In ferrite core with the dimension d the bulk resistivity is then given by $\rho_{bulk} = d/\bar{D}\,(\rho_{grain} + \rho_{gr.boudary})$. In MnZn ferrites where $\rho_{gr.bound.} > \rho_{gr.}$ we obtain for bulk resistivity $\rho_{bulk} \approx d/\bar{D}\,\rho_{gr.bound.}$

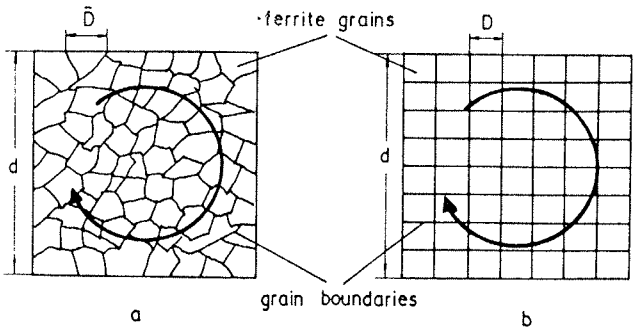

Fig. 2: A sketch of an actual (a) and an idealised (b) ferrite microstructure with grain boundaries permeable to the eddy current.

In a real material, Fig. 2, the grains have the shapes of irregular polyhedra. In this case only the components of

the grain boundaries which are perpendicular to the principal axis can effectively block the electric current.

At higher frequencies where the eddy current loss predominates the total loss is proportional to the average grain size $\bar{D}$;

$P \approx P_E = \bar{D}df^2B_m^2/\rho_{gr.bound.}$.

At frequencies where the grain boundaries are not short circuited by a high displacement current, the power loss can be effectively suppressed by a decrease in the average grain size.

To achieve a fine grained, homogeneous and dense microstructure, a small grained and equisized MnZn ferrite powder must be used. There are several non-conventional methods for producing a powder which exceeds the performance of conventionally prepared powders[9].

When engineering MnZn ferrites ceramics with the objective of forming fine grained, homogeneous and dense ceramics, one must proceed from a nonconventionally prepared ferrite powder. Among chemically prepared ferrite powders, those, prepared by the hydrothermal method offer enough advantages to realize this objective.

With ever increasing energy costs, the hydrothermal method could possibly become very attractive for the preparation of fine powders because of the low temperature involved during synthesis and their good sinterability. During hydrothermal syntheses equisized nanosized powders with a narrow grain size distribution can be achieved[10,11]. These samples sinter to a relative high density. In order to engineer the MnZn ferrite microstructure from the nanosized ferrite powder with an average grain size of 10 nm and a green density of 55% T.D., and prepare a ferrite core with an average grain size of around one μm, the average grain size should increase during sintering by a factor 10^2 and the density by 40%. So if we assume that the typical power loss of a ferrite core with an average size of 10 μm and 95 % T.G. at 50 mT, 80°C and 1MHz is about 10^3 mW/cm^3, then a ferrite core with an order of magnitude smaller average grain size and with all other parameters of similar magnitude, will have a power loss of an order of magnitude lower as well. By using hydrothermally prepared powder a fine grained ferrite core ($\bar{d} \approx 1$ μm) can be prepared by conventional sintering [12]. Such a microstructure can drastically decrease the high frequency power loss of MnZn ferrites.

Conclusions

- The power loss in MnZn ferrites at higher frequencies close to 1 MHz is mostly due to the eddy current loss, P_E.
- The average grain size is the most important microstructural parameter governing the power loss, P.
- The relationship between the eddy current loss and the average grain size is dependent on the extent of the eddy current and is governed by the microstructure of the ferrite.
- The most effective way to decrease the power loss in MnZn ferrites is to decrease the average grain size, provided that all other intrinsic properties stay constant.
- In order to prepare a fine grained and dense microstructure, a nanosized ferrite powder should be used. This offers the possibility of finding a compromise between a fine grained microstructure and a high density during sintering.

References

1. A. Goldman, "Modern Ferrite Technology", Van Nostrand Reinhold, N.Y. 1990

2. A. Kamade, K. Suzuki, "Optimum Ferrite Core Characteristic for 500 kHz Switch Mode Converter Transformer", in Advances in Ceramics, Ed. F.F.Y. Wand, pp. 507-12

3. C.R. Hendricks, V.W.R. Amarakoon, "Processing of MnZn Ferrites for High-Frequency Switch-Made Power Supplies", Cer. Bull. 70(5), 817-23

4. M. Guyot and A. Globus, "Determination of the Domain Wall Energy and the Exchange Constant from Hysteresis in Ferromagnetic Polycrystals", J. Phys., Suppl. 38(4), 157 (1977)

5. J. Smit and H.P.J. Wijn, Ferrites, Phil. Tech. Library, Eindhoven 1959, pp. 73-75

6. T.G. Stijntjes, J. Klerk, A.B. Groenon, "Permeability and Conductivity of Ti-Substituted MnZn Ferrites", Phillips Res. Rep., 25, 95-104 (1970)

7. Y. Sugaya, O. Inove and K. Kugimiya, "The Core Loss of Nano-Structure-Controlled Magnetic Materials", Ferrites; Proceedings of the Inter. Conf. on Ferrites (ICF6), Tokyo, Japan 1992, pp. 952-954

8. J.W.L. Köhler, C.G. Koops, "Absolute Measurements of the Time Constant of Resistor", Phillips Res.Rep. 1, 419-467 (1947)

9. Ceramic Processing before firing, Ed. G. Y. Onda, Jr. and L. L. Henck, John Wiley and Sons, NY, Toronto

10. S. Komarneni, E. Fregean, E. Breval, R.Ray, "Hydrothermal Preparation of Ultrafine Ferrites and their Sintering", J. Am. Cer. Soc., 71(1), C-26-C-28 (1988)

11. M. Rozman, M. Drofenik, "Hidrotermalna sinteza feritov", Zbornik referatov posvetovanja o materialih, Oct. 6.-8., 1993, Portorož, (in press)

12. T. Pannaparyil, R. Maranda, S. Komarneni, "Magnetic properties of high-density MnZn", J. Appl. Phys. 69(8), 5349 (1991)

Prispelo (Arrived): 16.02.94 *Sprejeto (Accepted): 22.02.94*

Dr. Miha Drofenik, dipl. ing.
Institut Jožef Stefan
Jamova 9
61000 Ljublajna, SLovenija
tel. + 386 (0)61 1259 199
fax. + 386 (0)61 1261 029

UDK 621.3:(53+54+621+66), ISSN0352-9045 Informacije MIDEM 24(1994)1, Ljubljana

NEW GENERATION OF PERMANENT MAGNET MATERIALS BASED ON Sm-Fe NITRIDES

Boris Saje, Spomenka Kobe Beseničar*
Iskra Magneti, Ljubljana, Slovenia
*** Jožef Stefan Institute, Ljubljana, Slovenia**

Keywords: permanent magnets, rare eart magnets, Sm-Fe-N magnets, material microstructures, thermomagnetic analysis, microelectronic analysis, X-ray analysis, metal alloys

Abstract: The microstructure and magnetic properties of the $Sm_2Fe_{17-x}Ta_x$ ($0< x <2$) cast and annealed alloys were investigated by means of the microstructural, X-ray diffraction and thermomagnetic analysis. A process for obtaining the Sm_2Fe_{17} phase free of iron in the as-cast state is described. The method consists of adding 5 at % of Ta in the melt. By this addition of Ta to the basic alloy two phase structure of the as-cast ingots consisting of the Sm_2Fe_{17} phase and Pauli paramagnetic $TaFe_2$ hexagonal Laves phase can be obtained. Less than 0.5 wt.% of free iron in the cast ingot with 5 at.% of Ta addition was determined with isothermal magnetic analysis.
X-ray diffraction showed an increase of the lattice spacing dependent upon the tantalum concentration in the alloy which indicated some possible solid solubility of Ta in the Sm_2Fe_{17} phase. Quantitative electron probe microanalysis confirmed the solid solubility of tantalum in the Sm_2Fe_{17} phase up to 2.3 at %. This resulted in an increase of the Curie temperature of the Sm_2Fe_{17} phase which was determined by means of thermomagnetic analysis.

Nova generacija trajno magnetnih materialov na osnovi Sm-Fe nitrida

Ključne besede: magneti trajni, magneti zemelj redkih, Sm-Fe-N magneti, mikrostrukture materialov, analiza termomagnetna, analiza mikroelektronska, X-žarki analiza, zlitine kovin

Povzetek: Z elektronsko mikroanalizo mikrostrukture in termomagnetno analizo so bile preiskane zlitine s sestavo $Sm_2Fe_{17-x}Ta_x$ ($0< x < 2$). Opisan je postopek priprave Sm_2Fe_{17} faze, ki se uporablja za pripravo trdomagnetne spojine $Sm_2Fe_{17}N_y$, v litem stanju z nizko vsebnostjo prostega mehkomagnetnega železa. Fazna modifikacija je bila dosežena z dodatkom 5 at% Ta, ki v nominalni sestavi Sm_2Fe_{17} zamenjuje železo. Tako dobljena zlitina je v litem stanju dvofazna in vsebuje Sm_2Fe_{17} fazo in Pauli paramagnetno $TaFe_2$ heksagonalno Lavesovo fazo. Vsebnost preostalega prostega železa v liti strukturi se giblje okoli 0.5 ut.%, kar je bilo ugotovljeno z izotermalno magnetno analizo. S termomagnetno, x-žarkovno in mikroelektronsko analizo vzorcev je bilo tudi ugotovljeno da obstaja območje trdne topnosti Ta v Sm_2Fe_{17} fazi (do 2.3 at.%) zaradi česar se Curiejeva temperature te faze zviša.

I. INTRODUCTION

The R_2Fe_{17} compounds with most of the rare earths (R) have been found to absorb large quantities of nitrogen when treated at about 500°C in gaseous NH_3 or N_2(1). The structures of the interstitial nitrides are related to those of the hexagonal Th_2Ni_{17} (for compounds with heavy rare earth) or rhombohedral Th_2Zn_{17} (for compounds with light rare earth) parent compounds (Fig. 1).

The $R_2Fe_{17}N_y$ with y = 2.8 have Curie temperatures that are in the range from 678 to 758 K, compared to those for y = 0 which are in the range from 214 to 477 K. This increase in Curie temperature in the nitrides is due to more than doubling of the Fe-Fe exchange interactions, associated with an increase in cell volume of about 7% (2). The R-Fe exchange interaction is slightly reduced in the nitrides. All compounds exhibit easy c-plane anisotropy at room temperature, except for R = Sm, which is easy c-axis. The negative sign of the Fe sublattice anisotropy constant K1 is unchanged after nitrogenation.

These materials possess a unique combination of high Curie temperature, strong uniaxial anisotropy and large iron moment. The comparison of intrinsic magnetic properties between $Nd_2Fe_{14}B$ and $Sm_2Fe_{17}N_y$ is the following; $Nd_2Fe_{14}B$: Tc= 588 K, Ms = 1.60 T, Ha = 7.5 T, BH max (teor.) = 509 kJ/m^3; $Sm_2Fe_{17}N_x$: Tc = 749 K, Ms = 1.55 T, Ha = 14 T, BH max (teor.) = 472 kJ/m^3. This is the reason that permanent magnets based on the $Sm_2Fe_{17}N_y$ ternary interstitial phase with rhombohedral Th_2Zn_{17} - type structure are considered to be competitive with the well-known Nd-Fe-B based magnets, especially because of the higher Curie temperature which is the main disadvantage in Nd-Fe-B based magnets.

Unfortunately the Sm_2Fe_{17} binary phase which is used for production of the $Sm_2Fe_{17}N_y$ interstitial ternary compound via the gas-phase interstitial modification process (2), is formed through a peritectic reaction between primary crystallised iron and Sm-rich liquid (3). This process always leads to considerable amounts of free iron (up to vol. 25 %.) and some Sm-rich phases in the as-cast state. Free iron especially, unless removed by a

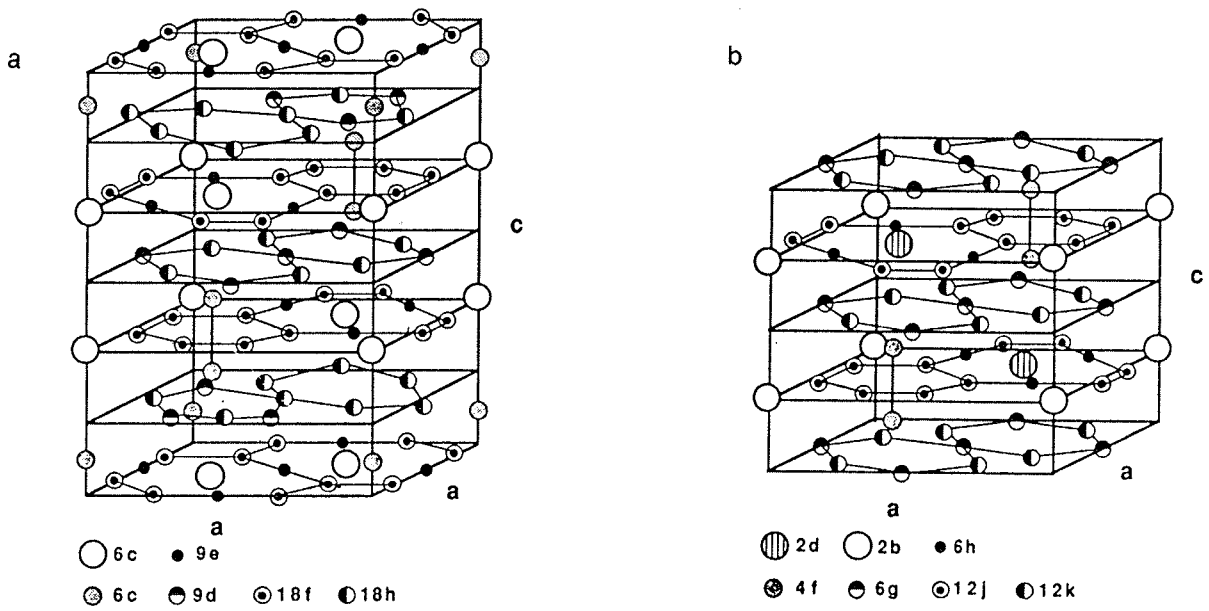

Fig. 1: Th_2Zn_{17} (A) and Th2Ni17 (B) crystall structures showing the octahedral interstitial 9e or 6h sites that may be occupied by N

subsequent isothermal homogenization treatment, reduces the coercivity of the subsequent Sm_2Fe_{17} nitride when used for permanent magnets.

Known methods for creating an alloy without soft magnetic phases are either high temperature-long term annealing of samarium-rich cast alloy or addition up to 5 at.% of Nb (4) which modifies crystallization and leads to two phase structure consisting of Sm_2Fe_{17} phase and $NbFe_2$ paramagnetic intermediate Laves phase.

From other transition elements it was shown that also Zr, Mo, Hf, V, Ti and Ta form intermediate Laves phases of AB_2 - type (5). $HfFe_2$ and $ZrFe_2$ are ferromagnetic (6) and thus inappropriate due to their magnetic interaction with demagnetising field, WFe_2 and $MoFe_2$ do not melt congruent but are formed through peritectoid reaction thus making formation kinetics unsuitable (7). Ti forms $TiFe_2$, antiferromagnetic Laves phase with Neel temperature of 272 K (8) but work in Sm-Fe-Ti system showed that Sm_2Fe_{17} and $TiFe_2$ are not in the equilibrium at melting temperature (9).

Tantalum forms Pauli paramagnetic $TaFe_2$ intermediate hexagonal Laves phase with iron (6). While it is possible in Sm-Fe-Nb to obtain two-phase as cast structure,similarity of Nb-Fe and Ta-Fe binary phase diagrams and while Nb and Ta form isomorphic system (5), we choose Ta as a promising candidate for addition element which would lead to a two phase structure in the as cast state consisting of Sm_2Fe_{17} and $TaFe_2$ without presence of soft magnetic free iron. This modification would lead to an precursor alloy suitable for producing $Sm_2Fe_{17}N_y$ ternary interstitial phase without isothermal annealing treatment of the cast ingots prior to nitrogenation.

We also expected some enhancement of the Curie temperature due to possible existence of solid solubility of Ta in the Sm_2Fe_{17} phase as it was reported for Sm-Fe-Ti (9) and Sm-Fe-Nb (10) systems.

II. EXPERIMENTAL WORK

As-cast alloys were prepared by arc-melting of 2 g samples in a Ti purified Ar atmosphere using elemental Sm (99.9 %, Johnson Matthey), Fe (99.9 %, Ventron) and Ta (99.9 %, Plansee). Excess Sm was added to a nominal composition of $Sm_2Fe_{17-x}Ta_x$ ($0< x <2$) to counterbalance Sm evaporation losses during melting. The samples were remelted four times to improve homogeneity.

Cast ingots were sealed in the evacuated quartz tubes with some addition of elemental Sm to counterbalance Sm vapour pressure at annealing temperature. Sealed samples were annealed at 1200°C for 5 hours and subsequently water-quenched.

Microstructural analysis was performed on a JEOL 840A SEM/EPMA electron probe microanalyser. Phase contents were calculated using digitised SEM micrographs and image analysis software.

XRD measurements of the powders were conducted on Phillips 1710 diffractometer using CuK a radiation.

Thermomagnetic analysis of the bulk samples (up to 100 mg) was carried out in vacuum in the temperature range from 300 to 1000 K at an applied field of 2 kOe , and isothermal magnetic analysis was performed at 550 K in an applied field from 0 to 15 kOe by means of sensitive

magnetometer- susceptometer (Manics) based on a Faraday principle.

III. RESULTS AND DISCUSSION

The microstructural analysis showed phase composition changes dependent upon increasing of Ta content of the investigated alloys. From Fig. 2, which shows microstructure of tantalum free alloy, we can observe the normal appearance of as cast state of nominally stoichiometric Sm_2Fe_{17} alloy. Dendrites of primary crystallised iron are surrounded by peritectically formed Sm_2Fe_{17} phase with some Sm-rich phase which was identified as $SmFe_2$. This is consistent with previous findings (3) that formation of $SmFe_3$ (which would be expected from the phase diagram) was suppressed due to its sluggish formation kinetics.

After annealing the nominally stoichiometric Sm_2Fe_{17} as-cast samples the microstructural image analysis

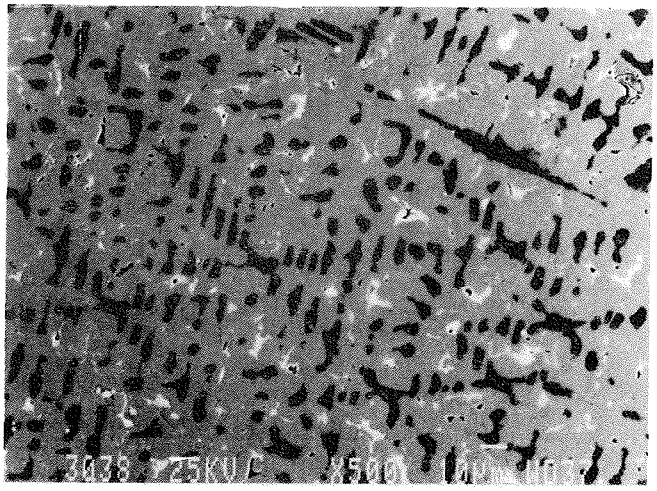

Fig. 2: SEM micrograph (SE/BSE Comp. Image) of the Sm_2Fe_{17} as cast alloy showing dendrites of primary Fe (dark), Sm_2Fe_{17} (grey), and $SmFe_2$ (white) phases.

revealed that the microstructure is still multiphase consisting of approximately 97 vol. % of Sm_2Fe_{17} phase, 2 vol % of Sm-rich phase and 1 vol. % of iron.

Microstructural analysis (supported by thermo magnetic analysis) also showed, that proportion of free iron dendrites as well as Sm-rich phases diminishes progressively with increase of Ta content (Fig. 3), and appearance of some $TaFe_2$ phase was identified which indicates some non- equilibrium solidification due to fast cooling.

The microstructure significantly changed for an alloy with 5 at % of tantalum which replaces iron in the nominal composition of $Sm_2Fe_{17-x}Ta_x$ as it is shown in Fig. 4. Image analysis of the digitised SEM micrograph showed that microstructure consists of approximately 85 vol % of Sm_2Fe_{17} phase and 15 vol % of $TaFe_2$ phase. It should be noted that due to the relatively large amount and

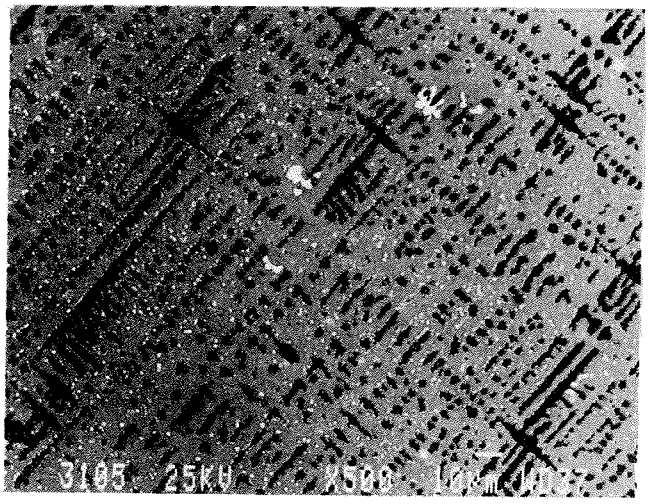

Fig. 3: SEM micrograph (SE/BSE Comp. Image) of the cast Sm-Fe-Ta alloy with 2 at.% of Ta showing Sm_2Fe_{17} (grey), Fe (dark), $SmFe_2$ (light grey) and $TaFe_2$ (white) phases

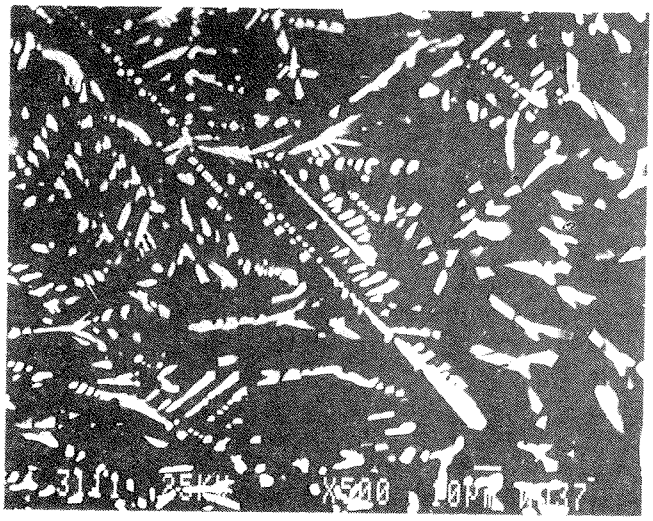

Fig. 4: SEM micrograph (SE/BSE Comp. Image) of the cast Sm-Fe-Ta alloy with 5 at. % of Ta showing Sm_2Fe_{17} (grey) and $TaFe_2$ (white) phases

dendritic appearance of the $TaFe_2$ phase optimal amount of Ta addition for preparation of Sm_2Fe_{17} precursor alloy for nitrogenation is somewhat lower than 5 at.% of Ta.

For qualitative confirmation of the present phases in as cast alloy we additionally used thermomagnetic analysis of the samples for Curie temperature determination of the existent phases.

The magnetic difference between the tantalum free alloy and 5 at% Ta material is evident from Fig. 5. The analysis of Ta free alloy showed three characteristic steps on M = f(T) curve, corresponding to the Curie temperature of Sm_2Fe_{17}, $SmFe_2$ and Fe respectively. Thermomagnetic curve of the 5 % Ta material shows only one large step, consistent with Curie temperature of Sm_2Fe_{17} phase. As expected, thermomagnetic scan of $TaFe_2$ phase showed the paramagnetic nature of the phase. It has to be noted from Fig. 5 (curve B) that after the Curie temperature of the Sm_2Fe_{17} phase a paramagnetic state of the alloy

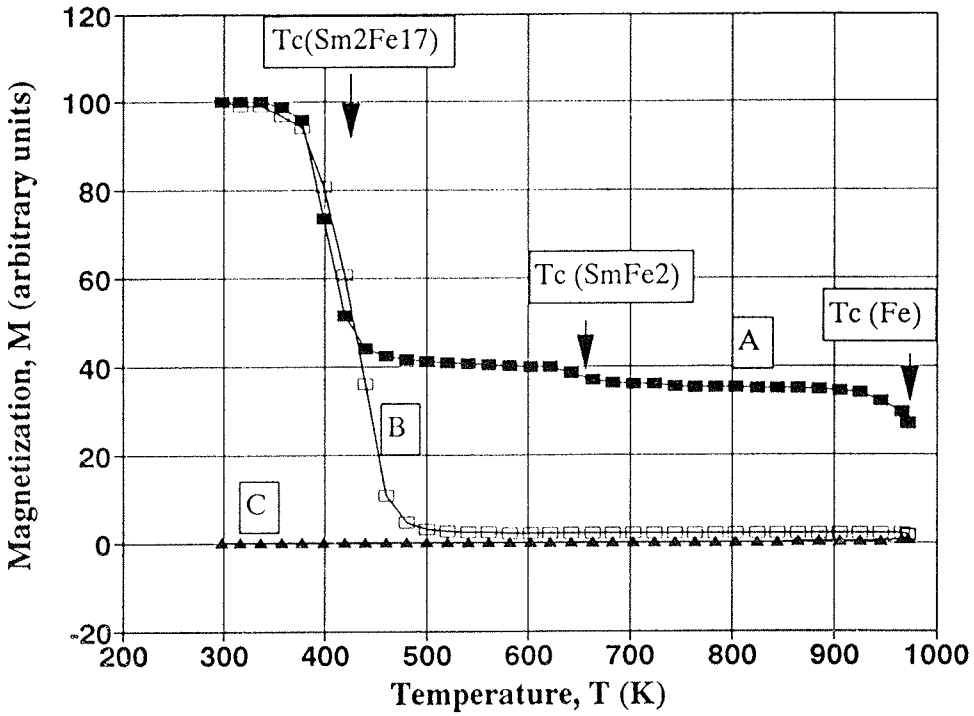

Fig. 5: Normalized thermomagnetic curves for A) as cast Ta free Sm_2Fe_{17} alloy, B) as cast Sm-Fe-Ta alloy with 5 at.% of Ta and C) $TaFe_2$ as cast alloy.

with 5 at. % was not attained. Therefore for quantitative determination of free iron dendrites or iron precipitates, which still might be present in the cast ingot, due to suspected inhomogeneous distribution induced by non-equilibrium solidification, isothermal magnetic analysis (ITMA) was used. The principle is originally based on the method of Honda (11) and Owen (12) for determination of ferromagnetic impurities in paramagnetic samples and applied in Rare-Earth -Transition Metals systems in work of Liu et all.(13).

Fig. 6 shows a typical M = f(H) curve of the as cast ingot with 5 at.% of Ta measured at 550 K. The measuring temperature is above the Curie temperature of Sm_2Fe_{17} phase therefore making its contribution to measured magnetisation paramagnetic. To estimate the amount of remaining free iron we separated the ferromagnetic and paramagnetic contribution from the measured M = f(H) curve. The ferromagnetic contribution (curve C on Fig.5) shows that the saturation magnetisation of residual ferromagnetic component in the alloy is 1.04 emu/g. Assuming this is free iron then this value divided by the value of saturation magnetisation of pure iron at measuring temperature gives 0.5 wt.% of remaining free iron in the alloy.

Quantitative electron probe microanalysis of the annealed samples revealed the existence of solid solubility of tantalum in Sm_2Fe_{17} phase as is shown in Table 1.

phase	element	concentration of the element (at %)		
		0 at % Ta	5 at % Ta	8 at % Ta
Sm_2Fe_{17}	Sm	10.85	10.55	10.83
	Fe	89.15	87.14	87.88
	Ta	-	2.31	1.29
Sm-rich	Sm	38.13	-	-
	Fe	61.87	-	-
$TaFe_2$	Fe	-	71.64	70.39
	Ta	-	28.36	29.61
Fe	Fe	100	-	99.35
	Ta	-	-	0.65

Table 1: Quantitative electron probe microanalysis of the phase composition of the phases present in the samples of the Sm-Fe-Ta alloys with different tantalum concentration

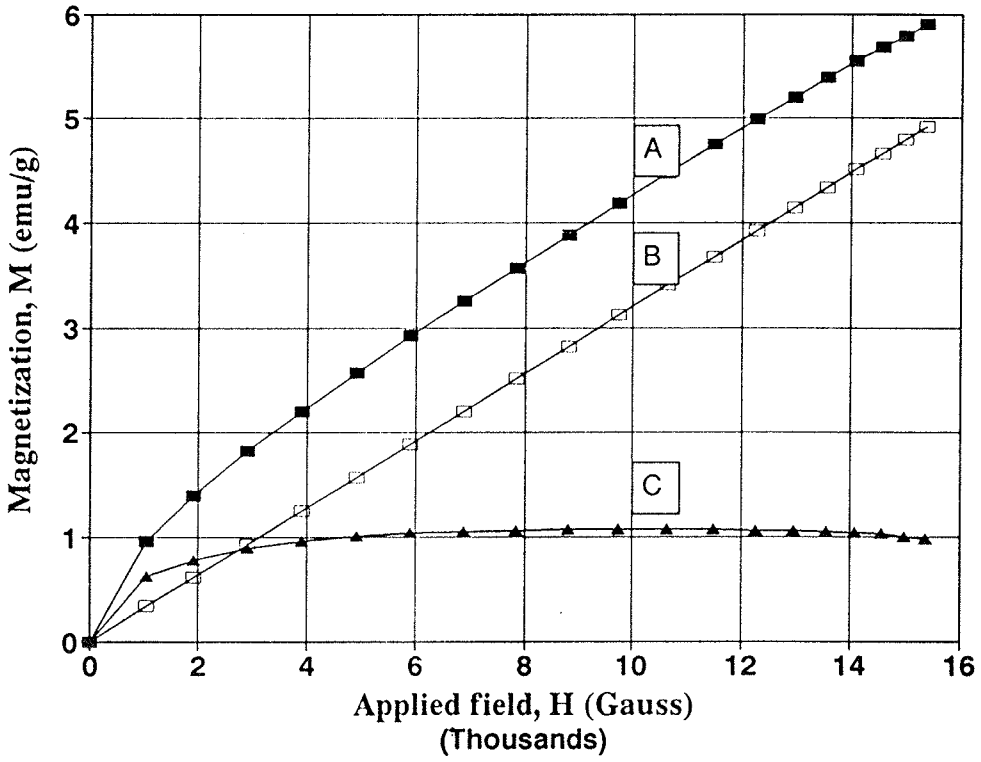

Fig. 6: *Magnetization as a function of applied field of as cast Sm-Fe-Ta alloy with 5 at.% of Ta measured at 550 K. Shown curves represents A) measured magnetization of the sample, B) paramagnetic contribution, C) free iron contribution.*

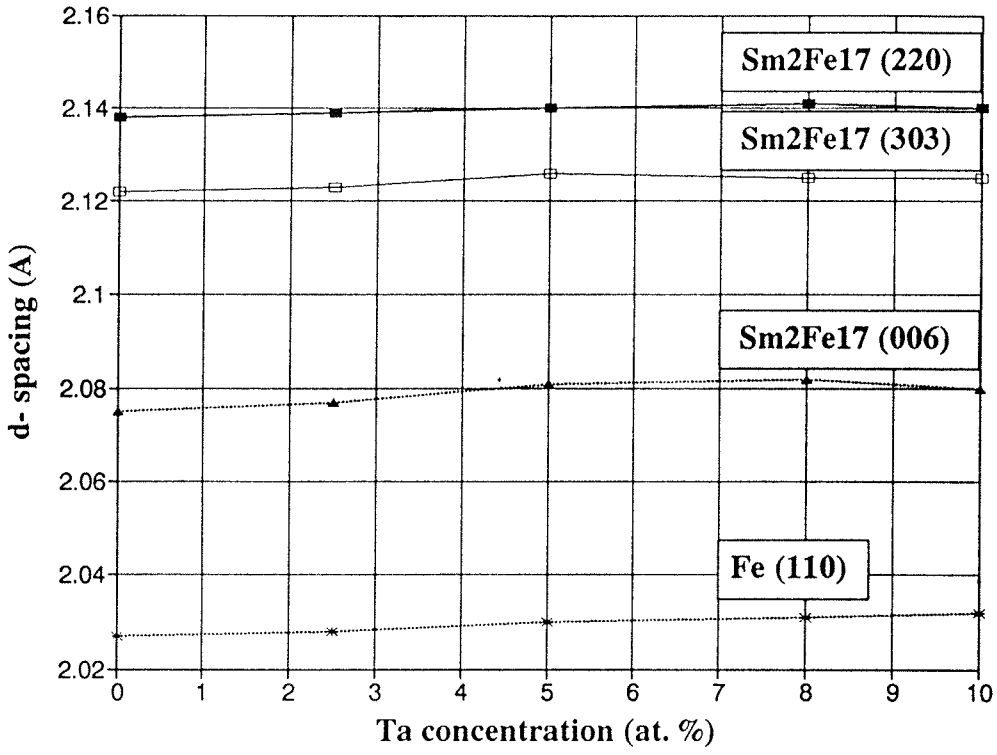

Fig. 7: *Enhancement of the d-spacings for characteristic reflections as a function of Ta concentration for Sm_2Fe_{17} phase and iron.*

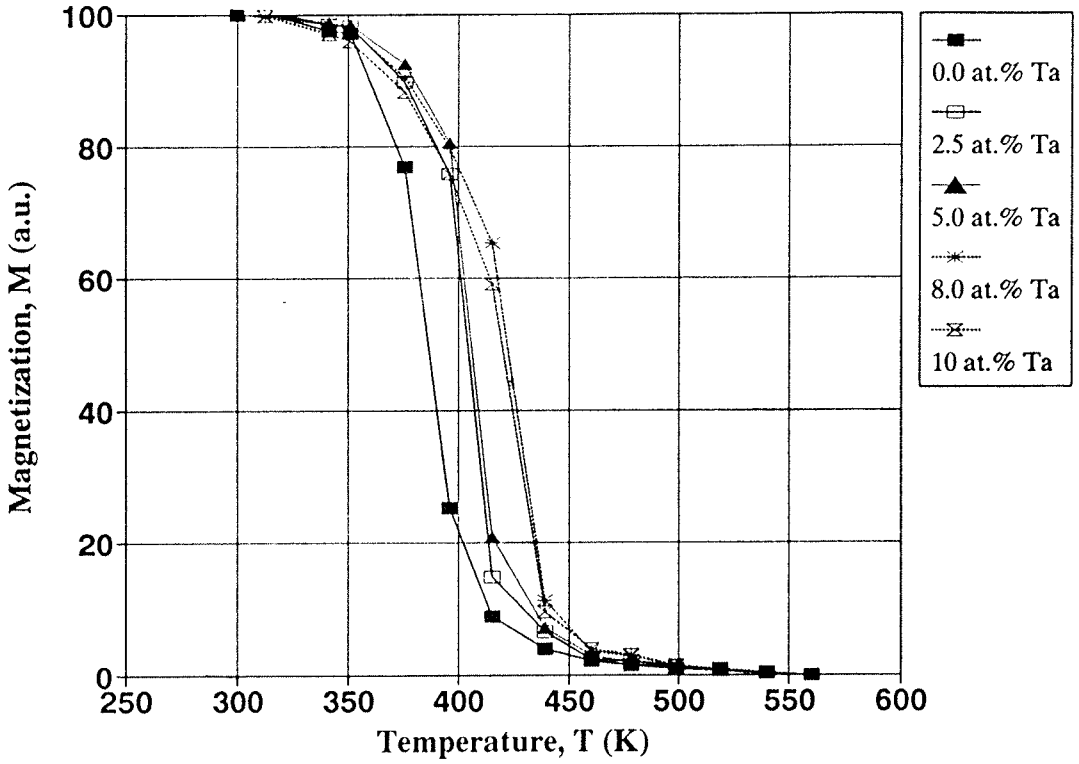

Fig. 8: Thermomagnetic curves normalized with respect to Sm_2Fe_{17} phase for Sm-Fe-Ta annealed alloys with different Ta content.

Quantification of the elemental analysis showed that Sm-rich phase in the sample is not purely stoichiometric $SmFe_2$ phase.

It has to be noted from Table 1 that $TaFe_2$ phase should be attributed to nearly stoichiometric Ta_3Fe_7 phase. Deviation from the stoichiometry of $TaFe_2$ originates from the homogeneity range of about 28 - 36 at % Ta which is consistent with the Fe-Ta phase diagram (7). It should also be noted from Table 1, that Fe is not pure iron, but solid solution of Ta in Fe which is also in good agreement with Fe-Ta phase diagram (7).

To confirm the solid solubility determined by quantitative electron probe microanalysis X-ray diffraction was used for measuring the changes of lattice spacings as a function of Ta concentration. The shift of the strongest diffraction lines ((220), (303) and (006) for Sm_2Fe_{17} phase and (110) for Fe) was measured to study the lattice expansion due to Ta solid solubility in the phases.

It is evident from Fig. 7 that the largest expansion appeared at 5 at % of Ta for the Sm_2Fe_{17} phase. However, it has to be noted, that maximum shift of d spacings is not uniform for all three reflections which may indicate some anisotropic deformation of the Sm_2Fe_{17} unit cell due to possible preferential substitution of the Ta into Fe sites.

Also it should be noted from Fig. 7 that there is some solid solubility of Ta in the Fe as well, which resulted in the shift of the d spacing corresponding to the (110) reflection.

Since the volume expansion of the unit cell in the Rare Earth Transition Metal systems usually results in the change of the Curie temperature thermomagnetic analysis was applied to study the effect of Ta concentration on the Curie temperature.

The thermomagnetic scans of the samples with tantalum concentration from 0 to 10 at %, normalised with respect to the Sm_2Fe_{17} phase (Fig. 8) showed increase of the Curie temperature of the Sm_2Fe_{17} phase by about 40 K. This enhancement is most likely attributable to changes of the Fe-Fe molecular field coefficient.

IV. CONCLUSIONS

We have described a process by which Sm_2Fe_{17} phase nearly free of iron dendrites or iron precipitates in as cast

state may be obtained via tantalum addition which replaces free iron in nominal composition. Microstructure of as cast alloy with 5 at.% of Ta consists therefore of Sm_2Fe_{17} and $TaFe_2$ paramagnetic phase. The overall remaining free iron content in the cast ingots was shown to be less than 0.5 wt.%.

It was also shown that in $Sm_2Fe_{17-x}Ta_x$ ($0< x < 2$) exist some solid solubility of tantalum in Sm_2Fe_{17} phase and in free iron. The maximum Ta concentration in the Sm_2Fe_{17} phase determined by means of electron probe microanalysis is 2.31 at % of Ta and for free iron is 0.65 at % of Ta. The solid solubility of Ta in Sm_2Fe_{17} phase gives rise to volume expansion of Sm_2Fe_{17} unit cell which was confirmed with XRD measurements of the d-spacing shift as a function of Ta concentration. This resulted in increase of the Curie temperature of the Sm_2Fe_{17} phase which was determined to be about 40 K by means of thermomagnetic analysis.

ACKNOWLEDGMENT

This work was financially supported by the Ministry of Science and Technology of Slovenia and by the British Council, UK.

REFERENCES

1. J. M.D. Coey, H. Sun, J. Magn. Magn. Mater., 87, (1990), L251.

2. J. M. D. Coey, H. Sun, D. P. F. Hurley, J. Magn. Magn. Mater., 101, (1991), 310.

3. K. H. J. Buschow, J. Less-Common Met., 25, (1971), 131.

4. A. E. Platts, I. R. Harris, J. M. D. Coey, J. Alloys and Compounds, 185, (1992), 251.

5. T. Massalski, Binary Alloy Phase Diagrams, ASM Int., Materials Park, Ohio, 1990.

6. K. Ikeda, T. Nakamichi, J. Phys. Soc. Jap., 39, (1975), 963.

7. O. Kubaschewski, Iron-Binary Phase Diagrams, Springer, Berlin, 1982. 8. T. Nakamichi, J. Phys. Soc. Japan, 25 (1968), 1189.

9. B. Reinsch, B. Grieb, E. Th. Henig, G. Petzow, IEEE Trans. Magn., in press.

10. L. Yi et all, Proc. 12th International Workshop on Rare-Earth Magnets and their Applications, Canberra, July 1992, 360.

11. K. Honda, Ann. Physik, 32, (1910), 1027.

12. M. Owen, Ann. Physik, 37, (1912), 657.

13. W. L. Liu, Y. L. Liang, L. Peeters, B. M. Ma, C. O. Bounds, same Ref. as 10, p. 168.

14. O. Kubaschewski, Iron-Binary Phase Diagrams, Springer Verlag, Berlin/Heidelberg, 1982.

Prispelo (Arrived): 05.11.93 *Sprejeto (Accepted): 23.2.94*

mgr. Boris Saje, dipl. ing. met.
Iskra Magneti, Stegne 37, Ljubljana
(MR na Institutu Jožef Stefan)
dr. Spomenka Kobe Beseničar, dipl. ing. kem.
Inštitut Jožef Stefan, Jamova 39, Ljubljana
tel: + 386 (0)61 1259 199
fax: + 386 (0)61 1261 026

CHARACTERISATION OF OUTGASSING CONTACT MATERIALS FOR MINIATURE RELAYS

L. Koller, M. Bizjak* and S. Spruk
Institute for Electronics and Vacuum Technology Ljubljana, Slovenia
* Iskra STIREL, Ljubljana, SLovenia

Keywords: miniature relays, electromagnetic relays, hermetical relays, component parts, vacuum outgassing, contact properties, Au electroplating, contact resistance, profesional electronics, testing, experimental results, AES, Auger electron spectroscopy

Abstract: Systematic investigations of vacuum outgassing for hermetic relays with AgCdO/AGPHOR and PdAg30 Au electroplated contacts were done. The experimental vacuum system constructed and built at our institute was additionally equipped with quadrupole mass spectrometer for residual gas analysis. Prior to the final encapsulation the relays were baked at the constant temperature of 125°C and outgassed in vacuum $1x10^{-5}$ mbar for several hours. The residual atmosphere was analysed every hour; in residual gas mixture, hydrogen, carbon monoxide, carbon dioxide, water vapour and remanents of cleaning chemical agents (ethanol, trichlorethylene) and hydrocarbons were found. Residual gas analysis showed that the concentration of impurity gases depends on materials and their treatments in different technological phases.

Karakterizacija razplinjenega kontaktnega materiala za miniaturne releje

Ključne besede: releji miniaturni, releji elektromagnetni, releji hermetični, deli sestavni, razplinjevanje vakuumsko, lastnosti kontaktov, pozlatitev elektrokemijska, upornost kontaktna, elektronika profesionalna, preskušanje, rezultati eksperimentalni, AES Auger spektroskopija elektronska

Povzetek: Sistematično smo raziskovali hermetične releje z AgCdO (AGPHOR lot folija) in PdAg30 elektrokemijsko pozlačenimi kontakti. Eksperimentalni vakuumski sistem, ki smo ga uporabljali, je bil konstruiran in narejen na našem inštitutu. Dodatno smo ga opremili s kvadrupolnim masnim spektrometrom za analizo preostale atmosfere v relejih. Pred dokončno inkapsulacijo smo preiskovane releje razplinjevali nekaj ur pri konstantni temperaturi 125°C v vakuumu $1x10^{-5}$ mbar. Vsako uro smo analizirali atmosfero v relejih. V izmerjeni mešanici plinov smo odkrili vodik, ogljikov monoksid, ogljikov dioksid, vodno paro, ostanke kemijskih čistil (etanola in trikloretilena) in klorovodike. Analiza je pokazala, da je koncentracija plinskih nečistoč odvisna od materialov samih pa tudi od njihove obdelave v različnih tehnoloških postopkih.

1. INTRODUCTION

Contamination film formed on the surface of electric contacts is one of the most serious causes of failure of hermetic relays. It deteriorates the contact resistance and device reliability. The most common types of contamination films are oxides and other corrosion products particles, layers formed by thermal diffusion processes, debris produced by mechanical wear and fretting, further evaporation outgassing, and condensation on contact surfaces of volatiles from isolation materials and those originating from manufacturing processes (1-9). Systematic investigations of vacuum outgassing of hermetic relays are done. The experimental vacuum setup was designed and assembled at Institute for Electronics and Vacuum Technique, Ljubljana. It has been additionally equipped with quadrupole mass spectrometer for residual gas analysis.

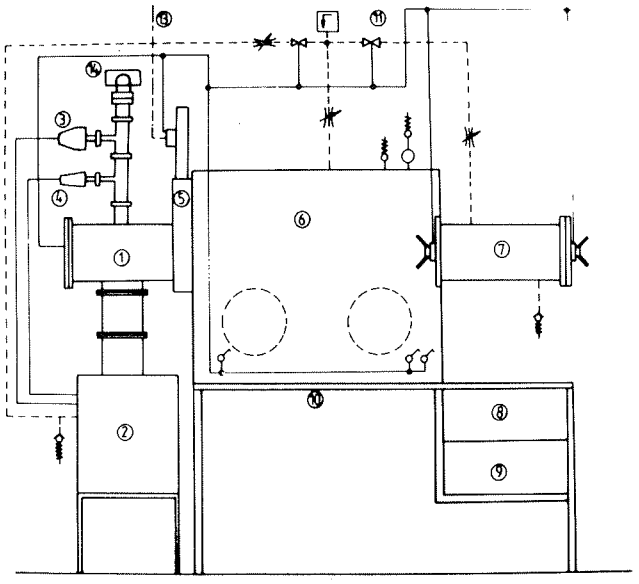

Fig. 1a: Experimental vacuum system (scheme) for outgassing process for hermetic relays: 1-vacuum chamber, 2-vacuum system, 3-PNG head, 5-mass spectrometer, 6-plate valve, 7-N_2 chamber for final hermetic relays incapsulation

2. EXPERIMENTAL

The experimental set up, designed and assembled specifically for vacuum outgassing of hermetic relays is shown in Fig. 1. The vacuum system consists of rotary

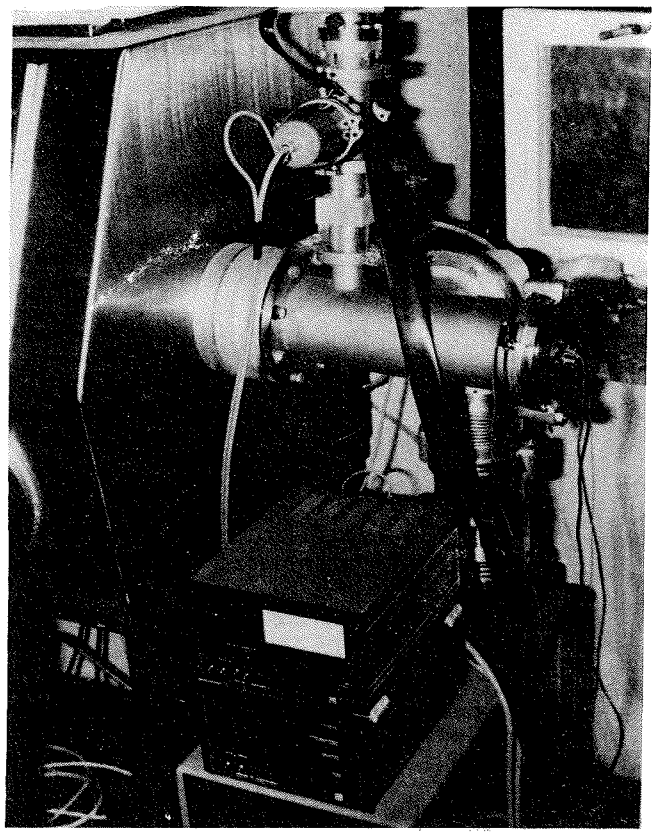

Fig. 1b: Experimental vacuum system (photograph)

vane pump and turbomolecular pump enabling to attain a vacuum of at least $1x10^{-6}$ mbar. The vacuum chamber which can be baked up to 300°C is equipped with a resistive heater. A thermocouple Fe-CuNi, 0.5 mm in diameter, is in thermal contact with one of the outgassed relays in the middle of the vacuum chamber. For residual gas analysis the quadrupole mass spectrometer Leisk 1000 M with AMU 2-100 has been used. Prior to the final hermetic incapsulation the relays are baked at constant temperature of 125°C in a vacuum of $1x10^{-5}$ mbar for several hours. The residual atmosphere has been analysed every hour.

3. RESULTS AND DISCUSSION

The first analysis of residual atmosphere was made in an empty and unbaked stainless steel chamber after a few days of continuous pumping. The base pressure in chamber was $2x10^{-6}$ mbar. Mass spectrum in Fig. 2 shows the outgassing products in the empty chamber. This spectrum is typical for a standard vacuum system with very small air leaks and no unusual gas sources; it shows that the most prominent outgassing product in the empty vacuum chamber is a mixture of water vapour, CO and N_2; small quantities of hydrogen and some hydrocarbons are also released in the empty chamber at this temperature as expected.

The spectrum in Fig. 3 was obtained after one hour's baking of the empty chamber at 125°C. This spectrum

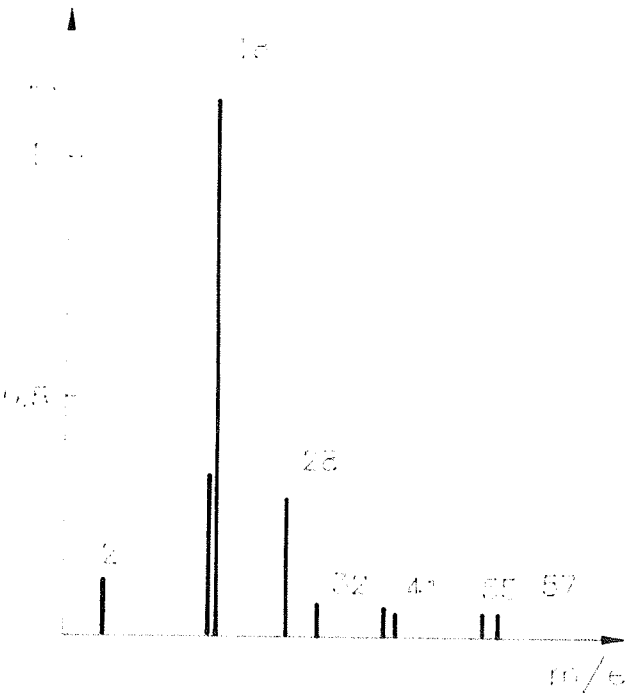

Fig. 2: Mass spectrum showing the outgassing products of the empty chamber

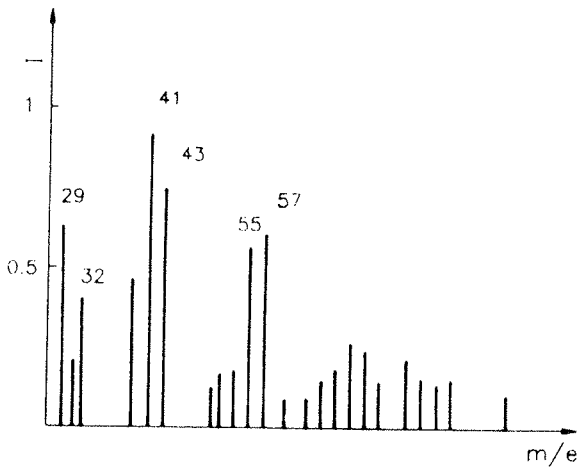

Fig. 3: Mass spectrum of the outgassing products of the empty chamber after one hour baking

shows the main outgassing product consisting of water vapour, CO and N_2 and unusual peaks typical for ethanol, trichlorethylene (mass 31, 45, 60) supposedly remanents from cleaning processes; some hydrocarbons are also released.

The spectrum in Fig. 4 was obtained after 24 hours baking of the empty chamber at the same temperature. Total pressure attained was $1.3x10^{-6}$ mbar. This spectrum is similar to that shown in Fig. 2, which shows the empty chamber without baking.

Finally, the mass spectrum represented in Fig. 5 shows the outgassing products of miniature relays baked at 125°C. The system pressure in this case was $1x10^{-5}$ mbar. The spectrum was registered 30 minutes after bringing the miniature relays up to the temperature. In the spectrum considerable partial pressures of ethanol,

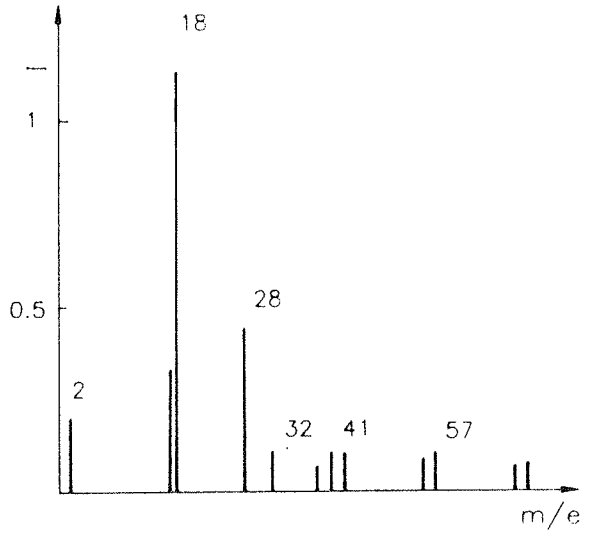

Fig. 4: Mass spectrum of the outgassing products of the empty chamber after 24 hours baking

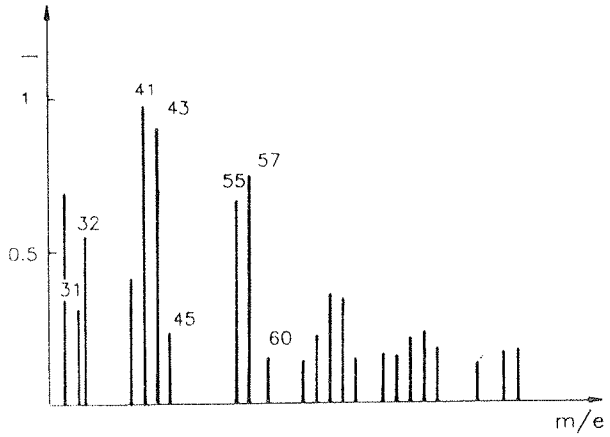

Fig. 5: Mass spectrum of the outgassing products of miniature relays (contacts PdAg30/Au) at 125°C in a vacuum of 1x10^{-5} mbar after 30 minutes

hydrocarbons, oxygen and CO_2 can be seen. Other spectra indicate also appreciable concentrations of water vapour, CO and N_2.

Residual atmosphere was analysed every hour. After 24 hours of relay outgassing process the spectrum in Fig. 6 was registered. The background system pressure was 3x10^{-6} mbar. A comparison of this spectrum with that shown in Fig. 4 for the empty vacuum chamber at 125°C, reveals that both spectra are quite similar, indicating that the baked relays are ready for final incapsulation. The most useful and often the simplest method for detecting contamination on an electric contact surface is to determine its contact resistance.

Contact resistance of vacuum outgassed relays with PdAg30/Au contacts was measured immediately after hermetic incapsulation and later in constant time intervals of 7, 14, 21 and 42 days. For a comparison the contact resistance of nonoutgassed relays was measured. The results are collected in Table 1. Initial contact resistances of nonoutgassed and outgassed relays were very similar. However, the difference in

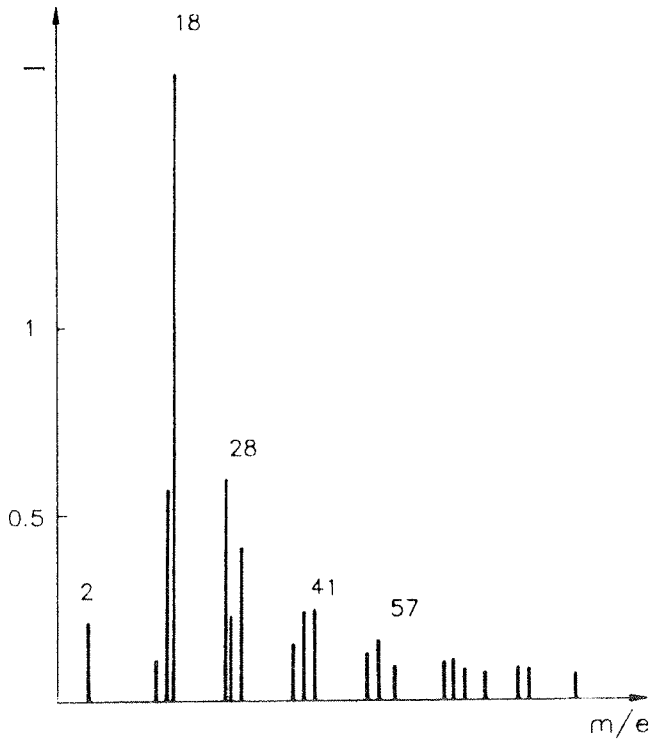

Fig. 6: Mass spectrum registered after 24 hours of the relay (contacts PdAg30/Au) outgassing process

Sample no. nonoutgassed relays	1	2	3	4	5	6	7	8	9	10
R (mΩ) after incapsulation	65	70	55	60	70	55	65	70	60	55
R (mΩ) after 7 days	120	130	110	140	100	90	120	145	100	90
R (mΩ) after 14 days	205	180	175	250	200	150	170	220	205	195
R (mΩ) after 21 days	230	190	175	255	205	160	170	230	210	205
R (mΩ) after 42 days	250	300	210	280	250	210	180	245	230	220

Sample no. outgassed relays	11	12	13	14	15	16	17	18	19	20
R (mΩ) after incapsulation	70	60	55	75	70	60	60	50	60	65
R (mΩ) after 7 days	70	60	55	80	70	60	60	50	60	65
R (mΩ) after 14 days	70	60	55	85	70	60	65	50	60	65
R (mΩ) after 21 days	70	60	55	85	70	60	65	50	60	65
R (mΩ) after 42 days	70	60	60	85	70	60	65	50	65	65

Table 1: Contact resistance of nonoutgassed and vacuum outgassed relays (contacts PdAg30/Au) measured immediately after hermetic incapsulation and in constant time intervals after 7, 14, 21 and 42 days

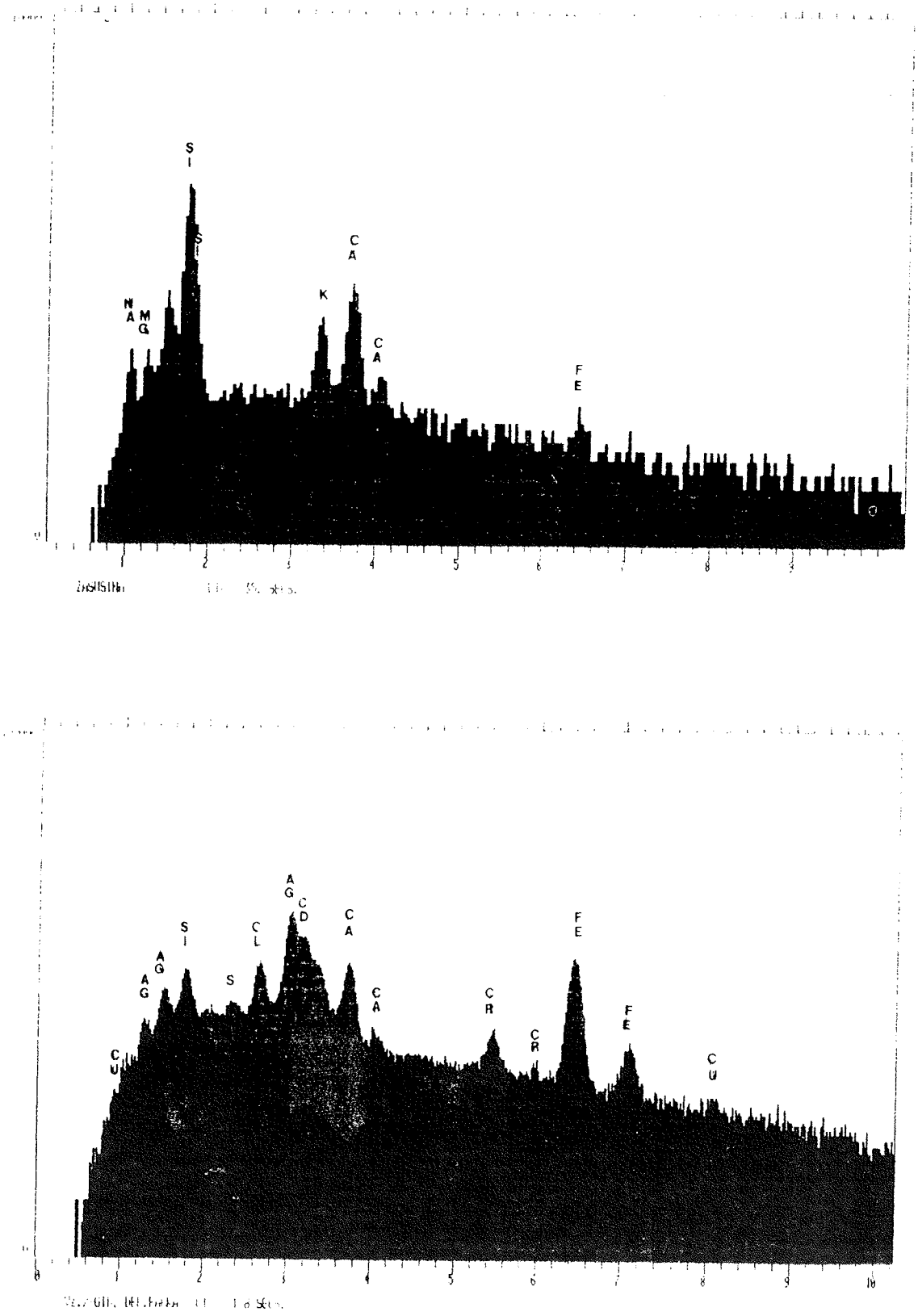

Fig. 7a: *Mass spectra of the outgassing products of contaminated miniature relay (contacts AgCdO/AGPHOR) at 125°C in a vacuum of 1x10^{-5} mbar after 24 hours*

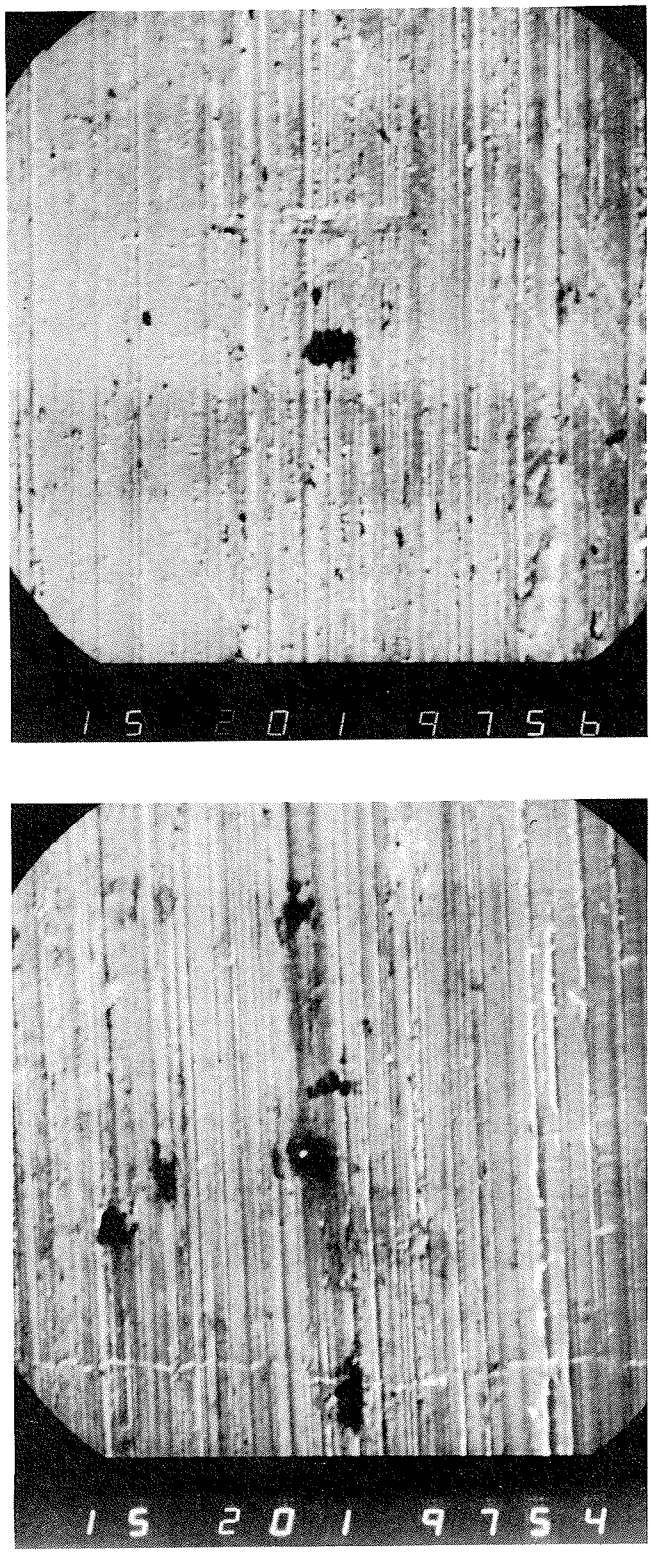

Fig. 7b: Pictures of the contaminated contact after outgassing

contact resistance was as early as after 7 days enormous. In relays which were not treated with vacuum outgassing contact resistance increased higher than it is qualified in current standards for miniature hermetic relays (0.1 ohm max).

When contact resistance of miniature relays with AgCdO contacts was measured after outgassing considerable increase was noticed. Therefore some relays were opened and their contacts analysed (Fig. 7a and 7b). Dark spots found on the contacts probably caused the increase of contact resistance. It seems that the relays mentioned were not sufficiently outgassed. Detailed examination of the phenomenon is planed in the near future.

4. CONCLUSIONS

The experimental vacuum system set up was designed and assembled specifically for vacuum outgassing of hermetic miniature relays. Systematic investigation of vacuum outgassing of hermetic relays were done. Residual gas analysis shows that outgassing products consist of remanents of cleaning chemical agents (ethanol, trichlorethylene), a mixture of water vapour, CO, N_2 and some hydrocarbons originating from rotary pump oil.

The results of experiments described above show clearly that the outgassing process is indispensable and should be included in the technology for producing of reliable hermetic relays qualified to MIL-R-3906 and MIL-R- 5757 standards.

REFERENCES

1. F.H. Reid and W. Goldie, Gold als Oberfläche, Eugen G. Lenze, Saulgau (Wuert) (1982).

2. S. Sinharoy, W.J. Lange, C.B. Friedhoff, J. Vac. Sci. Technol. A8, 2 (1990) 930.

3. A.G. Zalužin, Atomnaja Energ. 47 (1979) 113.

4. H.D. Fischer, Analysis of Volatile Contaminants in Microcircuits, Solid State Technology 1978.

5. R. Holm, Electric Contacts Handbook, Springer, New York 1967.

6. R.G. Alefeld, J. Folke, Vodorod v metallah, Mir, Moskva 1981.

7. M. Wutz, H. Adam, W. Walcher, Theorie und Praxis der Vakuumtechnik, Friedr. Vieweg und Sohn, Braunschweig, Wiesbaden 1982.

8. J.H. Leck, Pressure Measurements in Vacuum Systems, Chapman and Hall, London 1964.

9. N. Yushimura, T. Sato, S. Adachi, T. Kanezawa, J. Vac. Sci. Technol. A8, 2 (1990) 924.

Prispelo (Arrived): 18.01.94 *Sprejeto (Accepted): 16.02.94*

Lidija Koller
Inštitut za elektroniko in vakuumsko tehniko,
Teslova 30
Ljubljana, Slovenija
Martin Bizjak
ISKRA STIREL, Savska cesta 2
Ljubljana, Slovenija
Sonja Spruk
Inštitut za elektroniko in vakuumsko tehniko,
Teslova 30
Ljubljana, Slovenija
tel. 00 386-61-123 13 41

UDK 621.3:(53+54+621+66), ISSN0352-9045 Informacije MIDEM 24(1994)1, Ljubljana

COMPARISON OF DIFFERENT MOSFET THRESHOLD VOLTAGE DEFINITIONS*

Prepared from the paper presented on the Symposium MEET '93 (MIPRO), Opatija, May 1993.

Željko Butković
Faculty for Electrical Engeneering, Zagreb, Croatia

Key words: semiconductors, MOSFET transistors, threshold voltage, theoretical analysis, Poisson's equation, strong inversion, weak inversion, response characteristics

Abstract: Theoretically MOSFET threshold voltage is defined with the surface inversion and can be calculated using the MOS structure technological data. Device current-voltage characteristics are used to define threshold voltage in practice. In this paper both definitions are described and the connection between them has been determined in the example of real MOS structure.

Usporedba različitih definicija napona praga MOSFET-a

Pripremljeno prema referatu prezentiranom na Savjetovanju MEET '93 (MIPRO), Opatija, Svibanj 1993.

Ključne besede: polprevodniki, MOSFET transistorji, napetost pragovna, analiza teoretična, Poisson enačba, inverzija močna, inverzija šibka, karakteristike odzivne

Sažetak: Teorijski se napon praga MOSFET-a definira inverzijom površine silicija i može se računati iz poznatih tehnoloških podataka MOS strukture. U praksi se napon praga određuje iz strujno-naponskih karakteristika elementa. U radu su opisane obje definicije napona praga i određena je njihova veza na primjeru realne MOS strukture.

1. INTRODUCTION

Electrical characteristics of integrated circuits can be designed by fitting the individual electronic devices' parameters. One of the most important parameters, in MOS integrated circuits' design, is MOSFET threshold voltage U_{GS0}. Theoretical analysis of MOS structure determines the threshold voltage U^t_{GS0}. As the operation of integrated circuits is defined with the threshold voltage U^c_{GS0} obtained from the MOSFET current-voltage characteristics, connection of this parameter with the value of theoretically calculated threshold voltage U^t_{GS0} is needed. Both threshold voltage definitions are compared in this paper in the example of n-channel MOSFET.

2. THEORETICAL CALCULATION OF THRESHOLD VOLTAGE

Figure 1 shows the cross-section of the n-channel MOSFET. The device substrate (B) is a p-type silicon. The MOS structure, between two n^+ regions of source (S) and drain (D), consists of silicon substrate, thin silicon oxide layer (SiO_2) and the gate (G) material. For MOSFET operation, silicon surface under the oxide layer must be inverted and n-channel between source and drain must be formed. This is obtained electrically, by connection the voltage U_{GS} between gate and source. The voltage U_{GS} needed for surface inversion is the threshold voltage U_{GS0}.

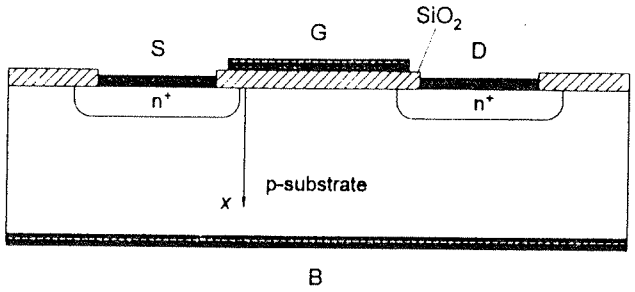

Fig. 1: Cross-section of n-channel MOSFET

Before channel formation, voltage U_{GS} decreases majority concentration of holes on the substrate surface,

* This paper is part of the scientific project "2-07-266 Electronics and Microelectronics" supported by "Ministry for Science" of the Republic of Croatia.

producing the thin depletion layer under the oxide. Potential distribution in the depletion layer, along the x coordinate perpendicular to the substrate surface (Fig. 1), determines the Poisson's equation /1/

$$\frac{d^2u}{dx^2} = \frac{q}{\varepsilon_{Si} \cdot U_T}(n - p - N), \quad (1)$$

where u is the normalized electrostatic potential ψ, $u = \psi/U_T$, n, p and N are electron, hole and net doping concentrations, q is the elementary charge, ε_{Si} is the silicon permittivity and U_T is the thermal voltage. If Fermi potential is chosen as reference potential, $\varphi = 0$, then in the case of low injection the majority hole concentration is

$$p = n_i \cdot exp\ (-u). \quad (2)$$

The minority electron concentration n is changed with the external potential /2/

$$n = n_i \cdot exp\ (u + u_V). \quad (3)$$

At the source end of the channel, normalized external potential u_V is the result of the voltage U_{BS} applied between bulk and source, $u_V = U_{BS}/U_T$. In the previous equations n_i is the intrinsic carrier concentration.

Generally, net doping concentration N is the difference between donor N_D and acceptor N_A concentration and corresponds to the difference between equilibrium carrier concentrations of electrons n_b and holes p_b in the bulk, far from the surface

$$N = N_D - N_A = n_b - p_b = n_i \cdot exp(u_b) - n_i \cdot exp\ (-u_b). \quad (4)$$

The doping concentration in the substrate of the n-channel MOSFET with homogeneously doped channel is acceptor concentration $N = -N_{AB}$, and this concentration is equal to the bulk majority hole concentration p_b. According to (4), normalized bulk potential is

$$u_b = -\ln\left(\frac{N_{AB}}{n_i}\right). \quad (5)$$

Depletion layer surface charge per unit area Q_{SD} is defined with Gauss's law

$$Q_{SD} = -\varepsilon_{Si} \cdot U_T \left(\frac{du}{dx}\right)\Big|_s, \quad (6)$$

where index s designates the silicon surface. Integration of Poisson's equation (1) yields

$$Q_{SD} = -\sqrt{2 \cdot q \cdot \varepsilon_{Si} \cdot U_T \cdot n_i} \cdot \left[\exp\left(u_s + u_v\right) - \exp\left(u_b + u_v\right) - \exp\left(-u_s\right) - \exp\left(-u_b\right) - 2 \cdot \left(u_s - u_b\right) \cdot sh\left(u_b\right)\right]^{1/2}. \quad (7)$$

The voltage U_{GS} is the result of potential distributions in the MOS structure,

$$U_{GS} = -\frac{Q_{SS} + Q_{SD}}{C'_{ox}} + \psi_s + \Delta\psi + U_{BS}. \quad (8)$$

In (8) Q_{SS} is the fixed surface charge per unit area in the oxide layer, and ψ_s is the surface potential, $\psi_s = u_s \cdot U_T$. The term $\Delta\psi = \phi_{MS} - \psi_b$ includes the work-function difference between gate and bulk ϕ_{MS} and the bulk potential $\psi_b = u_b \cdot U_T$. C'_{ox} is the oxide capacitance per unit area, $C'_{ox} = \varepsilon_{ox} / t_{ox}$, where ε_{ox} is the permittivity of SiO_2 and t_{ox} is the oxide layer thickness.

Theoretically, the threshold voltage U'_{GS0} is defined as the voltage U_{GS} that produces surface minority electron concentration equal to the bulk majority hole concentration, $n_s = p_b$. That is the case of strong inversion. The values of surface potentials $u_s = u_{s0} = -u_b - u_V$ and $\psi_s = \psi_{s0} = -\psi_b - U_{BS}$ included in (7) and (8), define the surface charge Q_{SD0} and the threshold voltage U'_{GS0}.

Surface inversion begins when surface minority electron concentration reaches the intrinsic carrier concentration, $n_s = n_i$. This case of weak inversion determines the surface potentials and $u_s = u_{si} = -u_V$, and $\psi_s = \psi_{si} = -U_{BS}$, corresponding charge Q_{SDi} and voltage U'_{GSi} are obtained from (7) and (8).

3. THE THRESHOLD VOLTAGE FROM CURRENT-VOLTAGE CHARACTERISTICS

In practice, the threshold voltage U^c_{GS0} is determined from the MOSFET current-voltage characteristic. The voltage U^c_{GS0} is defined as the voltage U_{GS} that breaks the flow of drain current I_D and can be read easiest from the MOSFET transfer characteristic $I_D = f(U_{GS})|_{U_{DS}}$. The problem is that the current I_D flow break is the continuous change and does not appear sharp at voltage $U_{GS} = U_{GS0}$. Namely, in subthreshold region, for voltages $U_{GS} < U_{GS0}$, there is a finite current I_D flow between source and drain that decreases exponentially with the voltage U_{GS}. Because of that the threshold voltage U^c_{GS0} is determined graphically, from extrapolation of the transfer characteristic and the coordinate with $I_D = 0$ /3/.

If the MOSFET operates in linear region, for voltages $U_{DS} \leq U_{GS} - U_{GS0}$, the drain current is

$$I_D = K \cdot \left(U_{GS} - U_{GS0} - \frac{U_{DS}}{2}\right) \cdot U_{DS}, \quad (9)$$

where K is the proportionality constant. At small voltages U_{DS}, the term $U_{DS}/2$ can be neglected. The current I_D changes linearly with voltage U_{GS}, and the transfer characteristic $I_D = f\ (U_{GS})|_{U_{DS}}$ is the line.

In saturation region, for voltages $U_{DS} \leq U_{GS} - U_{GS0}$, the current is

$$I_D = \frac{K}{2} \cdot \left(U_{GS} - U_{GS0}\right)^2, \quad (10)$$

and the transfer characteristic $I_D = f(U_{GS})|_{U_{DS}}$ is the parabola.

4. THE RESULTS OF CALCULATIONS

The comparison of two different definitions of the threshold voltage has been performed on the example of n-channel MOSFET. The homogeneously doped MOS structure, with the substrate acceptor concentration $N_{AB} = 10^{15}$ cm^{-3} and the oxide thickness $t_{ox} = 0{,}1$ μm, has been chosen. The oxide layer charge $Q_{SS} = 5 \cdot 10^{10}$ cm^{-2} and n-type oxide polysilicon layer have been supposed. Besides for those parameters, the threshold voltage has been calculated as the function of the concentration N_{AB}, the oxide thickness t_{ox}, and the bulk voltage U_{BS}.

The two values of threshold voltage have been determined with the theoretical approach: U^t_{GSO} for strong inversion and U^t_{GSi} for weak inversion. Current-voltage characteristics have been calculated numerically, using the MINIMOS device simulator /4/. The MOSFET with described MOS structure, and with the sufficiently large channel dimensions (the length $L = 10$ μm and the width $W = 10$ μm) has been analyzed to avoid short and narrow channel effects. The definition of the threshold voltage U^c_{GSO}, for the chosen parameters of MOS structure, is represented in Fig. 2a and 2b. Fig. 2a shows the transfer characteristics in linear region, calculated for small voltage $U_{DS} = 50$ mV. The transfer characteristic in saturation region (Fig. 2b) has been determined for voltage $U_{DS} = 5$ V. In order to maintain the linear relationship, as in the linear region, the square root of the current I_D, versus the voltage U_{GS}, has been drawn in Fig. 2b. In both Figures the straight line has been pulled through the MINIMOS data minimizing the root mean square error. The threshold voltage U^c_{GSO} has been determined by extrapolation of transfer characteristics to the current value $I_D = 0$.

The results of threshold voltage calculations, as the function of several technological and electrical quantities, are represented in Figures 3-5. According to Figure 3, the threshold voltage U_{GSO} increases with the substrate concentration N_{AB}. In the bulk the equilibrium majority hole concentration p_b increases and the equilibrium minority electron concentration n_b decreases with increase of concentration N_{AB}, so higher voltage U_{GS} is needed to equalize the surface electron concentration n_s with the hole concentration p_b. The enlargement of the oxide layer thickness t_{ox} increases, according to Figure 4, the threshold voltage U_{GSO}. The thicker oxide reduces the effectiveness of the gate electrode. The results of threshold voltage change with the bulk voltage U_{BS} are shown in Figure 5. As the higher voltage U_{BS} decreases the electron concentration n_b, the higher voltage U_{GS} is needed for channel inversion.

In all three Figures 3-5 the results of theoretical calculations U^t_{GSO} and U^t_{GSi} are compared with the voltages U^c_{GSO} obtained from current-voltage characteristics. As the smaller voltage U_{GS} is needed to increase the sur-

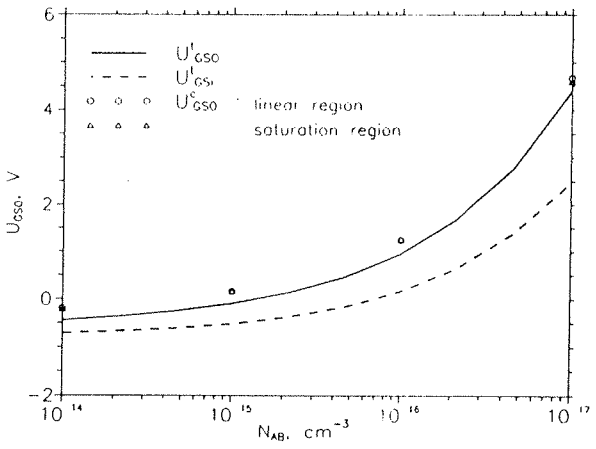

Fig. 3: Threshold voltage U_{GSO} versus bulk acceptor concentration N_{AB}

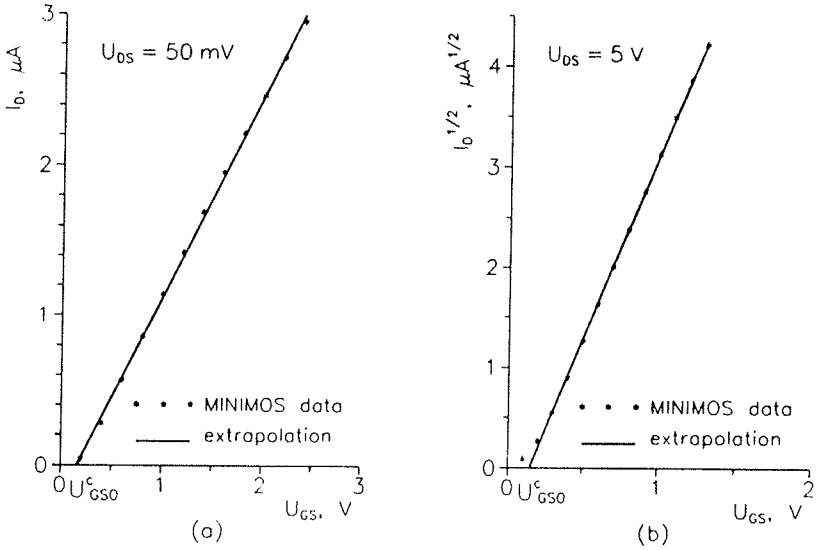

Fig. 2: MOSFET transfer characteristics: (a) in linear region, (b) in saturation region. MOS parameters are: $N_{AB} = 10^{15}$ cm^{-3}, $t_{ox} = 0{,}1$ μm and $U_{BS} = 0$V.

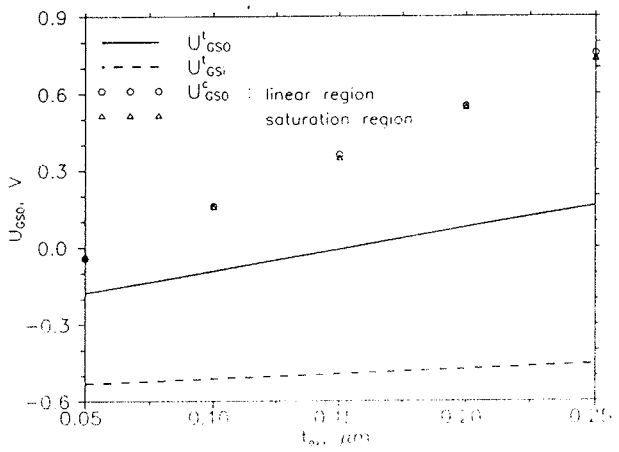

Fig. 4: Threshold voltage U_{GSO} versus oxide thickness t_{ox}

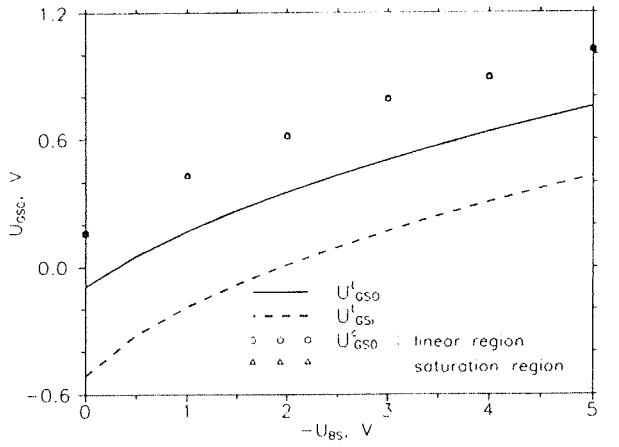

Fig. 5: Threshold voltage U_{GSO} versus bulk voltage U_{BS}

face electron concentration n_s to the value of intrinsic concentration n_i, than to the equilibrium hole concentration p_b, the theoretical threshold voltages U^t_{GSO} in weak inversion are lower than the threshold voltages U^t_{GSO} in strong inversion. The voltages U^c_{GSO} agree mutually regardless as they are obtained from transfer characteristics in linear or in saturation region. Also the voltages U^c_{GSO} show the better agreement with the values of the theoretical voltages U^t_{GSO} in strong inversion.

In Fig. 3 and Fig. 5 the voltages U^c_{GSO} are higher than the voltages U^t_{GSO} for practical the same value of 0,24 V. On the other hand, the voltage difference U^c_{GSO} - U^t_{GSO} in Figure 4 changes proportionally with the oxide thickness t_{ox}. The obtained values of voltages U^c_{GSO} can be calculated theoretically, including the correction factor

$$U^c_{GSO} = U^t_{GSO} + k \cdot t_{ox} = -\frac{Q_{SS} + Q_{SDO}}{C'_{ox}} - \\ - \psi_b + \Delta\psi + k \cdot t_{ox}, \qquad (11)$$

with the constant k = 2,4 V / μm.

5. CONCLUSION

The threshold voltage values U^t_{GSO} from theoretical analysis of MOS structure and U^c_{GSO} from current-voltage characteristics have been compared for typical example of n-channel MOSFET. The changes of threshold voltage U_{GSO} with basic technological and electrical quantities have been determined. Although the voltages U^t_{GSO} and U^c_{GSO} have been calculated for the same structure and with the application of the equal physical constants, the difference between the values U^t_{GSO} and U^c_{GSO} has been observed, and the dependence of the difference on the oxide layer thickness t_{ox} is described with the equation (11). The obtained relation is useful, because the threshold voltage can be technologically adjusted in accordance with the results. U^t_{GSO} from theoretical analysis, and the value U^c_{GSO} from current-voltage characteristics is essential for circuit application. More different examples must be analyzed to prove the generality of the equation (11).

REFERENCES

/1/ P. Biljanović: "Mikroelektronika - integrirani elektronički sklopovi", Školska knjiga, Zagreb, 1983.

/2/ S.M. Sze: "Physics of Semiconductor Devices" John Willey, New York, 1981.

/3/ P. Antognetti, G. Massobrio: "Semiconductor Device Modeling with SPICE" McGraw-Hill, New York, 1988.

/4/ S. Selberherr, A. Schötz, H. Pützl: "Two Dimensional MOS-Transistor Modeling" in: P. Antognetti, D. A. Antoniadis, R. W. Dutton, W. G. Oldham: "Process and Device Simulation for MOS-VLSI Circuits", Martinus Nijhoff, The Hague, 1983.

Prispelo (Arrived): 21.07.93 *Sprejeto (Accepted): 01.02.94*

dr. Željko Butković
University of Zagreb
Faculty of Electrical Engineering
Avenija Vukovar 39
41000 Zagreb, Croatia
tel. 00 385-41-629 924
fax. 00 385-41-629 653

UDK 621.3:(53+54+621+66), ISSN0352-9045 Informacije MIDEM 24(1994)1, Ljubljana

PARALELNI ULAZNO-IZLAZNI MEĐUSKLOP-PUI*

Pripremljeno prema referatu prezentiranom na Savjetovanju MEET'93 (MIPRO), Opatija, Svibanj 1993.

Goran Zelić, Krunoslav Martinčić, Mladen Skypala
Elektrotehnički fakultet, Zagreb, Hrvatska

Ključne riječi: polprevodniki, VLSI vezja, projektiranje vezij, celice standardne, PIO vmesniki vhodno-izhodno paralelni, PLA moduli, vodila mikroprocesorska, mikroprocesorji 8-bit, mikroprocesorji 16-bit

Sažetak: U ovom je radu opisan pristup projektiranju paralelnog ulazno-izlaznog sklopa (PUI sklop) kompatibilnog s 8 i 16 bitovnom sabirnicom mikroprocesora, koristeći modernu VLSI metodologiju projektiranja (standardne ćelije i PLA moduli). Opisan je koncept od razrade ideje do arhitekture koja je realizirana do razine maski.

Parallel Input-Output Interface-PUI

Prepared from the paper presented on the Symposium MEET'93 (MIPRO), Opatija, May 1993.

Key words: semiconductors, VLSI circuits, circuit design, standard cells, PIO parallel input-output interfaces, PLA programmable logic arrays, PLA modules, microprocessor buses, 8-bit mikroprocessors, 16-bit microprocessors

Abstract: This paper describes an approach to the design of parallel input-output interface (PUI device) compatible to 8 and 16 bit microprocessor buses using a modern VLSI design methodology (standard cells and PLA modules). Concept from idea to architecture, that is mask implemented, is described.

1. Uvod

Namjena PUI međusklopa je da olakša izgradnju različitih sklopova za upravljanje i nadzor industrijskih procesa koji su upravljani pomoću mikroprocesora. Premda za svaki mikroprocesor koji se koristi u takvim sklopovima postoji i paralelni međusklop za komunikaciju s vanjskim svijetom, povećani broj pristupa za prijenos podataka i upravljanje, mogućnost jednostavnog uklapanja na sabirnice postojećih 8 i 16 bitovnih porodica mikroprocesora (tipični predstavnici su: Intel /1/ i Motorola /2/) te ograničenje broja načina rada na šest koji se pretežno koriste u aplikacijama za industrijske potrebe, opravdava realizaciju PUI međusklopa.

Opisani međusklop ima slijedeće karakteristike: - programirljiv smjer prijenosa podataka (ulaz, odnosno izlaz) i način prijenosa (programski upravljan ili sklopovski upravljan preko upravljačkih linija);

- organizaciju perifernih linija u grupe od 8 ili 16 (ovisno o širini mikroprocesorske sabirnice, radi optimalnog iskorištenja ulazno izlazne propusnosti sustava);
- postavljanje zahtjeva za prekid (posebnom linijom zahtjeva za prijenos podataka, pojavom stanja na vanjskim linijama koje odgovaraju stanju maske koja se može programski postaviti ili bilo kakvom promjenom stanja na vanjskim linijama u odnosu na stanje maske) te
- nezavisno programiranje odvojenih pristupa.

PUI međusklop projektiran je pomoću automatiziranih topologija: standardnih ćelija tvrtke AMD u 2 μm SCMOS tehnologiji i PLA struktura.

2. Organizacija PUI međusklopa

PUI međusklop se sastoji od pet 8 bitovnih pristupa (AL, AH, BL, BH i C), upravljačke logike i internih sabirnica podataka (slika 1). U 8 bitovnoj konfiguraciji svi pristupi rade neovisno jedan o drugom i koriste samo osam nižih bitova mikroprocesorske sabirnice podataka (D0-D7). Gornjih osam bitova (D8-D15, odnosno C0-7) koristi pristup C za komunikaciju s perifernim sklopovljem. Ostala četiri pristupa imaju izvedene vlastite linije za komunikaciju (AL0-7, AH0-7, BL0-7, BH0-7). Priključenjem PUI međusklopa na 16 bitovni mikroprocesor pristup C se gubi (njegova je uloga da iskoristi osam podatkovnih linija koje se ne koriste kada je međusklop priključen na 8 bitovni mikroprocesor), a pristupi AL i AH te BL i BH se stapaju u dva 16 bitovna:

* Ovaj rad je dio znanstvenog projekta 2-07-266 Elektronika i mikroelektronika financiranog od Ministarstva znanosti Republike Hrvatske

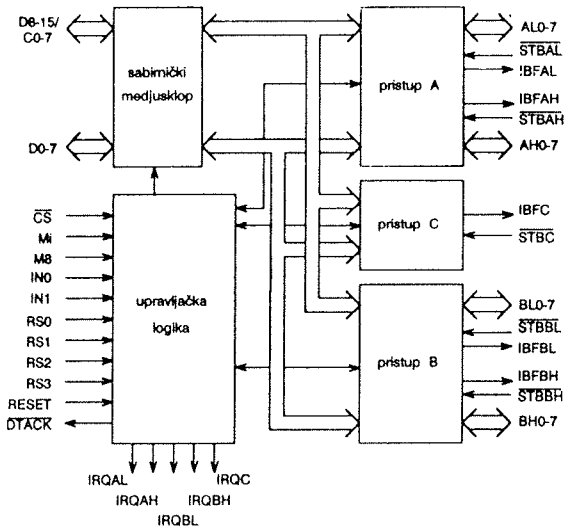

Slika 1: Blok shema PUI međusklopa.

A i B. U ovoj konfiguraciji signalne linije pristupa AL i BL (zahtjev za prekid i linije za upravljanje prijenosom podataka sa perifernog sklopa, odnosno na periferni sklop) zadržavaju svoju funkciju, dok se one vezane uz pristupe AH i BH ne koriste.

Upravljačka logika, na temelju odabranog tipa mikroprocesora s kojim komunicira PUI međusklop i stanja upravljačkih signala na vanjskoj sabirnici, generira interne signale kao što su signali čitaj, odnosno piši i aktivira pristupe na koje se ti signali odnose. Interne sabirnice podataka služe za prijenos podataka između vanjske mikroprocesorske sabirnice podataka i pojedinih pristupa. U 8 bitovnoj konfiguraciji PUI međusklop koristi četiri linije (RS0-RS3) za odabir pristupa ili upravljačke riječi, dok u 16 bitovnoj konfiguraciji koristi samo dvije (RS1-RS2). Adresni prostor 8 i 16 bitovne konfiguracije prikazan je u tablici 1, odnosno u tablici 2. Svaki pristup ima lokaciju za podatke (AL, AH, BL, BH i C, odnosno A i B) i lokaciju za upisivanje upravljačke riječi (CWAL, CWAH, CWBL, CWBH i CWC, odnosno CWA i CWB), kako bi se omogućilo neovisno programiranje pojedinih pristupa.

RS3	RS2	RS1	RS0	Lokacija
0	0	0	0	AL
0	0	0	1	AH
0	0	1	0	BL
0	0	1	1	BH
0	1	0	0	C
0	1	1	0	CWAL
0	1	1	0	CWAH
0	1	1	1	CWBL
1	0	0	0	CWBH
1	0	0	1	CWC

7 0

Tablica 1: Adresni prostor 8 bitovne konfiguracije.

Tablica 2. Adresni prostor 16 bitovne konfiguracije.

RS2	RS1	Lokacija
0	0	A
0	1	B
1	0	CWA
1	1	CWB

Upravljačka riječ koristi četiri bita (vidi tablicu 3): B3 određuje način komunikacije sa mikroprocesorom (0 programski, 1 s zahtjevom za prekid); B2 određuje da li se koriste upravljačke linije za komunikaciju s periferijom (0) ili se radi o uspoređivanju s maskom (1); B1 određuje način uspoređivanja s maskom (0 na pojavu, 1 na promjenu); B0 određuje smjer prijenosa podataka (0 ulaz, 1 izlaz).

Tablica 3. Upravljačka riječ 8 i 16 bitovne konfiguracije.

ne koristi se	B3	B2	B1	B0

15/7 0

Postoji šest načina rada koje PUI međusklop podržava i oni su dani u tablici 4. Kada se koriste načini s uspoređivanjem na masku potrebno je prvo upisati masku u željeni pristup pa tek onda promjeniti upravljačku riječ. Prilikom uključenja i reseta, svi bitovi upravljačke riječi prelaze u stanje 0 (programski upravljiv ulaz).

Tablica 4. Načini rada PUI međusklopa.

B3	B2	B1	B0	Način rada
0	X	X	0	programski upravljiv ulaz
0	X	X	1	programski upravljiv izlaz
1	0	X	0	ulaz (prekidni način rada)
1	0	X	1	izlaz (prekidni način rada)
1	1	0	X	prekid na pojavu stanja
1	1	1	X	prekid na promjenu stanja

PUI međusklop može se povezati sa četiri tipa mikroprocesora: Intel 8080 i 8086 te Motorola MC6800 i MC68000. Dvije signalne linije PUI međusklopa određuju o kojem se tipu mikroprocesora radi: Mi (1 Motorola, 0 Intel) i M8 (1 8bitovni, 0 16bitovni). Ove linije, ovisno o tipu mikroprocesora, spajaju se na napajanje odnosno masu. Upravljačka logika na temelju stanja na navedenim linijama tumači dvije dodatne linije (IN0 i IN1) koje su spojene na vanjsku upravljačku sabirnicu mikroprocesora. Način spajanja pojedinih signala mikroprocesora na linije IN0 i IN1 prikazan je u tablici 5. Linije zahtjeva za prekid (IRQ) i linija RESET razlikuju se u aktivnom nivou za porodice Intel (aktivno visoko) i Motorola (aktivno nisko). Te linije se interno dekodiraju

u samom čipu (ovisno o stanju linije Mi) tako da nije potrebna dodatna logika.

Tablica 5. Povezivanje PUI međusklopa na upravljačku sabirnicu procesora.

Mi	M8	IN0	IN1
0	0	RD	WR
0	1	W / RD	-
1	0	AS	R / W
1	1	ENABLE	R / W

3. Realizacija PUI međusklopa

Za realizaciju PUI međusklopa korištene su automatizirane topologije: standardne ćelije i PLA strukture. Na topološkom prikazu PUI međusklopa (slika 2) vidljive su makroćelije od kojih se čip sastoji te veze između njih. Makroćelije **hc, irq, cData** i **xnormux** realizirane su standardnim ćelijama; **conPla** i **cPla** realizirane su PLA strukturama, dok **porta, portb** i **portc** koriste oba pristupa (slika 3). Na obodu čipa nalaze se vanjski priključci koji su razmješteni u makroćelije **left, right, top** i **bottom**. Razmještaj ćelija i povezivanje unutar makroćelija provedeno je ručno. Razmještaj makroćelija proveden je također ručno, dok se za povezivanje koristio program za globalno povezivanje **TimberWolfMC** i program za kanalno povezivanje **YACR2** /3/

Upravljačka logika, komparatori i dodatna logika u pristupima opisana je u jednoj varijanti jezika za opis ponašanja BDL (engl. behavioral description language) iz kojega se automatski generira PLA struktura za opisanu logičku funkciju. Jedan takav primjer dan je na slici 4 i predstavlja opis makroćelije **conPla**. U opisu su

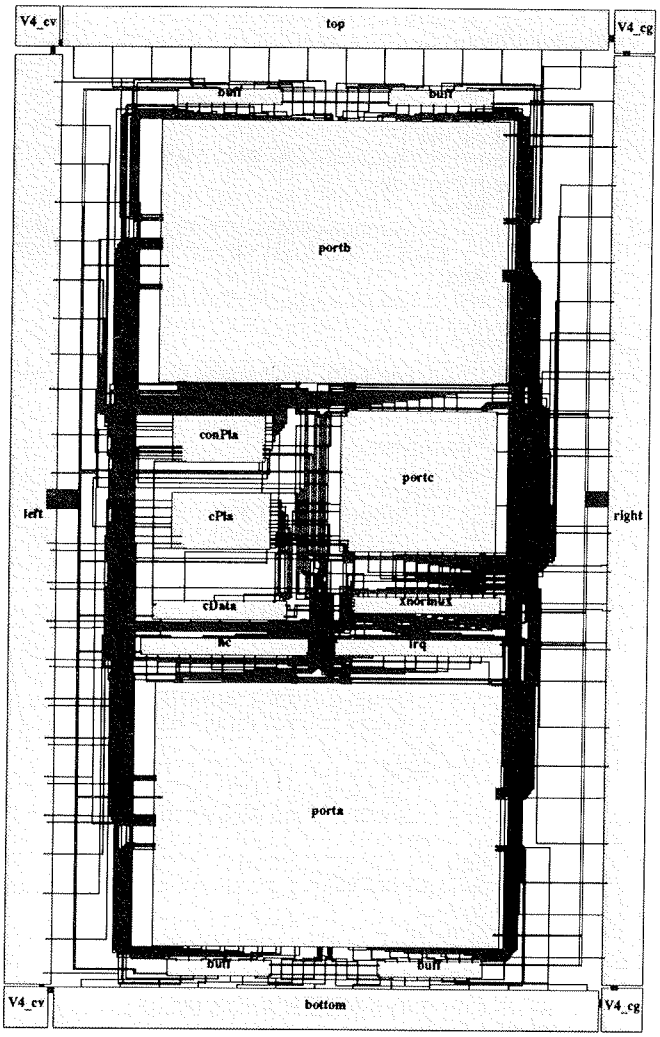

Slika 2: Topološki prikaz PUI međusklopa

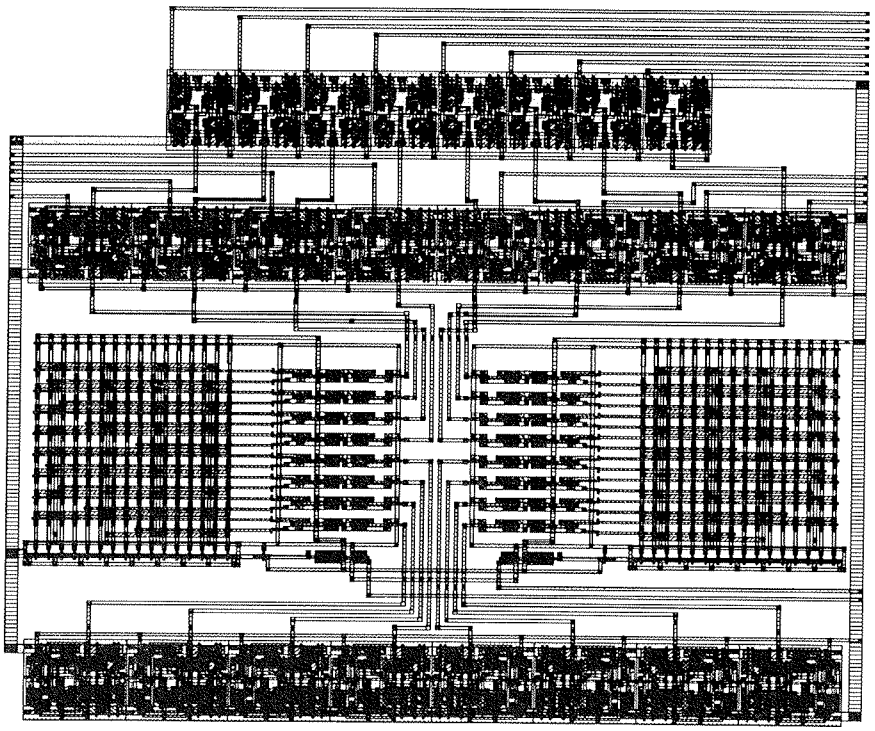

*Slika 3: Topološki prikaz makroćelije **portc**, koja se sastoji od standardnih ćelija i Pla struktura.*

```
model  con Pla
        PSAL, PSAH, PSBL, PSBH, PSC, SCWAL, SCWAHM, SCWBL, SCWBH, SCWC, DCTACKB, RD, WR =
        IN0,IN1,Mi, M8, CS, RS3, RS2, RS1, RS0;
routine PostSel <9:0 > (rs < 3:0 >, mikro < 0 >, cs < 0 >);
        state 0 <>,  ps < 9:0 >;
        for i from 0 to 9 do ps <i>= (rs EQL i) AND mikro;
        for i from 0 to 3 do
                begin
                    ps<i>=ps<i>OR((rs<2:1>EQL(i SR0 1))AND(NOT mikro));
                    ps<5+i>=ps<5+i>OR((rs<2:1> EQL((4+i)SR0 1))AND(NOT mikro));
                end;
        for i from 0 to 9 do ps<i>=ps<i> AND cs;
        return ps<9:0>;
endroutine PortSel;
routine ReadWrite<1:0>(in1<0>,in0<0>,mib<0>,mikro<0>,cs<0>);
        state temp<1:0>,svar<1:0>;
         temp=0;
        svar=2*mib+mikro;
        select svar from
                |0|:begin
                        temp<0>=NOT in1;
                         temp<1>=NOT in0;
                    end;
                |1|:begin
                         temp<0>=in0;
                        temp<1>=NOT in0;
                     end;
                |2|:begin
                        temp<0>=(NOT in0)AND(NOT in1);
                        temp<1>=(NOT in0)AND in1;
                    end;
                |3|:begin
                        temp<0>=in0 AND(NOT in1)
;                       temp<1>=in0 AND in1;
                     end;
        endselect;
        temp=temp AND(3*cs);
        return temp;
endroutine ReadWrite;
routine main;
        state temp<9:0>;
        temp<1:0>=ReadWrite(IN1,IN0,Mi,M8,CS);
         WR=temp<0>;
        RD=temp<1>;
        temp<9:0>=PortSel(8*RS3+4*RS2+2*RS1+RS0,M8,CS);
        PSAL=temp<0>;
        PSAH=temp<1>;
        PSBL=temp<2>;
        PSBH=temp<3>;
        PSC=temp<4>;
        SCWAL=temp<5>;
        SCWAH=temp<6>;
         SCWBL=temp<7>;
        SCWBH=temp<8>;
        SCWC=temp<9>;
        DTACKB=dont_care;
        if (Mi EQL 1)AND(M8 EQL 0) then
                DTACKB=NOT(WR OR RD);
endroutine main;
endmodel conPla;
```

Slika 4: Ponašajni prikaz upravljačke PLA strukture.

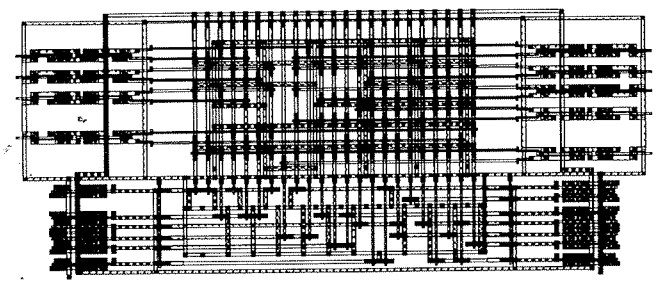

Slika 5: Topološki prikaz upravljačke PLA strukture

navedene ulazne i izlazne signalne linije, te dvije procedure (PortSel i ReadWrite) koje opisuju interne signale. Nakon prevođenja prikazanog opisa u **PLA format** zapisa, te naknadne optimizacije logičkih funkcija, kreira se PLA struktura **conPla** čija je topologija prikazana na slici 5.

4. Zaključak

U ovom je radu opisan projekt paralelnog ulazno-izlaznog međusklopa i njegova realizacija upotrebom

moderne VLSI metodologije projektiranja. Upotrebom automatiziranih topologija (standardne ćelije i PLA strukture), te programa za automatsko povezivanje, znatno je smanjeno vrijeme potrebno za projektiranje topologije čipa. Grafičko sučelje i jezik za opis ponašanja također su pridonijeli uštedi vremena. Najveću teškoću prilikom realizacije topologije čipa predstavljao je razmještaj standardnih ćelija i PLA struktura. Budući da nam nije bio na raspolaganju odgovarajući programski modul za automatski razmještaj, on je proveden ručno. Trenutne mogućnosti dozvolile su realizaciju PUI međusklopa samo do razine topologije ali ne i do konkretne realizacije u siliciju.

Reference:

/1/ Intel: Microprocessor and Peripheral Handbook, Volume II-Peripheral, 1987.

/2/ J. Michael Bennett: 68000 Assembly Language Programmung A Structured Approach, Prentice-Hall international Editions, New Jersey, 1987.

/3/ J.Reed, A.Sangiovanni-Vincentelli, M.Santomauro: A New Symbolic Channel Router: YACR2, IEEE Trans. on CAD, vol. 4, no. 2, July 1985, pp. 208-219.

Prispelo (Arrived): 21.07.93 ***Sprejeto (Accepted): 16.02.94***

mr. Goran Zelić,
Krunoslav Martinčić, dipl. ing.
Mladen Skypala, student
Elektrotehnički fakultet, Zavod za elektroniku
Avenija Vukovar 39, Zagreb
tel. 00 85-41-629 924
fax. 00 385-41-629 653

Testiranje polprevodniških in mikroelektronskih komponent

TESTIRANJE KOMPLEKSNIH MIKROELEKTRONSKIH VEZIJ ZA UPORABO V MODERNIH TELEKOMUNIKACIJSKIH SISTEMIH

Zlatko Bele
MIKROIKS d.o.o., Ljubljana, Slovenija

Ključne besede: mikroelektronska vezja z mešanimi funkcijami, codec, digitalno procesiranje signalov, modem, PCM (Pulse Coded Modulation), A/D konverzija, Fourier transformacija

Povzetek: Članek podaja osnovne značilnosti kompleksnih mikroelektronskih vezij z mešanimi funkcijami za uporabo v modernih telekomunikacijskih sistemih in problematiko povezano s kvalitetnim testiranjem takih vezij.

Testing of Complex Integrated Circuits for Use in a Modern Telecommunications Systems

Keywords: mixed-signal integrated circuits, codec, digital signal procesing, modem, PCM (Pulse Coded Modulation), A/D conversion, Fourier transformation

Abstract: Article deals with the typical characteristics of complex mixed- signal integrated circuits for use in a modern telecommunications systems and the problems encountered with the comprehensive testing of such devices.

UVOD

Pri današnjih telekomunikacijskih sistemih gre za prenos raznovrstnih informacij na zelo velike razdalje. Poleg, lahko bi rekli običajnega prenosa govornih signalov, pa se že takorekoč rutinsko s pomočjo satelitov prenašajo TV signali praktično po celotni zemeljski obli, poslovni, znanstveni in tudi domači računalniki pa že komunicirajo med sabo na razdaljah, ki gredo v tisoče kilometrov. Da ne omenjamo prenosa posebnih podatkov v vojaške in druge namene kot npr.vesoljske raziskave.

Izredno hiter in dinamičen razvoj telekomunikacijskih oz. teleinformacijskih sistemov je vsekakor posledica neslutenega razvoja na področju polprevodniških tehnologij in izdelave izredno kompleksnih mikroelektronskih vezij. Tipični predstavniki takoimenovanih "telecom" mikroelektronskih vezij, ki jih najdemo praktično v vsakem modernem telekomunikacijskem sistemu so codec (koder/dekoder za pretvorbo analognega signala v digitalnega in obratno), SLIC (Subscriber Line Interface-povezava med telefonskim naročnikom in telekomunikaciskim sistemom), digitalni filter, telefonsko vezje, tonski pozivnik, DTMF (Dual Tone Multi Frequency) generator in sprejemnik, modem (modulator/demodulator), delta modulator in dušilec odmeva. Skupna značilnost praktično vseh teh vezij je poleg same kompleksnosti in visoke integracije tudi vsebovanost tako digitalnih kot analognih funkcij. To pa postavlja proizvajalce telecom mikroelektronskih vezij in seveda testnih sistemov pred izredno zahtevno nalogo, kako čim kvalitetneje in celoviteje stestirati omenjena vezja ter s tem zagotavljati tako funkcionalnost kot zelo ozke tolerance vrste parametrov, zahtevane po mednarodnih standardih.

TESTNE ZAHTEVE ZA TELECOM MIKROELEKTRONSKA VEZJA

Za ilustracijo si oglejmo telecom vezje "codec", katerega vloga v okviru telekomunikacijskega sistema je podana na sliki 1, ki prikazuje tipično telefonsko linijo. Codec mora biti sposoben sprejeti analogni signal iz enega telefonskega aparata, ga pretvoriti v digitalno obliko in prek digitalnega komunikacijskega kanala posredovati drugemu ter obratno.Torej mora dvosmerna telefonska linija vsebovati po eno codec vezje na vsaki strani.

Čeprav gre pri testiranju codec vezja prvenstveno za preverjanje, kako kvalitetno je bila izvedena konverzija signala iz analogne v digitalno obliko in obratno, torej

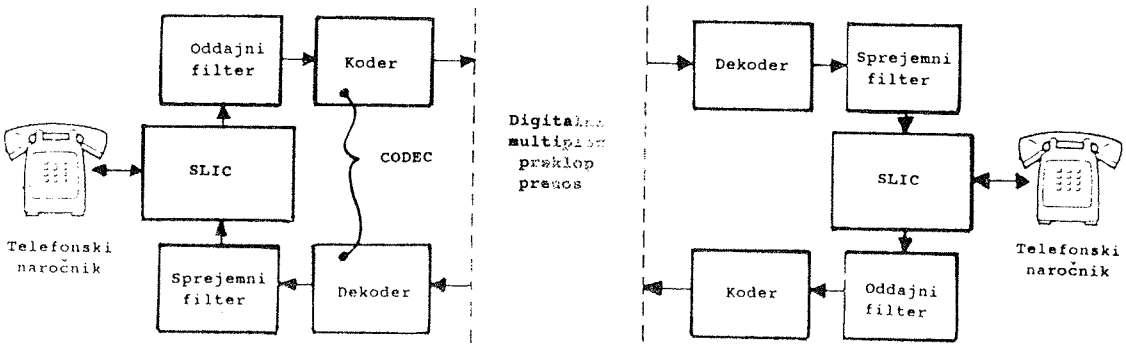

Slika 1: Tipična dvosmerna telefonska linija

preverjanje funkcionalnosti koderja in dekoderja, pa ločimo še takoimenovane "transmisijske" ali "PCM" teste, ki se morajo ravnati po zahtevah, ki so postavljene najprej s strani mednarodnega komiteja CCITT, nato pa še posameznih državnih institucij. S transmisijskimi testi preverjamo vpliv vezja na kvaliteto prenosa govornih in podatkovnih signalov glede na celotni komunikacijski kanal.Ti testi tako vključujejo meritev parametrov kot so ojačanje, razmerje signal/šum, nelinearno popačenje in drugi. Pri vezju codec so ti testi zelo zahtevni saj je potrebna visoka točnost meritev, prisotni so interaktivni efekti vzorčenja in kvantizacije, kanal je delno analogen, delno digitalen in ne nazadnje test ne sme biti predolg. Poleg transmisijskih pa ločimo še digitalne funkcionalne teste, s katerimi preverimo npr. signalno funkcijo, izbiro kodiranja, izklop napajanja, izbiro testnega načina in še parametrične DC in AC teste kot so kontaktni test (kratki stik, odprte sponke), meritev logičnih nivojev, meritev impedance itd.

Drugi tipični predstavnik telekom mikroelektronskih vezij je modem, ki je ključni element pri prenosu računalniških podatkov prek telefonskih linij.Modem sprejema digitalne signale, ki mu jih posreduje računalnik in jih pretvori v analogne, ki so primerni za prenos prek telefonske linije. Hkrati poteka proces tudi v obratni smeri.

V splošnem lahko razdelimo testno proceduro za modem v naslednje segmente:

- DC parametrični testi kot so meritev porabe pri različnih pogojih delovanja, meritev tokov puščanja, zmogljivosti izhodov itd.
- karakterizacijo oddajnika, ki vsebuje meritev DC offseta, osnovne amplitude in frekvence signala, celotno razmerje signal/šum, meritev popačenja od druge do pete harmonske in energije zunaj pasu
- funkcionalni preizkus oddajnika;modem deluje v več načinih. Izbira vrste modulacije je odvisna od načina, ki diktira hitrost prenosa. Odvisno od uporabljene tehnike (FSK, PSK ali QAM), izhod digitaliziramo in analiziramo ali gre za pravilno frekvenco, amplitudo in fazo izhodnega signala glede na digitalno kombinacijo na vhodu.
- funkcionalni preizkus sprejemnika; modem lahko prepozna več kot 15 različnih frekvenc in amplitud vhodnega signala. Zato je potrebno sprejemnik preveriti na vsako frekvenco posebej, kakor tudi na spremembo frekvence. Prav tako je zelo pomemben preizkus dela vezja za detekcijo nosilnega signala. Za natančne rezultate je potrebno izmeriti tako vhodni nivo histereze kot časovne parametre.
- karakterizacija sprejemnika; to je vsekakor najzahtevnejši test modema, saj zahteva izredno natančno sinhronizacijo analognega in digitalnega dela vezja.Pri karakterizaciji sprejemnika ugotavljamo naprimer koliko napak naredi sprejemnik pri detekciji posameznega bita pri različnih nivojih vsiljenega šuma. Potem preverjamo tendenco modema, da traja stanje logične enke dalj časa kot logične ničle. Nato merimo takoimenovani "jitter" in isohrono popačenje. Pravimo, da sta dva signala isohrona, če sta identična v časovni domeni. Isohrono popačenje pa je razlika oz. stopnja variacije med signaloma. Le to konkretno dobimo, da odštejemo digitalni vzorec, ki ga dobimo iz modema od idealnega izhodnega vzorca in ga izrazimo v procentih.
- funkcionalnost Self-testa; večina današnjih modemov vsebuje samopreizkus. To pomeni, da lahko delujejo v takoimenovanem "analog- loopback" načinu, kar kontroliramo prek podatkovnega terminala. Pri tem se digitalni vzorec vsili v oddajnik, ki generira analogni signal, tega pa sprejemnik ponovno pretvori v digitalni signal. Običajna zakasnitev med obema signaloma je tipično med 3-3.5 msek.

Iz zgoraj povedanega sledi, da je testna procedura za telekom mikroelektronsko vezje v splošnem izredno kompleksna in zbir množice zelo zahtevnih segmentov(pripravljalnih, forsirnih, merilnih), ki morajo biti med seboj natančno sinhronizirani in usklajeni. To pa pomeni, da za to potrebujemo zelo kompleksne in s tem seveda tudi drage testne sisteme (tudi 1-2 mio. $), ki poleg visoko profesionalnega merilnega inštrumentarija,

uporabljajo posebna dodatna programska orodja in tehnike ter seveda kar precejšnjo računalniško moč.

TESTNI SISTEM ZA TELEKOM MIKROELEKTRONSKA VEZJA

V grobem lahko rečemo, da testni sistem za testiranje telekom mikroelektronskih vezij sestavljajo:

- zmogljiv računalnik nivoja miniračunalnika z več uporabniškim operacijskim sistemom in takoimenovanim array procesorjem
- programska oprema (splošna, posebna)
- analogni del z vrsto posebnih modulov
- digitalni del za generacijo in komparacijo digitalnih vzorcev
- testna glava, za kontakt med vezjem in testnim sistemom

Primer takega univerzalnega testnega sistema, ameriškega proizvajalca SCHLUMBERGER-TECHNOLOGIES, je prikazan na sliki 2.

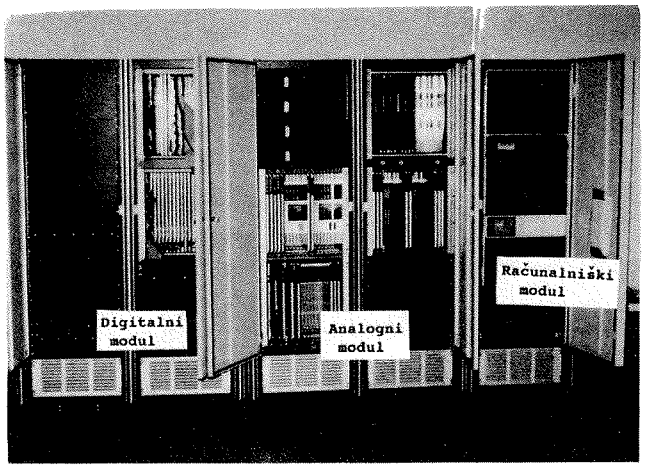

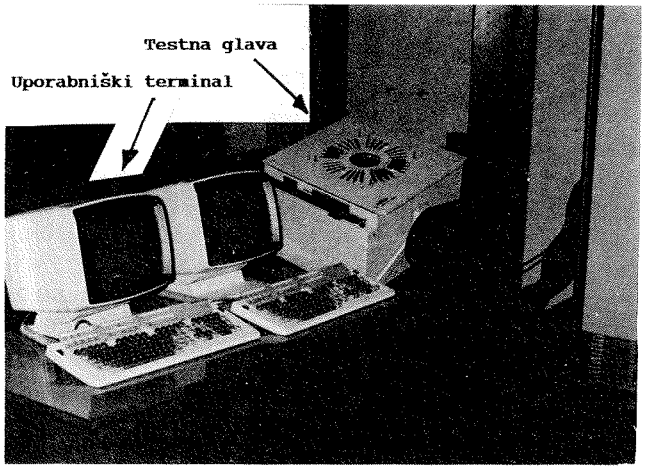

Slika 2: Testni sistem za Telekom mikroelektronska vezja

Ključni moduli

Pri podrobnejšem opisu je potrebno vsekakor omeniti naslednje testne (strojne) module, ki so praktično nepogrešljivi pri vsakem takem sistemu, in sicer:

- **programsko nastavljivi napajalniki** (tako napetosti kot toka)
- **funkcijski generator**, ki na podlagi poljubnega digitalnega vzorca na vhodu generira poljuben analogni signal na izhodu
- **signalni digitalizator**, ki poljubni analogni signal s pomočjo sistemskega računalnika pretvori v digitalno obliko in shrani v poseben spomin, Tako je moč pozneje ta signal temeljito analizirati.Poleg lastne ure, lahko digitalizator krmilimo tudi z zunanjim urinim signalom.
- **precizni merilnik napetosti in toka** za zelo natančne meritve napetosti in tokov, tako pri samem testiranju kot kalibraciji in diagnostiki sistema.
- **audio izvor**, ki mora biti sposoben generirati zelo "čiste" sinusne signale s popačenjem manjšim od 0.02%.
- **array processor**, dodatni računalnik za izvajanje izključno matematičnih (matričnih)operacij v povezavi s tehniko digitalnega procesiranja signalov, kar je opisano v nadaljnem tekstu.

Vsi omenjeni moduli so seveda v celoti programsko krmiljeni in popolnoma vključeni v programsko opremo sistema.

Sinhronizacija

Kot že rečeno vsebujejo telekom mikroelektronska vezja tako digitalne kot analogne funkcije. Za kvalitetno testiranje je zato ključnega pomena popolna sinhronizacija med temi funkcijami, kar je zagotovljeno z dvosmernimi vodili med CPU in digitalnimi moduli, CPU in analognimi moduli, analognimi in digitalnimi moduli in analognimi oz. digitalnimi moduli in vezjem, ki ga testiramo. Vsekakor pa je potrebno zagotoviti tudi asinhrono delovanje kot možnost proženja testnih dogodkov s strani vezja samega.

Zato ima običajno generator digitalnih vzorcev kristalni oscilator, ki ga uporabimo ali samo za digitalni del, lahko pa tudi kot urin signal celega sistema. Prav tako ima svojo uro tudi analogni generator, običajno pa imamo še tretji zelo precizni referenčni urin signal.

Digitalno procesiranje signalov (DSP)

Digitalno procesiranje signalov ali krajše DSP (Digital Signal Processing) je tehnika, ki je praktično postala nepogrešljiva na področju testiranja telekom in tudi ostalih analognih oz. vezij z mešanimi funkcijami.

Osnovna ideja DSP sloni na Fourierovih enačbah, po katerih je moč vsako periodično funkcijo predstaviti kot vsoto posameznih višjeharmonskih frekvenc. Vsaka periodična funkcija ima tako svoj diskretni frekvenčni spekter. S pomočjo Fourierovih enačb lahko določimo amplitudo in fazo vsake posamezne frekvence oziroma izvedemo transformacijo funkcije iz časovnega v frekvenčni prostor in obratno.

DSP tehnika tako omogoča, da pri testnih sistemih za testiranje kompleksnih telekom mikroelektronskih vezij nadomestimo konvencionalne merilne instrumente in signalne izvore z računalniškimi modeli. Kakor pri klasičnih aplikacijah pogosto uporabljamo DSP za analizo relativno neznanih signalov in umetno obogatitev signalov kot npr.slik, pa gre pri testnih sistemih predvsem za sintezo stimulus signalov in analizo odzivnih signalov pod strogo kontroliranimi in koordinirami pogoji.

DSP omogoča vrsto prednosti pred konvecionalnim instrumentarijem. Ena prvih je vsekakor dosti krajši testni čas, saj DSP "instrumenti" ne potrebujejo nobenih preklopnih in nastavitvenih časov, kot je to primer pri resničnih instrumentih.

Ker odziv vezja shranimo v spomin je zadosti, da test izvedemo samo enkrat, odziv pa naknadno poljubnokrat obdelamo pač glede na iskane lastnosti vezja.

Druga velika prednost pa je dosti večja točnost in ponovljivost rezultatov. To pa zato, ker pri meritvah, ki slonijo na DSP tehniki v splošnem uporabimo manj realnih komponent, ki same po sebi vnesejo v rezultat določen pogrešek, ali pa jih uporabimo na mestu, kjer je ta kontribucija manj zaznavna, poleg tega pa lahko pri računalniških modelih uporabimo izračune z dosti večjo točnostjo.

DSP meritve omogočajo tudi bistveno večjo fleksibilnost pri analizi odziva. Predpostavimo, da nas zanima tudi vsebovanost višje harmonskih frekvenc v merjenem signalu, ali pa enosmerni nivo oz. maksimalna (konica) vrednost signala. V tem primeru nam ni potrebno ponovno izvesti meritve, temveč samo zaukažemo testnemu sistemu, naj ponovno obdela shranjen odziv. Pri tem ne rabimo nobenih dodatnih modulov, ki jih je potrebno, najprej seveda kupiti, potem pa tudi kalibrirati in vzdrževati. DSP merilniki nam po navadi posredujejo tudi bistveno več informacij kot konvencionalni merilniki, kot je na primer faza ali zakasnitev ovojnice signala, pri detekciji konice signala pa nam npr. povedo ne samo, kakšna je ta konica, ampak kje v signalu se tudi nahaja.

Poleg omenjenega nam testni sistem, ki uporablja DSP pristop lahko simulira ne samo instrumente, ampak tudi samo vezje, ki ga testiramo. To je zelo uporabno pri karakterizaciji vezij in korelacijskih analizah. Tako ima običajno programska oprema DSP testnega sistema že "vgrajene" modele osnovnih gradnikov telekom vezij, ki jih lahko pri taki simulaciji uporabimo.

Seveda DSP pristop testiranja zahteva znatno računalniško moč in seveda tudi čas. Zato imajo testni sistemi poleg osnovnega računalnika, ki nadzira in izvaja vse testne korake tudi dodatni računalniški modul, takoimenovani "array processor", ki izvaja izključno matematične operacije (Fourier transformacija, matrične in vektorske kalkulacije) in to seveda zelo hitro, ki so potrebne pri simulaciji merilnega instrumentarija. S tem izredno pospešimo samo računalniško modeliranje kakor tudi celotno testiranje, saj lahko osnovni računalnik med delovanjem array procesorja istočasno izvaja ostale testne in druge podporne funkcije.

ZAKLJUČEK

Iz vsega povedanega sledi, da postaja problematika testiranja telekom mikroelektronskih vezij vedno zahtevnejša naloga, kljub novim in vedno močnejšim orodjem, ki so na voljo zaradi skokovitega razvoja računalniške tehnologije.

Hkrati pa lahko rečemo, da DSP testiranje ni samo dodatna testna tehnika, ampak kar drugačna filozofija oziroma nov način razmišljanja, ki je in bo verjetno še znatno vplivala na sam pristop in tudi zasnovo testnih sistemov za testiranje kompleksnih mikroelektronskih vezij.

Zlatko Bele, dipl.ing.
MIKROIKS d.o.o.
Dunajska 5
61000 Ljubljana

PREDSTAVLJAMO PODJETJE Z NASLOVNICE

MIL Radovljica d.o.o.

Podjetje MIL Radovljica, d.o.o. je bilo ustanovljeno v začetku leta 1990. Podjetje je 100 % v družinski lasti. Glavno področje dela je mikroelektronski inženiring, montaža in testiranje tankoplastnih hibridnih in integriranih vezij (P-MOS, N-MOS IN C- MOS). Ustanovitelji podjetja so strokovnjaki z dolgoletnimi izkušnjami na področju montaže integriranih vezij in načrtovanja ter izdelave tiskanih vezij.

Sedež podjetja je v Radovljici, proizvodnja pa se odvija v prostorih bivše ISKRA Mikroelektronike v Ljubljani. Poleg šestih redno zaposlenih sodelavcev v montaži, sodelujemo še z večjim številom zunanjih strokovnjakov, predvsem iz ISKRE, IJS, MIPOT, MIKROIKS in LMFE iz Ljubljane.

Na razpolago imamo 250 m^2 proizvodnih prostorov od katerih je 160 m^2 prostorov v klasi 100.000 (lokalno 10.000), ki so kompletno opremljeni z vso infrastrukturo in tehnološko opremo za montažo in testiranje. V preteklih dveh letih smo namreč uspeli kupiti vso potrebno opremo za montažo v CERDIP in KERAMIČNA ohišja, ter proizvodne prostore.

Podjetje smo prvotno ustanovili z namenom, da finaliziramo nedokončano proizvodnjo, ki je ostala po stečaju ISKRE Mikroelektronike, pozneje pa so se pokazale potrebe po nadaljevanju montaže nekaterih vezij po naročilu za znane kupce kot so: ISKRA Števci, ISKRA AVI, ISKRA TELTIM, ISKRA Transmission itd. Tudi manjša nova zasebna podjetja so se zaradi konkurenčnosti že pričela zanimati za montažo integriranih vezij, tako da smo prvotno najemno pogodbo za opremo in prostore z likvidacijskim upraviteljem podaljšali do konca leta 1992.

Čipe na silicijevih rezinah, ki jih uporabljamo v montaži, nam procesirajo v AMS v Gradcu, kjer še vedno vzdržujejo 5 in 3 µ procese, tako da lahko uporabljamo vsa orodja (maske in testne programe) za vezja, ki so bila razvita v Mikroelektroniki ali na Fakulteti za elektrotehniko.

Naše proizvodne kapacitete v montaži so naslednje:

- montaža v CERDIP, CERPAC ohišja (8 do 10-pin) 200.000 kosov/leto
- montaža v keramična ohišja in CHIP-CARRIER (8 do 64 pin) 100.000 kosov/letno
- montaža tankoplastnih hibridov (8 do 200-pin) 5.000 kosov/letno

Te kapacitete lahko z minimalnimi vlaganji podvojimo.

Naša ponudba obsega:

- Načrtovanje tankoplastnih hibridnih vezij, izdelava filmov in MASTER ter delovnih mask
- testiranje-sortiranje čipov na silicijevih rezinah (do premera 125 mm), digitalno in delno analogno na testnem sistemu Sentry VII (katerega lastnik je MIKROIKS, d.o.o.)
- Montaža integriranih vezij v CERDIP, CERPAC (SMD), CHIP CARRIER in KERAMIČNA ohišja
- Montaža tankoplastnih hibridnih vezij v keramična in kovinska ohišja do velikosti 80x80 mm.
- Zagotavljanje kvalitete integriranih in tankoplastnih hibridnih vezij z izločilnimi testi v skladu s standardi MIL STD 883. Na zahtevo kupcev pa vezja preizkušamo še po drugih postopkih in parametrih.
- Funkcionalno testiranje integriranih vezij na testnem sistemu Sentry VII
- Funkcionalno testiranje tankoplastnih hibridnih vezij na aplikacijah
- Izdelava raznih kartic za parametrično in funkcionalno testiranje čipov na silicijevih rezinah ali že zaprtih v ohišju
- Izdelava testnih programov
- Usposabljanje kadrov za montažo in svetovanje na področju montaže
- Izdelave tehnoloških projektov in elaboratov za montaže

Poleg naštetih dejavnosti na področju mikroelektronike pa se naše podjetje ukvarja tudi z načrtovanjem (CAD PCB), izdelavo filmov in mask za tiskana vezja (od ene do 20 plasti in debeline 5 mm) ter samo izdelavo tiskanih vezij v vseh tehnologijah po zahtevah naročnikov. Smo pooblaščeni predstavnik za prodajo CAD programov ameriške firme WINTEK CORP, za načrtovanje tiskanih vezij za področje Slovenije, Hrvaške in držav Vzhodne Evrope. Ti programi so zaradi svoje preprostosti in cenenosti primerni predvsem za dijake in študente elektrotehnike in načrtovalce v manjših podjetjih, ki maloserijsko izdelujejo elektrotehnične izdelke. Programi so nastali že pred 20 leti in se sproti dopolnjujejo vsako leto tako, da so res izredno zmogljivi in kvalitetni (autoruter je 100%). Vsi uporabniki so evidentirani in program lahko dograjujejo z minimalnimi doplačili.

Naslednja dejavnost v našem podjetju pa je zastopanje ameriške tovarne za izdelavo helikopterjev THE ENSTROM HELICOPTER CORP. Smo pooblaščeni predstavnik za prodajo in servisiranje njihovih lahkih 3 in 5 sedežnih helikopterjev za Slovenijo, Hrvaško in

države Vzhodne Evrope. Prek servisa prodajamo tudi vse rezervne dele za vse modele. Pri nas se lahko šolajo piloti helikopterjev, nudimo pa tudi vse vrste komercialnih prevozov potnikov in blaga, snemanja iz zraka, nadzor prometa, daljnovodov in drugih energetskih sistemov. Z veljavnim pilotskim dovoljenjem lahko pri nas helikopter tudi najamete. Prodajamo tudi vse vrste rabljenih helikopterjev, urejamo certifikate potrebne za registracijo itd.

Imamo tudi lastno trgovino, kjer lahko poleg ostalega kupite tudi vse naše izdelke. Na zalogi imamo večje količine integriranih vezij kot so:

- matrike 1005 A,B in C
- 4-bitne mikroprocesorje 1001 K
- časovna vezja 1002 B,D,E,F in 1150
- pulzni izbiralec 2560
- števec 1315
- smerni diskriminator 1317
- vezje za merilne letve 1201
- vezje MTK 1404, 1405 in 1406

Vsa vezja imajo potrdila o kakovosti, cene pa niso pretirane.

Tako široko paleto uslug in izdelkov vam lahko nudimo predvsem zaradi lastnega znanja in sposobnih sodelavcev ter dobrega poznavanja tujih partnerjev in trdne povezanosti z našimi zunanjimi sodelavci. Vedno smo vam pripravljeni svetovati in nuditi strokovno pomoč in podporo v trenutkih, ko je potrebno rešiti kak VAŠ problem.

Vsi naši izdelki in ponujene usluge so priznane svetovne kvalitete največjih in najbolj poznanih svetovnih proizvajalcev.

Na področju mikroelektronike se mislimo v bodoče še bolj povezovati s sorodnimi podjetji doma, predvsem pa v tujini, pa ne samo v smislu širitve znanja in strokovnega dopolnjevanja ampak tudi v proizvodnem in tehnološkem navezovanju. Zato smo že pričeli s pogovori o prenosih montaže v našo tovarno, kar se bo odrazilo tudi skozi posodobitev naše obstoječe opreme in povečanju kapacitet. V bodočnosti računamo tudi na kakšno pomoč Ministrstva za znanost in tehnologijo, ki se sedaj do mikroelektronike dokaj mačehovsko obnaša.

Referenčna lista naših kupcev:

- ISKRA Števci
- ISKRA AVI, TELAVI, TELTIM
- ISKRA Transmission
- ISKRA Elektooptika
- ISKRA Avtoelektrika
- ISKRA Telkom
- ISKRA Mehanizmi
- IJS
- Siemens Nemčija
- RSF Avstrija
- Avtotehna Canon
- REPRO
- TIPRO
- GALLILEO Italija

direktor Ivan Milatovič, ing.
MIL Radovljica, d.o.o.
Gradnikova 121
64240 Radovljica
Tel/fax: (061) 573 007
h.c. (061) 1591 133/37

PRIKAZ MAGISTERSKIH DEL IN DOKTORATOV, LETO 1993

Naslov naloge: **Načrtovanje analognih aktivnih filtrov za realizacijo v CMOS tehnologiji integriranih vezij**
Avtor: **Stanislav Gruden**, dipl. ing., Ljubljana
Mentor: **prof. dr. Baldomir Zajc**
Univerza v Ljubljani, Fakulteta za elektrotehniko in računalništvo

To delo se ukvarja z realizacijo linearnih analognih vezij v CMOS tehnologiji integriranih vezij. Kot sestavni deli vezja so uporabljeni elementi, ki jih je vse mogoče izdelati z obstoječo tehnologijo. To so transkonduktančni ojačevalniki, kondenzatorji in tokovna zrcala. Prikazali smo zgradbo vezja, s katero lahko realiziramo želene prenose funkcije.

Izdelani postopek načrtovanja omogoča izračun tokovnih prestavnih razmerij za tokovna zrcala vezja tako, da je dinamično področje izdelanega filtra optimalno. Sledi načrtovanje transistorskega vezja, ki upošteva izračunana tokovna prestavna razmerja.

Celoten postopek je vgrajen v računalniški program, ki zahteva v vhodni datoteki opis grafa pretoka signala, katerega prenosna funkcija je enaka želeni, v izhodni datoteki pa vrne opis vezja v formatu, ki ga podpira programski paket SPICE. Opisali smo delovanje programa, način, kako program označuje sestavne elemente in vozlišča vezja v izhodni datoteki in uporabo programa. Obdelali smo vplive neidealnosti sestavnih elementov na delovanje vezja in možne kompenzacije teh neidealnosti. Neidealnosti, na katere je možno učin-

kovito vplivati, so predvsem nenatančno preslikovanje prek tokovnih zrcal in odvisnost vrednosti transkonduktanc ojačevalnikov in kapacitivnosti kondenzatorjev od zunanjih vplivov.

Podana ocena je omejitev območij vrednosti, v okviru katerih je možno izdelati sestavne elemente vezja in ocena območja prenosnih funkcij, ki jih lahko izdelamo ob upoštevanju teh omejitev.

Naslov naloge: **Deljenje digitalnih vezij za izvedbo z FPGA vezji**
Avtor: **Roman Kužnar**, dipl. ing.
Mentor: **prof. dr. Baldomir Zajc**
Univerza v Ljubljani, Fakulteta za elektrotehniko in računalništvo

V tem magistrskem delu obravnavamo problem deljenja logičnega vezja v več manjših podvezij, kjer bo vsako izmed njih izvedljivo z izbranim FPGA (Field Programmable Gate Array) vezjem.

Osnovni kriteriterij delitve je doseganje čim nižje cene izvedbe celotnega logičnega vezja. Vsako FPGA vezje je določeno z naborom parametrov, ki so shranjeni v knjižnici: logična zmogljivost FPGA vezja, število vhodnih/izhodnih priključnih sponk in njegova cena. Motiv za magistrsko delo izhaja iz potrebe po orodju za avtomatsko deljenje obsežnejših logičnih vezij, ki jih ne moremo izvesti v enem samem FPGA vezju. Avtomatizirano računalniško orodje za deljenje vezij olajša načrtovalcu veliko načrtovalnih naporov ter prihrani mnogo načrtovalskega časa.

Osnovni rezultat naših raziskav je delitveni algoritem, ki temelji na rekurzivni uporabi delitvene hevristike, katero sta predlagala Fiduccia in Matheyses. To hevristiko smo razširili tako, da (a) je dosežena najnižja cena izvedbe logičnega vezja in (b) so upoštevane omejitve, ki nastajajo pri deljenju vezja za izvedbo z FPGA vezji. Čeprav je opis in zasnova algoritma splošna, smo učinkovitost in uporabo metode prikazali na pestrem izboru logičnih vezij, ki so bila deljena za izvedbo s Xilinx FPGA vezji.

Eksperimentalni delitveni program imenovan k-way.x, ki smo ga razvili skozi raziskovalno delo, je pokazal zelo spodbujajoče rezultate. Za mnoga testna vezja je končna cena izvedbe deljenega logičnega vezja zelo blizu teoretično določljivi najnižji ceni izvedbe.

Naslov naloge: **Študija uporabe nevronskih mrež na področjih senzorjev in metrologije**
Avtor: **Rok Rape**, dipl. ing.
Mentor: **prof. dr. Dušan Fefer**
Univerza v Ljubljani, Fakulteta za elektrotehniko in računalništvo

Magistrsko delo predstavlja sistematično študijo apliciranja nevronskih mrež na področjih senzorjev in metrologije. Nevronske mreže je smotrno uporabiti kot dopolnilo in nadgradnjo k ustaljenim in preizkušenim orodjem za obdelavo signalov in podatkov. Do izraza pridejo v primerih, ko z njimi rešimo probleme bolje, enostavneje, učinkoviteje. Osnovni namen in cilj vključevanja nevronskih mrež v senzorske, merilne in metrološke sisteme je zato bil povečati kvaliteto in zanesljivost metroloških parametrov teh sistemov ter zagotoviti njihovo sledljivost. Ker je ta tematika še dokaj neraziskana, teoretičnih možnosti za uporabo nevronskih mrež pa je veliko, je s tako majhnim obsegom dela nemogoče predstaviti celovit pregled možnosti, raziskav in rezultatov. Pričujoče delo zato predstavlja le skromen poskus obravnave treh s stališča omenjenih področij najzanimivejših problemov: posrednega merjenja veličin, kvalitativne obdelave signalov in predikcije časovnih signalov. Vsako poglavje nudi nov pogled na praktično uporabo nevronskih mrež. Vse raziskave so vezane na realne probleme, ker je le tako mogoče oceniti njihovo uporabnost.

V uvodu so najprej opisani motivi za uporabo nevronskih mrež. Nakazane so njihove splošne prednosti in slabosti. Nadalje je predstavljena kratka zgodovina nevronskih mrež od začetka do osnovne prelomnice v razvoju - odkritja učilnega algoritma za večnivojske perceptrone. Na koncu uvoda so opisane domene znanosti in tehnike, kjer je mreže mogoče s pridom uporabiti.

Drugo poglavje je posvečeno uporabi nevronskih mrež pri posrednem merjenju veličin. Raziskave in rezultati raziskav so vezani na primer določanja relativne vlažnosti zraka. Ker je to značilen primer, raziskave s tem ne izgubijo na splošnosti. Nakazani so problemi v zvezi z izbiro topologije nevronske mreže, predstavitvijo realnega problema in določitvijo parametrov mreže. Posebno pozornost zasluži razdelek o načinu predstavitve učilnih vzorcev, saj odločilno vpliva na točnost preslikave in hitrosti konvergence. Rezultati raziskav so zelo zadovoljivi in podajajo splošne smernice pri reševanju tovrstnih problemov.

Tretje poglavje obravnava uporabo nevronskih mrež pri razpolavljanju in razvrščanju signalov. Kot realen problem je bilo izbrano ugotavljanje prisotnosti skupin Pc-2-5 geomagnetnih mikropulzacij v signalu geomagnetnega polja. Pri problemih takega tipa je predprocesiranje še večjega pomena, zato je tej temi namenjenega precej prostora. Spet so predstavljene primerne topologije mrež in rezultati, ki smo jih z njimi dosegli. Z naučenimi mrežami smo lahko uspešno izvedli analizo transformacije geomagnetnega polja pri prehodu v moderno stavbo.

V četrtem poglavju je govora o predikciji signalov. Za obravnavo je bil izbran netipičen primer - sledenje obnašanja referenčnih napetostnih elementov v DC modulu AC/DC transfer etalona. Orisali smo, kako bi bilo nevronske mreže mogoče v kombinaciji z ostalimi klasičnimi metodami uporabiti za ocenjevanje trenutnega in napovedovanje bodočega stanja napetostnega etalona. Rezultati so pokazali, da je tudi v tem primeru

nevronske mreže možno uporabiti kot dodatno orodje za obdelavo informacij.

Zadnje, peto poglavje je namenjeno fizičnim implementacijam nevronskih mrež. Ločena razdelka sta namenjena implementacijama, ki sta bili tudi dejansko preizkušeni. V prvem primeru je šlo za implementacijo z diskretnimi komponentami, v drugem pa z digitalnim signalnim procesorjem. V ostalem delu poglavja so bežno prikazani moderni pristropi in tehnologije, ki si prizadevajo doseči čim višjo stopnjo paralelizma pri obdelovanju informacij.

Naslov naloge: **Funkcijska verifikacija in diagnoza napak v programabilnih vezjih**
Avtor: **Andrej Žemva**, dipl. ing.
Mentor: **prof. dr. Baldomir Zajc**
Univeza v Ljubljani, Fakulteta za elektrotehniko in računalništvo

V delu je predstavljen pristop k testiranju, funkcijski verifikaciji in diagnozi napak v FPGA (Field Programmable Gate Arrays) vezjih. FPGA vezja se danes zaradi hitre, enostavne in cenene realizacije vse pogosteje uporabljajo pri načrtovanju digitalnih integriranih vezij. Delež napak, ki se pojavlja v teh vezjih, je spričo novih tehnologij izdelave vezij še nadpovprečno visok, zato se je v praksi pojavil problem zanesljivega in učinkovitega testiranja FPGA vezij.

V delu so najprej opisane napake do katerih lahko pride v postopku realizacije FPGA vezij. Študij napak obsega napake v osnovnih logičnih gradnikih (logičnih modulih) vezja in napake v povezovalni arhitekturi. Vzrok napak je lahko tudi v nepravilnem vrstnem redu programiranja programabilnih elementov. V delu smo pokazali, da s klasičnim modeliranjem enojnih napak ne dobimo zadovoljivega podatka o pravilnosti delovanja vezja.

V naslednjem poglavju je predstavljen naš pristop modeliranja napak, s katerim lahko funkcijsko preverimo delovanje vsakega logičnega modula. Za logični modul z N vhodi s predstavljenim modelom preiskusimo izhodno vrednost logičnega modula za vse 2^N vhodne kombinacije. Osnova modela je v predstavitvi logične funkcije v najbolj osnovni obliki, to je v PDN (popolni disjunktivni normalni) obliki in PKN (popolni konjuktivni normalni) obliki (1). Napake, s katerimi funkcijsko preverimo delovanje logičnega modula, so enojne napake v 0 na izhodu vseh vrat v IN ravnini pri PDN obliki in vse enojne napake v 1 na izhodu vseh vrat v ALI ravnini pri PKN obliki zapisa logične funkcije. Nadalje je prikazano, da s tem načinom modeliranja napak odkrijemo tudi večino napak v povezovalni arhitekturi vezja in sicer vse napake na vhodih logičnih modulov ter napake, ki nastanejo kot posledica stika dveh ali več vhodov posameznega logičnega modula.

Predstavljeni model napak smo uporabili v hierarhičnem generatorju testnih vzorcev, kjer se vsi koraki v postopku generiranja testnih vzorcev izvajajo na nivoju logičnih modulov. Funkcija posameznega logičnega modula je predstavljena v obliki glavnih in zaznavnih logičnih vsebovalnikov. V fazi testiranja vezja je v PDN in PKN obliki predstavljen le logični modul, ki ga funkcijsko testiramo. Vsi ostali logični moduli so predstavljeni hierarhično, s čimer povečamo učinkovitost generiranja testnih vzorcev. Osnova hierarhičnemu algoritmu so metode na katerih temeljijo algoritmi za testiranje vezij, ki so predstavljena z osnovnimi logičnimi vrati.

Algoritem smo realizirali v programskem jeziku C ter preizkusili na vezjih realiziranih z Actel FPGA vezji. Rezultati, ki smo jih dobili na testnih vezjih, so obetajoči. Pokazali smo, da je delež funkcijskih napak odkritih s testnimi vzorci dobljenih na osnovi modela enojnih napak med 75% do 95%. Število napak, s katerimi preverimo funkcijsko delovanje vezja, ni bistveno večje od števila enojnih napak v vezju, kjer so logične funkcije posameznih logičnih modulov predstavljene v minimalni obliki z osnovnimi logičnimi vrati. Hkrati v postopku testiranja odkrijemo tudi morebitne redundantne napake ter na ta način zmanjšamo število uporabljenih logičnih modulov in izboljšamo dinamične lastnosti vezja. Pristop k testiranju FPGA vezij je splošen in ga lahko uporabimo tudi za FPGA vezja ostalih proizvajalcev.

Naslov naloge: **Testiranje analognih vezij z uporabo metod umetne inteligence**
Avtor: **Marina Santo Zarnik**, dipl. ing.
Mentor: **prof.dr. Dušan Kodek**
Komentor: **doc.dr. Igor Mozetič**
Univerza v Ljubljani, fakulteta za elektrotehniko in računalništvo

V magisterskem delu je obdelana možnost testiranja analognih vezij z uporabo orodja umetne inteligence. Opisana je splošna problematika testiranja analognih vezij in podan pregled stanja področja, ki vključuje klasifikacijo različnih diagnostičnih metod. Poseben poudarek je na problematiki testiranja in načrtovanja testiranja aktivnih RC filtrov. Omenjeni razred analognih vezij je izbran kot problemska domena, v kateri sem predstavila postopek avtomatskega testiranja z uporabo CLP($\Re$). Naloga vsebuje kratko predstavitev CLP ($\Re$) sistema in opisuje možnost uporabe pri analizi analognih vezij (modeliranje in simulacija). Omenjeno orodje omogoča tudi preprosto diagnosticiranje napak v vezju, kar sem ponazorila pri opisu osnovne ideje diagnostičnega postopka. Osrednji del naloge opisuje metodo, ki združuje postopek načrtovanja testiranja in možnost diagnosticiranja aktivnih RC filtrov z uporabo CLP ($\Re$). Podani so eksperimentalni rezultati in nakazane smernice za nadaljni razvoj.

Naslov naloge: **Prehodni pojavi v amorfnem siliciju pri svetlobnem vzbujanju**
Avtor: **Elvis Bassanese**, dipl. ing.
Mentor: **prof. dr. Jože Furlan**
Univerza v Ljubljani, Fakulteta za elektrotehniko in računalništvo

V zadnjih letih je bilo vloženo veliko truda v iskanje alternativnih virov energije, ki bi zadostili dvema pogojema: ekološki neoporečnosti in nizki ceni. Sončna

energija je ena najbolj obetajočih virov, ker je enostavno dostopna in nima kvarnih vplivov na okolje.

Za pretvorbo sončne energije v elekrično so danes v uporabi t.i. sončne celice, izdelane iz različnih materialov. Med njimi je tudi amorfni silicij (a-Si). Za dosego čim višjega izkoristka pri pretvorbi energije je potrebno zaradi optimizacije čim bolje poznati lastnosti tega materiala.

Najpomembnejši parameter kvalitete a-Si je gostota lokaliziranih stanj ('density of states' = DOS) v mobilnostni reži. Zaradi porušene kristalne zgradbe amorfnega silicija obstajajo večja ali manjša odstopanja v dolžinah in kotih valenčnih vezi, kar povzroča lokalizirana stanja v energijski reži. Ta stanja odločilno vplivajo na njegove električne lasnosti v stacionarnem stanju med prehodnim pojavom.

Večina spoznanj s področja fizike polprevodnikov in izolatorjev je izpeljana iz transientnih eksperimentov. Transientne karakteristike imajo v delovanju večine polprevodniških elementov bistveno vlogo, tudi stacionarni pojavi so pogosto natančneje analizirani s pomočjo predhodnih pojavov. Transientni eksperimenti nam dajo manj dvomljive rezultate kot stacionarni, ki so vedno povprečja na daljši časovni interval.

Interpretacija transientnih eksperimentov je v splošnem zelo zahtevna in je zato grajena na osnovi večjih poenostavitev in enostavnih modelov. Problem transientnih analiz je očiten tudi v analizi hidrogeniranega amorfnega silicija (a-Si:H). Veliko vprašanj in kontraverzij glede fizikalnega ozadja tega pomembnega polprevodnika izvira iz naše omejene sposobnosti za interpretacijo rezultatov, dobljenih s pomočjo transientnih eksperimentov. Popolnejša razlaga teh eksperimentalnih rezultatov pa ima velik pomen pri načrtovanju boljših elementov na osnovi amorfnega silicija.

Za lažje razumevanje rezultatov transientnih eksperimentov si ponavadi pomagamo tako, da jih primerjamo s tistimi, ki smo jih dobili z reševanjem ustreznega fizikalnega modela materiala. To reševanje je lahko popolnoma analitično ali pa vključuje tudi numerično reševanje. Z uporabo numeričnih metod je možno rešiti cele sisteme integro - diferencialnih enačb, ki opisujejo trasientne eksperimente na polprevodnikih. Na ta način lahko koreliramo eksperimentalno merljive količine z mikroskopskimi, ki niso direktno merljive. To nas vodi do boljšega razumevanja procesov, ki potekajo v polprevodniškem vzorcu med eksperimentom, in njihovega vpliva na dobljene eksperimentalne rezultate. Vsakič pa se moramo vprašati, kaj je vzrok za transport nosilcev naboja in kaj nam eksperimentalni rezultati dejansko povedo o materialu.

Z opisovanjem merilnih rezultatov transientne fotoprevodnosti poskušamo pojasniti mikroskopske razmere v mobilnostni reži med predhodnim pojavom nosilcev naboja. Izhodišče večine teoretičnih del sloni na poenostavljenem modelu večkratnega lovljenja, ki sta ga opisala Tjedje in Rose ter neodvisno od njiju Orenstein in Kastner (TROK model). V tem modelu je uveden časovno odvisni demarkacijski nivo $E_d(t)$, ki ob vsakem času deli mobilnostno režo na dve energijski področji. Predpostavljeno je, da so plitva stanja nad $E_d(t)$ v kvazi-ravnovesju s prevodnim pasom,zasedenost globokih stanj pod to energijo pa je enakomerna. Osnovna MT teorija zanemarja vse prehode nosilcev naboja med lokaliziranimi stanji in valenčnim pasom zaradi majhne koncentracije vrzeli v nedopiranem a-Si. S pomočjo teh predpostavk so izpeljali poenostavljene analitične izraze, ki opisujejo prehodni pojav fotoprevodnosti. Največje število experimentalnih in teoretičnih del je bilo izvedenih z impulznim svetlobnim vzbujanjem. Z analizo prehodnih pojavov koncentracij nosilcev naboja pri stopničastem vzbujanju z uporabo MT pristopa sta se ukvarjala Kastner in Monroe /3/, ter kasneje Mendoza, Pickin in Alonso /4-7/.

V tem delu sem numerično analiziral prehodni pojav nosilcev naboja pri različnih svetlobnih vzbujanjih brez vnaprej vnešenih poenostavitev. V nasprotju z drugimi pristopi, ki zanemarijo prisotnost prostih vrzeli, sem v analizo vključil tudi verjetnosti prehodov nabojev med valenčnim pasom in stanji v mobilnostni reži. Za model gostote stanj sem uporabil model stanj z akceptorskimi in donorskimi lokaliziranimi stanji. sestavljajo ga stanja na repih prevodnega in valenčnega pasu ter stanja bingljajočih vezi, ki se nahajajo bolj v sredini mobilnostne reže in so opisana z Gaussovo funkcijo porazdelitve. Iz časovnih sprememb koncentracij nosilcev naboja sem sestavil sistem štirih nelinearnih diferencialnih enačb, ga razrešil numerično za različne primere svetlobnega vzbujanja in dobljene rezultate fizikalno razložil.

Z analizo izračunanih prehodnih pojavov prostih in ujetih nosilcev naboja sem za različne časovne intervale vpeljal specifične poenostavitve, ki so vodile do analitičnih rešitev prehodnega pojava. Tako dobljene rešitve razmeroma dobro opisujejo prehodne pojave nosilcev naboja. Cilj izpeljave analitičnih izrazov za prehodni pojav je enostavno ugotavljanje odvisnosti med mikroskopskimi količinami, ki jih lahko izmerimo z določeno merilno metodo. Uvajanje specifičnih poenostavitev v analizo omogoča izpeljavo izrazov za ekstrakcijo nekaterih značilnih parametrov materiala, kot je na primer porazdelitev gostote stanj v mobilnostni reži a-Si. Pri tem lahko za vhodne podatke uporabimo rezultate, dobljene z meritvami prehodnih pojavov fotoprevodnosti.

Naslov naloge: **Uporaba mikroobdelave za realizacijo 3D silicijevih struktur**
Avtor: **Drago Resnik**, dipl.ing.
Mentro: **prof.dr. Slavko Amon**
Univerza v Ljubljani, Fakultta za elektrotehniko in računalništvo

Vzporedno z razvojem visoko integriranih mikroelektronskih vezij so se nekako bolj v senci v osemdesetih razvijale tudi periferne enote, kot so senzorji, aktuatorji in pretvorniki, ki pretvarjajo fizikalne veličine v električne , oziroma obratno. Vse te enote so bile še pred

leti diskretnega značaja, v zadnjih nekaj letih pa so doživele izredno hiter in nesluten razvoj v povsem novih dimenzijah.

Tak razvoj je omogočil novo področje mikroelektronike, takoimenovana mikroobdelava silicija (micromachining). Pri mikroobdelavi silicija se poslužujemo vseh orodij, ki so na voljo dandanes v mikroelektronski industriji z dodatkom novih ali izpopolnjenih tehnik, povsem specifičnih za področje mikroobdelave. Pomemben pogoj pa je , da so vse te dodatne tehnike združljive z mikroelektronskimi procesi, saj se izvajajo v istih okoljih.

Silicijeve mikrostrukture izdelamo ponavadi z jedkanjem kristala prek definiranih oblik maskirnih materialov ali pa s tehnikami nanašanja. Predvsem prva je danes še največ v uporabi. Take 3D strukture, ki jih izdelamo v silicij zaobjemajo celo paleto membran, vpetih peres, mostičev, vse do prosto gibajočih (rotirajočih) mehanskih delov. Pri tako izdelanih mikrostrukturah se izkoriščajo poleg električnih tudi izredne mehanske lsnosti silicija, svojstvene določenim kristalnim orientacijam, posebej orientaciji (100).

Dve glavni lastnosti silicija, ki omogočata današnjo stopnjo 3D prostosti v mikroobdelavi silicija sta anizotropija (smerno odvisna hitrost jedkanja) in samoustavitvene tehnike jedkanja, ki zelo natančno določajo, kje se bo jedkanje ustavilo v z smeri.

Razvoj mikreelektronskih struktur, kot jih danes radi poimenujejo, je usmerjen na takoimenovane "smart" strukture. Pod temi pojmi razumemo integrirane sisteme, kjer so na istem substratu realizirani eden ali več perifernih enot, ki pretvarjajo električne veličine v neelektrične ali obratno, skupaj z vsem krmilnim vezjem in vezjem na procesiranje zajetih signalov. Tako zasnovani sistemi dopuščajo nadaljno miniaturizacijo, kar je ob nižji ceni, povečani zanesljivosti in zmogljivosti gibalo razvoja te veje znanosti.

Vsekakor mikroobdelava silicija skriva neslutene možnosti, kar lahko sodimo že po bogatih objavljenih dosežkih zadnjih dveh, treh let.

V magistrski nalogi, ki je razdeljena na osem poglavij, so predstavljeni osnovni pojmi mikroobdelave, orodja, tehnike, vse do konkretne izdelave senzorske strukture.

Prva tri poglavja nas uvedejo v specifičnosti kristalne zgradbe silicija in njegovih kristalografskih lastnostih. Te specifičnosti nam v končni fazi omogočijo izdelavo 3D mikrostruktur s pomočjo orodij, ki se jih poslužujemo. Poznavanje teh orodij, posebej mokrega jedkanja, njegove aplikacije za izdelavo specifične strukture, je bistvenega pomena.

V naslednjem poglavju smo pristopili k razlagi mehanizma, ki vodi reakcijo mokrega anizotropnega jedkanja (100) silicija v KOH anizotropnem jedkalu. Eden od parametov, ki določajo kvaliteto 3D strukture, je tudi gladkost jedkane površine. raziskali smo parametre, ki na to vplivajo.

Nadalje smo pozornost usmerili na odpornost raznih maskirnih materialov na jedkanje ter na anomalije, ki nastopajo, če so robovi, ki obdajajo strukturo konveksni.

Jedkalne tehnike, ki omogočajo samoustavitev jedkanja na vnaprej definiranih plasteh, so podane v naslednjih dveh poglavjih, s tem da je največji poudarek tega dela na tako imenovanem elektrokemijskem anizotropnem jedkanju silicija s samoustavitvijo na zaporno polariziranem spoju N/P silicijeve rezine. Za primer te samoustavitvene tehnike smo izvedli številne eksperimente, ki so izredno zadovoljivo pojasnili sliko dogajanj okrog napetostno tokovnega obnašanja silicija, ko se jedka pri priključenih zunanjih potencialih. Razdelana je bila tvorba pasivacijskega oksida, ki je glavni vzrok za samoustavitav jedkanja in sicer eksperimentalno in teoretično.

Ob vseh spoznanjih, združenih iz zgornjega dela smo zasnovali zadnje poglavje, ki predstavlja realizacijo naše mikrostrukture, to je izdelavo tanke silicijeve membrane. Orisani so uspešni eksperimenti izdelave membrane za silicijev piezorezistivni senzor tlaka s tehniko samoustavitve na N/P in N/P^+ epitaksijskih vzorcih.

V dodatku je predstavljen polprevodniški del izdelave senzorja tlaka, ki zaobjema vse tehnološke korake s podrobnejšimi opombami na mestih z uvedenimi modifikacijami in posebnim poudarkom na spremljanju procesnih parametrov na testnih rezinah z meritvami med procesom.

Naslov naloge: **Simulacija odziva in optimizacija tehnologije silicijevega piezoresistivnega senzorja tlaka**

Avtor: **Uroš Aljančič**, dipl. ing.
Mentor: **prof.dr. Slavko Amon**
Univerzav Ljubljani, Fakulteta za elektrotehniko in računalništvo

Silicij je zelo uporaben material za izdelavo senzorjev, saj:

- ima dobre mehanske lastnosti;
- z veliko natančnostjo se ga da oblikovati v različne geometrijske oblike;
- zahvaljujoč mikroelektronski industriji je dosegljiv na trgu v izredno čisti obliki in v pravilnih kristalografskih strukturah;
- je občutljiv na vrsto fizikalnih veličin, med drugimi tudi na mehanske napetosti.

Slednjo lastnost - občutljivost na mehanske napetosti - se že vrsto let uporablja za izdelavo silicijevih piezoresistivnih senzorjev tlaka. Le-te lahko najdemo v celi

vrsti aplikacij, tako v avtomobilski in letalski industriji kot tudi v robotiki in medicini.

Fizikalne veličine, na katere je silicij občutljiv lahko razdelimo na:

svetloba - fotoelektrični efekt, fotoupornost;

mehanske sile in napetosti - piezoresistivni efekt;

magnetno polje - Hallov efekt, magnetoupornost;

temperatura - temperaturno odvisna upornost;

kemikalije - ionsko občutljiv poljski efekt.

Silicijev senzor tlaka, o katerem govori to delo, je sestavljen iz tanke membrane in v Wheatstoneov mostič povezanih uporov na membrani. Za pretvorbo mehanske napetosti v električni signal izkorišča piezoresistivni efekt.

Naloga je razdeljena na štiri poglavja. V prvem poglavju si bomo pogledali osnovne enačbe, s katerimi lahko opišemo matematični model senzorja tlaka in numerično metodo, s katero bomo enačbe tudi rešili.

Računalniški program, s katerim izračunamo porazdelitev mehanskih napetosti po tanki neenakomerno debeli silicijevi membrani predstavlja drugi del naloge. Poznavanje porazdelitve mehanskih napetosti na membrani je osnova za pravilno načrtovanje senzorja tlaka in za oblikovanje novih elementov.

V tretjem poglavju so opisani optimizacijski postopki na tehnoloških korakih, s katerimi smo zmanjšali temperaturno odvisnost odziva senzorja tlaka, izboljšali homogenost izhodnih karakteristik izdelanih senzorjev ter zmanjšali izmet.

V zadnjem delu je opisana primerjava rezultatov računalniških simulacij in rezultatov meritev, ki smo jih opravili na izdelanih senzorjih.

Naslov naloge: **Polprevodniški senzor svetlobnega spektra**
Avtor: **Žarko Gorup**, dipl.ing.
Mentro: **prof.dr. Jože Furlan**
Univerza v Ljubljani, Fakulteta za elektrotehniko in računalništvo

Delo zajema fizikalno zgradbo, analizo in realizacijo polprevodniškega senzorja svetlobnega spektra. Teorija delovanja temelji na odvisnosti absorbcijskega koeficienta od valovne dolžine pri prehodu svetlobe skozi kristal polprevodnika in selektivnem zbiranju svetlobno generiranih nosilcev v področju zunanjega električnega polja. Poznavanje absorbcijske funkcije omogoča izračun poteka svetlobnih generacij prek strukture in povezavo fotonskega fluksa s tokovnim odzivom senzorja. Senzor, ki je predmet predstavitve, v integrirani obliki združuje dve klasični funkciji: detekcijo in filtriranje svetlobnega fluksa. V osnovi deluje kot dvojni optoFET, modulacija debeline kanala pa omogoča določitev področja svetlobnih generacij, katerih tok je neposredno merjen. Delovanje elementa zahteva nesimetrično zaporno plast v kanalu, ki je s pomočjo zunanje zaporne napetosti zvezno nastavljiva.

V Laboratoriju za elektronske elemente FER je bil senzor projektiran in procesiran. Struktura je dala pričakovani odziv na spremembe valovne dolžine merjene svetlobe v nekaj intervalih valovnih dolžin. Uvodne meritve so bile zadovoljive in prvi rezultati kažejo pot, ki lahko pripelje do izboljšav ter praktične uporabe opisane strukture za manj zahtevne spektralne meritve.

Naslov naloge: **Postopki meritev debeline in oblike materiala z laserskim merilnikom**
Avtor: **Darjan Gradišnik**, dipl.inž.el.
Mentor: **red.prof.dr. Dali Đonlagić**
Univerza v Mariboru, Tehniška fakulteta Maribor

V magistrski nalogi "Postopki meritev debeline in oblike materiala z laserskim merilnikom" je opisan prototipno izdelan merilnik debeline in simulacijsko opisan merilnik oblike. Meritev debeline je postopek, ki ga srečujemo v vseh panogah industrije. Kvaliteten merilnik je nujen pri kontroli in regulaciji valjanja, vlečenja, stiskanja, kovanja itd. raznih materialov.

V avtomatski regulaciji debeline (AGC) nas zanimajo zvezne meritve, ki pa so lahko stične ali brezstične. Zaradi doseganja večjih pretokov materiala se vse bolj uveljavljajo brezstične meritve, pri katerih tudi ne prihaja do poškodb na merilnem mestu. V ta razred sodi tudi laserski merilnik debeline, ki ima pred ostalimi tudi to prednost, da je merjenje debeline njegova primarna funkcija, medtem ko ostali podobni merilniki merijo debelino posredno prek drugih fizikalnih veličin.

Naslov naloge: **Analiza vodenja indukcijskega motorja**
Avtor: **Ludvik Kumin**, dipl. inž. elektrotehnike
Mentor: **prof. dr. Karel Jezernik**
Univerza v Mariboru, Tehniška fakulteta Maribor

V delu je obdelana problematika vodenja pogona z indukcijskim motorjem. Predstavljeni so modeli indukcijskega motorja v različnih koordinatnih sistemih in model uporabljenega bremena. Opisan je postopek za določitev parametrov modela motorja iz rezultatov meritev praznega teka in kratkega stika ter postopek za verifikacijo tako dobljenih parametrov. Na primeru nelinearnega SISO sistema je predstavljena input-state linearizacija nelinearnega modela objekta vodenja. Enak postopek je nato uporabljen za linearizacijo in razklopitev modela indukcijskega motorja. Obdelana sta dva algoritma vodenja indukcijskega motorja, zasnovana na modelu motorja v koordinatnem sistemu rotorskega magnetnega polja: indirektna vektorska regulacija in algoritem vodenja z uporabo input-state

linearizacije. Opisan je eden od možnih načinov za diskretno realizacijo omenjenih algoritmov vodenja. Obnašanje reguliranega pogona je ilustrirano z rezultati simulacij zveznega in hibridnega simulacijskega modela z digitalnim računalnikom.

Naslov naloge: **Modeliranje in vodenje elektronsko komutiranega motorja s permanentnimi magneti**
Avtor: **Marko Lutar**, dipl. inž. elektrotehnike
Mentor: **Prof. dr. Karel Jezernik**
Univerza v Mariboru, Tehniška fakulteta Maribor

Delo vsebuje predstavitev elektronsko komutiranega motorja s permanentnimi magneti (EKM s PM) in primerjavo s podobnimi motorji (enosmerni motor in sihronski stroj). Izpeljan je model v naravnih koordinatah, primeren za računalniške simulacije, in model v d-q koordinatah, na osnovi katerega je opravljeno načrtovanje vodenja z mikrokrmilnikom. Zasnovana je večzančna regulacijska struktura z notranjo tokovno zanko in zunanjo zanko za vodenje gibanja. Predlagana sta dva različna algoritma za vodenje navora oz. toka, ki zmanjšujeta valovitost, ki jo vnaša digitalna realizacija. Predstavljen je princip pulzno-širinske modulacije in narejena primerjava med sinusno in izboljšano modulacijo, ki povečuje izkoristek napetosti razsmernika. Opravljene so simulacije tako zgrajenega servo pogona. Na osnovi rezultatov simulacij je opravljen pregled vplivov perturbacije parametrov na obnašanje regulacije. V laboratoriju smo na EKM s PM preizkusili vodenje navora oz. toka s krmilnikom, ki mu je za povečanje hitrosti izračunavanja dodan transputer. Rezultati simulacij in eksperimenta so potrdili teoretično delo.

Naslov naloge: **Numerično računanje tridimenzionalnih problemov s permanentnimi magneti po metodi končnih elementov ob uporabi reduciranega skalarnega potenciala**
Avtor: **mag. Igor Tičar**, dipl.inž.el.
Mentor: **red.prof.dr. Božidar HRIBERNIK**
Univerza v Mariboru, Tehniška fakulteta Maribor, Elektrotehnika, računalništvo in informatika

Delo predstavlja prikaz izboljšav pri računanju statičnih magnetnih polj z metodo končnih elementov, ob uporabi reduciranega magnetnega skalarnega potenciala. Izkaže se, da se lahko izognemo računskim napakam v področju visoke permeabilnosti z uporabo t.i. "robovnih" elementov. Z njihovo pomočjo opišemo vrtinčni del magnetnega polja. Prikazane so metode za reševanje problemov stacionarnega magnetnega polja, vsebujoče predstavitev z robovnimi elementi. Posebej je nakazana možnost reševanja v primeru, ko je poznana tokovna porazdelitev. Podan je model permanentnega magneta, ob predpostavki konstantne remanentne gostote ter poznanih krivuljah magnetenja v direktni in prečni smeri.

Dana sta dva tridimenzionalna problema, v prvem primeru s permanentnimi magneti, v drugem pa tudi z dodatnim vzbujanjem. Pokazana je primerjava med računalniško rešitvijo in med merjenimi vrednostmi.

MIEL-SD'94 Announcement and call for papers

September 28. - 30. 1994
TERME ZREČE - ROGLA, SLOVENIA

ORGANIZER

MIDEM - Society for Microelectronics, Electronic Components and Materials
Dunajska 10, 61000 Ljubljana, SLOVENIA

SPONSOR

Ministry of Science and Technology of Republic Slovenia

PROGRAM COMMITTEE

Borut Lavrenčič, Slovenia
Iztok Šorli, Slovenia
Slavko Amon, Slovenia
Giovanni Soncini, Italy
Radomir Kužel, Czech Republic
Marko Hrovat, Slovenia
Janez Trontelj, Slovenia
Marija Kosec, Slovenia
Spomenka Beseničar, Slovenia
Bojan Jenko, Slovenia
Monika Jenko, Slovenia

ORGANIZING COMMITTEE

Franc Jan, Slovenia
Darko Belavič, Slovenia
Meta Limpel, Slovenia
Miloš Komac, Slovenia
Brane Kren, Slovenia
Rudi Ročak, Slovenia

GENERAL INFORMATION

MIEL-SD'94 is an international conference organized by MIDEM, uniting two meetings with long tradition: 22nd International Conference on Microelectronics and 30th Symposium on Devices and Materials.

Both conferences are well known through the distinguished guest speakers. Several hundred scientists from all over the world took part in the MIEL-SD conferences in the past. The goal of connection and building of friendship among the scientists and their companies remains the keystone of the organizer.

The conference will be held in TERME ZREČE - ROGLA, Slovenia, a picturesque tourist resort, **SEPTEMBER 28th - 30th.**

ORIGINAL PAPERS IN THE FOLLOWING AREAS ARE SOLICITED:

- Novel monolithic and hybrid circuit processing techniques
- New device and circuit design
- Process and device modeling
- Semiconductor physics
- New electronic materials and applications
- Electronic materials science and technology
- Optoelectronics
- Reliability and failure analysis
- Microelectronics education

Presentation of microelectronics companies and laboratories will be held after afternoon sessions.

INVITED PAPERS:

The following speakers will present introductory review papers before sessions:

1. N. SETTER, Ecole Polytechnique Federal de Lausanne , Switzerland:
   "Ferroelectric Thin Films for Micro Electro Mechanical Applications"
2. J.TRONTELJ, Faculty of Electrical and Computer Engineering, Ljubljana, Slovenia:
   "Trends in Mixed Signal ASIC Design"
3. R.DELL' AQUA, MiTeCo Microelectronics Technology Consultants, Pavia Italy:
   "Sensors: A Great Chance for Microelectronics Technologies"
4. Z. SITAR, Institute of Quantum Electronics, ETH, Zuerich, Switzerland:
   "MBE in Ferrolelectrics, Technique and Analysis"
5. H.VIEFHAUS, Max Planck Institute für Eisenforschung GmbH, Düsseldorf, Germany:
   "Surface, Interface and Thin Film Analysis in Material Science"

PREPARATION OF SUMMARY AND ABSTRACTS

A summary not longer than 60 lines is required for review. This summary must state clearly what new results have been obtained and what techniques have been used.

RECEIPT DEADLINE:

Deadline for receiving the summaries is **May 15th.**

PREPARATION OF THE PAPERS

The papers have to be prepared on maximum **6 pages A4** format, ready for reproduction in the Proceedings. Further information will be given to the authors of accepted papers by **June 1st.**

RECEIPT DEADLINE

Deadline for the manuscript of the paper is **September 1st.**

CONFERENCE PROCEEDINGS

Invited papers and accepted papers will be published in the conference proceedings distributed at the conference registration.

LANGUAGE

Official conference language is English.

REGISTRATION

The registration fee is US$ 300. Members of the MIDEM Society and Conference sponsors have 20% discount while MIDEM members have 30% discount. The fee includes free access to all conference events, including welcome cocktail party and the conference dinner on September 29th.

IMPORTANT DATES

Summary deadline: May 15th
Notification of acceptance: June 1st
Advanced Program: August 1st
Paper deadline: September 1st
Final conference program: at registration, September 28th

Program and organizing committee:

MIDEM
Dunajska 10
61000 Ljubljana, SLOVENIA
tel.+386-61-312 898, fax.+386-61-319170
Secretary of the conference:
Mrs.Meta Limpel

Vesti

SAJMOVI I KONFERENCIJE

EXPONET VIENNA 94

U Beču je u vremenu od 8. do 10. februara ove godine održan "Exponet Vienna 94"-međunarodni sajam i konferencije. Evo što o sajmu kaže Angela Rummel, Project Manager of "Exponet Vienna 4":

The secret of the exponent success is its concentration on the market. Companies require a professional platform for the high tech products and services. Exacting fair visitors desire competent consultation, convincing demonstrations and complete solutions. By utilizing this concept, exponet has become the largest and most successful trade fair for networking, enterprise computing and telecommunications in Germany and Europe.

"Exponet Vienna 94" adapts the valued principles of this successfull concept to a highly specific market situation: Not only does it fill the needs of the Austrian and eastern neighboring countrie's trade fair demands, but also offers the Austrian and European information and communciations industry its first international trade forum in order to raise the level of discussion concerning the eastern market's investment demands for information and communications technology to the decision-making level.

"Exponet Vienna ", as turntable of trade for the information and technology transfer between West and East, is the ideal event to pave the way to valuable business relations in various levels. The "East/West Cooperation Talks" not only offers first hand to all those interested in East-West business through economic institutions and chambers of commerce of Eastern European countries, information concerning business partnerships, business locations etc., but also brings potential partners at the fair into first talks and makes contacts happen.

Vienna being international market place, gateway to the East, and geographical and historical mediator of western economic power, inventiveness and technology, is certainly predestined for an international market event such as "Exponet Vienna 94."

Na sajmu je učestvovalo 78 izlagača iz 11 država. Zastupljenost izlagača iz pojedinih država bila je:

Austrija	38 izlagača
Belgija	2 izlagača
Engleska	3 izlagača
Holandija	1 izlagač
Hrvatska	5 izlagača
Izrael	1 izlagač
Luksemburg	1 izlagač
Mađarska	5 izlagača
Njemačka	15 izlagača
Slovenija	4 izlagača
Švicarska	3 izlagača

Posebno je još na "East/West Cooperation Talks" bilo prijavljeno 19 učesnika i to iz:

- Austrije 5 učesnika
- Češke 2 učesnika
- Hrvatske 3 učesnika
- Poljske 2 učesnika
- Rusije 3 učesnika
- Slovačke 1 učesnik
- Slovenije 1 učesnik
- Ukrajine 1 učesnik

Nemoguće je u kratkome prikazu opisati i spomenuti što se sve nudilo na sajmu. Da bi se dobila približna slika o raznovrsnosti ponude dovoljno je spomenuti da je sajam bio podijeljen u 12 tematskih sekcija:

1. INFORMATION AND COMUNICATIONS SYSTEMS
2. COMUNICATIONS NETWORKS
3. TERMINALS
4. NETVORK MONITORING SYSTEMS
5. TRANSMISSION TECHNOLOGY/ SYSTEMS
6. TRANSMISSION ACCESSORIES
7. UNITS AND MODULS
8. SOFTWARE
9. CONSULTANCY
10. SERVICES
11. INFORMATION SERVICES
12. OTHERS

Prisustvo izlagača iz Hrvatske i Slovenije na sajmu bilo je zamjećeno, iako čudi da, obzirom na blizinu Beča, broj izlagača iz Hrvatske i Slovenije nije bio veći.

NAJBOLJE PRODAVANE KNJIGE U KALIFORNIJI

ELEKTRONIKA

1. *Art of Electronics*, 2. izdanje
   Pisci: Paul Horowitz i Winifield Hill.
   Izdavač: Cambridge University Press, 1990.
   Cijena: $27,95.
2. *Art of Electronics Student Manual*
   Pisac:Paul Horowitz
   Izdavač: Cambridge University Press, 1992.
   Cijena: $47,95
3. *Basic Electronics*, 7. izdanje
   Pisac: Bernard Grob.
   Izdavač: Glencoe
   Cijena: $47,95
4. *JPEG Still Image Data Compression*,
   Pisac: William Pennebaker,
   Izdavač: Van Nostrand Rinehold, 1992
   Cijena: $59,95

KOMPJUTERSKE ZNANOSTI

1. *TCP/IP Network Administration*,
   Pisac: Craig Hunt
   Izdavač: O'Reilly & Associates, 1992
   Cijena: $29,95
2. *Nanosystems Molecular Machinery*,
   Pisac: Eric Drexler,
   Izdavač: John Wiley & Sons, 1992,
   Cijena: $24,95
3. *Ciberats*
   Pisac: Linda Jacobsen,
   Izdavač: Publisher's Group West, 1992.
   Cijena: $22,95
4. *Nanotechnology Research*
   Pisac: B.C. Crandall,
   Izdavač: MIT Press, 1993
   Cijena $39,95

Ovu listu je sastavila, za časopis "Electronic Design",knjižara "Stacey's Bookstore", Palo Alto, Kalifornija.

POSLOVNO TEHNOLOŠKE NOVOSTI

E-MAIL HELPS ENGINEERS DO HIGH-LEVEL DESIGN

Engineers can get quick help with their high-level design problems through an innovation that exploits both e-mail and advanced information-retrieval technology. The solv-It! customer-support system, developed by Synopsys inc, Mountain Wiew, Calif., consist of a large knowledge base that users access through e-mail to find answers at any time of the day or night. Solv-It! includes more that 1000 articles with about 200 additional articles expected to be added every month. All articles are indexed and ranked for their relevance to solving users' questions. It also includes information directly from Synopsys' technical staff, such as answers to questions frequently asked of the company's hotline engineers. Excerpts from documentation, application notes, and release notes; bug fixes and workarounds; information on library development; and system-administration issues can all be accessed without delay through the e-mail syste. Response time averages between two and five minutes.

MODEL REPLACE POWER DEVICE PROTOTYPES

A technology agreement between Analogy Inc., Beaverton, Ore., and Motorola's Semiconductor Products Sector, Phoenix, Ariz., aims to eliminate hardvare prototypes of new power components and reduce design-cycle time. Under the terms of the agreement, Analogy and Motorola will jointly develop virtual prototypes (software models) of components that will replace actual hardware samples for customer evaluation. Ultiately, by eliminating an often lengthy prototype-evaluation phase, time to market will be shortened substantially. Motorola will provide proprietery process-technology information, and Analogy will then create the models with its Saber mixed- signal simulator. Analogy's Mast analog hardware-description language is the enabling technology behind the virtualparts. It can accurately model electrical, mechanical, and hydraulic behavior. And because native units are employed rather than electrical eqivalents, the models are intuitive drive. The library will ultimately comprise 50 parts ranging from IGBTs and MOSFETs to fluorescent ballast drivers.

AGREEMENTS SPURS ZINC-AIR BATTERY DEVELOPMENT

A licensing agreement between AER-Energy Resources Inc., Smyrna, Ga., and Westinghouse Electric Corp., will accelerate the development of long- running and rechargeable zinc-air batteries, potentially doubling or even quadrupling the run time of portable computers. Run times for portable notebook and pen-based computers of 8 hours or more are being pursued by AER. The agreement is exclusive for portable computers and non-exclusive for all other portable products. The proprietary technology licensed from Westinghouse - an air cathode that absorbs oxygen from air to charge - allows the batteries to achieve a high energy-density-to-weight ratio. This is partly de to the fact that zinc-air batteries don't require heavy metal electrode like nickel or lead. The technology was orifinally developed at Westinghose's Science and Technology Center, Youngwood, Pa. This past august, AER began manufacturing zinc-air batteries.

SILICON ICs TO CUT NOISE POLLUTION

Signal-processing ICs and highly efficient power amplifiers developed by Harris Semiconductors, Melbourne, Fla., are expected to aid in the war on noise pollution. Harris and Noise Cancellation Technologies NTC), Stamford, Conn., will yointly develop and manufacture proprietary silicon ICs that can implement NTC's active noise-reduction technology. The basis noise- cancellation technology involves using a michrophone to pick up the noise sources, digitizing the noise signals, and then applying those signals to a DSP IC. The processor analyses the signal in real time and "calculates" a train of digital words equal and opposite to the noise signal. This so- called "anti-noise" signal is converted to analog form, amplified for both amplitude and power levels, and applied to one or more loudspeakers whose outputs cancel (nul out) the original noise. Harris brings its analog signal-processing IC techniques to the project along with its on-chip high- frequency (1-MHz) power pulse width-modulation (PW) IC process. Harris' wide-band op aps, multiplexers, and data converters will handle the analog signals between the microphone and the DSP circuit, and between the DSP circuit and the power amplifier. The PWM circuits can be used in class-D switching power amplifiers with efficiencies topping 0%.

NEXT-GENERATION GAMES TO USE 64-BIT MUSCLE

A 3D-capable game for under $250 is the ultimate goal of designers at Nintendo Co. Ltd., Tokyo, Japan, and Silicon Graphics Inc., Mountain View, Calif., who will collaborate to develop a 64-bit chip set for the game console. The joint agreement couples the game expertise of Nintendo and the visual computing technologies of Silicon Graphics (used it such movies as Jurassic Park and Terminator 2). Together, they will produce Reality Immersion Technology (RIT) to allow players to step inside real-time 3D worlds. At the heart of the system will be the MIPS multimedia Engine chip set-a 64-bit MIPS RISC micro processor, a graphics coprocessor, and one or more custom chips. The chip set's computing power will exceed the throughput of most workstations. For instance, at a 100-MHz clock, the CPU executes over 100 mips and 100 MFLOPS. The graphics subsystem also matches most moderate-performance more workstations. It handles 24-bit color images and generates more than 100,000 polygons (50-pixel meshed triangles) per second while performing real-time antialiased 3D texture mapping to produce realistic graphic iages. The set will also handle CD-quality audio and provide video resolution better than NTSC or PAL. Graphics' graphic library. The technology's firs implementation will debute this year as an arcade-style game, and is expected in a hoe game console by late 1995.

3D DISPLAY USES POSITION SENSING, FAST GRAPHICS

Engineers at NEC Corp.'s Central Research Laboratories in Tokyo, Japan have come up With a novel 3D graphic viewer that doesn't require special glasses or viewing screens. The system consist of very fast 3D graphics software, a sophisticated 3D position sensor, and a conventional 2D LCD screen mounted on a mechanical arm that can move in any direction. When the user moves the screen into a new orientation, the position sensor reports the new orientation to the graphic software, which calculates the new perspective of the object from the user's point of view. In addition to the basic ability to obtain a new view of the object by moving the screen, the real- time graphics software also supports zooming for closer observation, section cutting for internal views of the object. recording and playback of viewpoint-position data, and data conversion to third-party CAD software tools. NEC expects the technology to find applications in CAD-tool environments, education, entertainment and a presentation device.

COLOR PRINTER CONSORTIUM FORMED

A newly formed industry consortium, the Assocation of Thermal Transfer Technology (ATC), will help supply more advanced color-printer-based products while promoting the technologi's application-specific advantages. The color termal-transfer printers are based on ink-jet technology, which is responsible for the high-quality output. They're suitet for such applications as CAD, imaging, graphic arts, and electronic publishing.

The ACT consortium consists of color termal-transfer printer manufacturers and suppliers, including Armor Nantes, Calcop, Diafoil, Fujicopain, International Imaging Materials, Mitsui Plastics, and Tektronix. Headquartered in Buffalo, N.Y., the group will serve as an umbrela for the effort and will work with members on technology-advancement seminars and other pursuit.

SILICON BIPOLAR FTs CHASE GaAs FETs

For two decades, Galium Arsenide has been "tomorrow's" technology. As ever- faster silicon bipolar-junction transistors (BJTs) arrive from R&D labs, this may remain true. At the LSI Lab of NTT developped a 0.5 μm, double- polysilicon bipolar process SST1C), builds npn transistors providing an f_t of 40.7 GHz at a collector-emitter voltage (V_{ce}) of 1V. When employed in an ECL circuit, gate delays run 23 ps at a collector current of 2.4mA. 8:1 frequency dividers were made that handled input signals of 22 GHz. The developers say combining trench isolation with a "damage free" diffusion technique, which creates the shallow base, is the key to SST1C's performance. the technique consists of ion implanting a thin oxide with boron, following it with rapid thermal annealing (RTA), which form the active base region, and the removing the thin oxide. After an emitter opening is created, an arsenic-doped polisilicon emitter is formed and driven in with more RTA. The result is a BJT with minimum base resistance and parasitic capacitance so that f_{max} approaches f_t . Hitachi researchers come up with a biCMOS process that combines very small npn transistors (9.47 μm^2) with CMOS FETs with a gate lenght from 0.4 to 0.6 μm. The npns employ a sidewall polycide-base technology, which builds npns needing less silicon area that the FETs. These npns achieved an f_t of 38 GHz at a V_{ce} 3 V. The use of low-energy base implantations followed by RTA helps the achieve the performance. In a comparasion of gate delays between CMOS and biCMOS gates on the process, the biCMOS gates showed delays about half that of the CMOS gates. For example , while driving 0.6 pF, the biCMOS gate delay run 0.5 ns; the CMOS gate delay ran 1 ns. The BCTM covers a wide range of analog, digital, circuit design process, and simulation technologies.

New CMOS Process for up to 35V at AMS

AMS announces the availability of a new CMOS process suited for high voltage ASIC solutions. Besides the standard low voltage MOS transistors also high voltage N and P MOS transistors up to 35V, N-junction FETs up to 35V, isolated bipolar transistors and DMOS transistors can be realized on the same ASIC through the new AMS technology; until recently products in CMOS could be implemented only for applications ranging from 5.5 to 10V, depending on the process. The 2μ single-poly double-metal CMOS process (designated as "CBK" at AMS) was primarily developed for ASICs incorporating complex digital parts with high speed, high density elements.

Lower power consumption, fast switching capabilities and applicability to a wide range of automotive and industrial performance requirements are further key benefits of this advanced AMS process, being especially suited to withstand high voltage spikes which typically occur in such environments.

AMS, with its in-house research and development department and state-of-the-art manufacturing equipment, now can provide more than 40 proven BiCmos and CMOS processes.. Because of AMS's parallel suport of new, traditional and mature process technologies, AMS' process flexibility guarantees the duration of any one process as long as a specific product is required.

Afurther advantage for the AMS customer is the availability of 2 μ, 1.2 μ and 1 μ AMS CMOS cell libraries. Since all three libraries are functionally equivalent, the customer can easily migrate with an existing design to more advanced technologies. Together with the proven 2m digital library the new 2m process represents the ideal solution for high voltage ASICs.

Schloß Premstätten
A-8141 Unterpremstätten, Austria
Telex 312547 ams a
FAX (03136)52 501, 53 650
TEL (03136) 500-0
Dr. Conrad Heberling, ext. 277

1993: AMS sucessful in the international telecom market

As in the past years, AMS - the No. 1 in the European market in the field of analogue/digital ASICs - has succeeded to continuously increase its **order entry:** from 735 MAS 1992 **to more than one billion AS (1,066.8**

MAS·) 1993. Gross sales were increased from 734.4 MAS 1992 to **823 MAS· 1993** with 600 employees.

A reason for the further positive development of AMS - 45% growth in the order entry 1993 relative to 1992 - results in the use of ASICs in the strongly growing telecommunications market, mainly mobile phones. According to Dataquest, the market for mobile phones has increased at a rate of 650,000 units sold 1993 in Europe and will grow at a rate of 212% per year to 4.3 milion units till 1997. Outside of Europe higher growth rates will be expected, though in smaller markets. It is especially for this market segment that AMS develops and produces taylor made solutions and product innovations which are today state-of-the- art.

In the field of **telecommunications** AMS is not only furnished with relevant concepts and specific products for the segment mobile communications but also serves the analogue and strongly evolving digital markets with innovative products: single chip telephones, diallers, line adapters, modems, codecs, filters, ringers and speech amplifiers.

Important market segments which AMS serves: **Automotive** (electronics for safety belt tensioners, ignition and motor controls, airbags and lighting) and **industrial electronics** (ICs for analogue and digital controls for civil aviation, advanced instrumentation, enhanced robotics and environmental protection).

Further reasons for the continued dynamic growth of AMS are:

- the continuity in its internationalization process: Worldwide cooperations with universities and companies as well as the securing of international markets and partnerships under the aspect of new technologies and products;
- the fact that AMC houses IC design and production "under one roof". Full production is in Unterpremstätten, i.e. from the concept up to the finished product; the advantage - shortest lead times and highest quality.

Note: Only recently AMS has introduced the first single chip featuring all the functions required of an electronic telephone and reducing the component count of the average telephone by 80%! (Licencing of this AMS product to SAMES, South Africa)

· preliminary figures

Schloß Premstätten
A-8141 Unterpremstätten, Austria
Telex 312547 ams a
FAX (03136)52 501, 53 650
TEL (03136) 500-0
Dr. Conrad Heberling, ext. 277

South African Micro-Electronic Systems Ltd. (SAMES) and Austria Mikro Systeme International AG (AMG) announce first Product Licence and Wafer Foundry Agreement

South African Micro-Electronic Systems Ltd. (SAMES), currently the only commercial manufacturer of integrated circuits in Southern Africa and **Austria Mikro Systeme International AG (AMS)**, the Number One mixed signal ASIC (application specific integrated circuits) manufacturer in Eurpoe, announce the first major international licence and wafer foundry agreement.

The terms of the agreement are that SAMES will, for a lincencing fee, endeavour in the production and sale of the AMS Single Chip Telephone Circuit - recently developed by AMS - and that SAMES will engage in the sale of this product for the entire region of South Africa: The Single Chip Telephone is programmable for use worlwide and utilizes new speech amplifier and repertory functions,a melody generator and dialler all on a single chip - an integrated circuit that performs all the functions required of an electronic telephone. The advantage of this new product is its simple use and high comfort, the very low operating power consumption, the optimum high integration and the fact that it drastically reduces the external component count by 80%. The announcement of the AMS single chip has spun off a worldwide demand for this highly innovative product.

SAMES was established to bring the benefits of microelectronics technology to industries on the Southern African subcontinent. SAMES and AMS are both privately owned companies and have, both in their fields, become international players offering state-of-the-art technology from design through all aspects of manufacturing and test, to field support of its internationall customers.

"The agreements between SAMES and AMS represent a further important strategic goal in the internationalization of SAMES' activities", said Mr. Heinz Fellinger, Managing Director and CEO of SAMES, when announcing the deal. SAMES has established itself as a major vendor for telephone ICs in the international market place. The innovative single chip telephone circuit

developed by AMS is a logical extension of the SAMES product range for telephony and cements SAMES' leadership in this market.

SAMES has recently commissioned its state-of-the-art 6 inch wafer fabrication facility with submicron fabrication capabilities at the cost of $50 000 000 and can thus offer AMS very competitive silicon foundry manufacturing services. Backed by major multinational concerns in the electronics field, e.g. Siemens Ltd. and Altech, SAMES is the ideal partner for AMS.

According to AMS President and CEO, Mr. Horst Geber, the agreement between SAMES and AMS represents a new accomplishment and milestone in the history of the company in that it sets the start for the worldwide transfer of Austrian know-how, R & D and engineering in ASIC technology - the proof that AMS has successfully invested its resurces.

This product licence agreement follows a number of highly successful cooperations and agreements between AMS and a number of international partners in the recent past such as with Pioneer Semiconductor Corporation, USA and Semiconductor Complex Limited, India.

AMS has invested a figure equivalent to 20% of 1993 first half sales in capital equipment to increase capacity following a 31% increase in bookings over the same period. The investment gives the company a strong platform for growth during 1994.

The results for the first half of 1993 - the first ever to be released since thr company was floated on the Vienna Stock Exchange and the SEAQ in London on July 12, 1993 - reveal a growth to 359 million ATS (Austrian Schiling) in sales (from 346 million ATS), a significant achievement in the current recessionary climate. Earnings have also incresed by more than 10% over the same period of the last year.

Particularly strong in the telecommunications, automotive and industrial sectors, AMS is anticipating that the growth in bookings will be considerable increase over the target set at the beginning of the year.

Schloß Premstätten
A-8141 Unterpremstätten, Austria
Telex 312547 ams a
FAX (03136)52 501, 53 650
TEL (03136) 500-0
Dr. Conrad Heberling, ext. 277

1994: More process technologies with more frequent departures of AMS' Multi-Product Wafer Train™

Austria Mikro Systeme International AG (AMS) announces its new 1994 Multi-Product Wafer (MPW) Train Service Schedule for the 0.8 µ, 1 µ, 1.2 µ and 2 µ CMOS processes and now also for the 1.2m BiCMOS process. This capability, also known as shared silicon technology, allows the parallel processing of several devices on one wafer. AMS is believed to be one of the only semiconductor fascilities in Europe currently handling and providing full in- house services for Multi-Product Wafer Projects.

The benefits of AMS' MPW Train Service for customers is that circuit development charges are reduced by up to 50% due to reduced mask shop and fabrication costs. Span times are also kept at a minimum. Furthermore, MPWs allow at a very little extra cost the parallel study of design options which lowers the risk of redesign; the customer can evaluate the performance of several design options at once without lengthening development times.

AMS groups devices with compatible processes on a wafer. AMS receives a tape input from the customer and delivers packaged parts. More runs are now available from each 0.8µ, 1µ, 1.2µ and 2µ CMOS process and for the new 1.2 µ BiCMOS process.

Participation is guaranteed provided customer's data input arrives on time. The practical implementation of MPW runs at AMS has succeeded in the recent past due to significant efforts initiated in data preparation, mask making and assembly and the coordination of these activites. AMS' successful installation of a MPW service was made possible because of the company's highly flexible and integrated facility which provides the necessary in- house mask making, data preparation, wafer fabrication, assembly and test.

For the "Wafer Train" schedules please contact your local sales office or AMS, Corporate Communications, Schloß Premstätten, 8141 Unterpremstätten, Austria.

AMS MPW runs 1994/95

Process	Tape in	Samples out
2.0 µ CMOS: CBA/CBB/CBE CBH•/CBM•/CBO• CBQ•/CBR•/CBS•	25.03.94	20.05.94
	03.06.94	29.07.94
	12.08.94	07.10.94
	21.10.94	16.12.94
	06.01.95	03.03.95
1.2µ CMOS: CAB/CAE CAQ•	18.02.94	15.04.94
	29.04.94	24.06.94
	08.07.94	02.09.94
	16.09.94	11.11.94
	25.11.94	20.01.94
	03.02.95	31.03.95
1.0µ CMOS: CZB/CZE	04.03.94	29.04.94
	01.07.94	26.08.94
	04.11.94	30.12.94
	10.02.95	07.04.95
0.6µ CMOS: CYB	18.03.94	13.05.94
	17.06.94	12.08.94
	30.09.94	25.11.94
	20.01.95	17.03.95
1.2µ BiCMOS: BAE	25.02.94	20.05.94
	25.05.94	19.08.94
	30.09.94	23.12.94
	27.01.95	21.04.95

•These processes share only the mask set with the MPW, but are processed on a seperate wafer run. ES are available two weeks later than shown in the calendar. There is also an extra charge.

Schloß Premstätten
A-8141 Unterpremstätten, Austria
Telex 312547 ams a
FAX (03136)52 501, 53 650
TEL (03136) 500-0
Dr. Conrad Heberling, ext. 277

KOLEDAR PRIREDITEV 1994

APRIL

10.04. - 15.04. 1994
PHOTOVOLTAIC SOLAR ENERGY CONFERENCE AND EXIBITION
Netherlands
(Info.: Robert Hill, Tel.: 44 91-227-4594)

11.04. - 14.04.1994
1994 INT. RELIABILITY PHYSICS SYMPOSIUM
San Jose, California, USA

12.04. - 14.04.1994
SEMICON EUROPA
International Conference and Exibition
Geneva, Switzerland

21.04. - 24.04.1994
CONFERENCE ON SEMI-INSULATING III-V MATERIALS
Krakow, Poland
(Info.: William Ford, Tel.: (408) 433-2222,CA)

39th Annual Gathering KOREMA
ZAGREB, Hrvatska
(info. 385 41 611 944 Ext.127)

MAJ

01.05. - 04.05. 1994
44th ELECTRONIC COMPONENTE AND TECHNOLOGY CONFERENCE
Washington DC, USA
(Info.: Dr. Rao Tummals, Tel.: (914) 894-5647)

15.05. - 18.05. 1994
CCIC '94 CUSTOM INTEGRATED CIRCUITS CONFERENCE
San Diego, CA, USA
(Info.:Melissa Wilderkehr,Tel.:(202) 986-1137)

23.05. - 27.05. 1994
MIPRO 94
OPATIJA, Hrvatska
(Info. 385 51 211 051)

30.05. - 03.06. 1994
ESREL '94 EUROPEAN SAFETY AND RELIABILITY
La Baule, France
(Info.: Claude Salmon (33) 61 27 34 72)

JUNIJ

06.06. - 08.06.1994
MICROTECH 94
Anugrana, Italy

07.06. - 10.06. 1994
ICRMS '94 INT. CONFERENCE ON RELIABILITY, MAINTAINABILITY AND SAFETY
Beijing, China
(Info.: Xu Fu Rong, Tel.: (861) 838 1147)

07.06. - 09.06.1994
VLSI TECHNOLOGY SYMPOSIUM
Honolulu, Hawai
(Info.: James T. Clemens (908) 582-2800)

12.06. - 15.06. 1994
TTFS 94 (WORKSHOP ON THICK AND THIN SENSORS

AND THEIR APPLICATIONS IN EKOLOGY
Szklaska Poreba, Poland

21.06 - 23.06. 1994
INT.CONFERENCE ON APPLIED SYNERGETICS & SYNERGETIC ENGINEERING
Erlangen, Germany
(Info.: Thomas Wagner Tel.: 49-9131-776-544)

21.06 - 24.06.1994
INT.CONFERENCE ON NUMERICAL ANALYSIS OF SEMICONDUCTOR DEVICES & INTEGRATED CIRCUITS
Dublin,Ireland
(Info.: Paulene McKeever Tel.: 353-1-679-7655)

JULY

04.07. - 07.07.1994
INTERNATIONAL VACUUM MICROELECTRONICS CONFERENCE
Grenoble, France
(Info.: D: Celier, Tel.:33 1 42 78 15 82)

13.07. - 15.07. 1994
INTERNATIONAL ELECTRON DEVICES & MATERIALS SYMPOSIUM
Hsin Chu, Taiwan
(Info.: Chien Ping Lee, Tel.: 886-35-726100)

AUGUST

23.08. - 26.08. 1994
INTERNATIONAL CONFERENCE ON SOLID STATE DEVICES AND MATERIALS
Yokohama, Japan
(Info.: SSDM '94 Business Center, Tel.: 81-3-5814-5823)

SEPTEMBER

05.09. - 07.09. 1994
ELECTROCERAMICS IV
INTERNATIONAL CONFERENCE ON ELECTRONIC CERAMICS & APPLICATIONS
RWTH Aachen, Germany

28.09. - 30.09. 1994
22nd INTERNATIONAL CONFERENCE ON MICROELECTRONICS, MIEL '94
30th SYMPOSIUM ON DEVICES AND MATERIALS, SD '94
TERME ZREČE,Rogla, Slovenija
(Info.: Meta Limpel, Tel.: 386 61 312 898)

OCTOBER

04.10. - 07.10. 1994
ESREF '94
5th EUROPEAN SYMPOSIUM ON RELIABILITY OF ELECTRON DEVICES, FAILURE PHYSICS AND ANALYSIS
Glasgow, Scotland
(Info.: G.M.Brydon, Tel.: 44 604 408647)

NAVODILA AVTORJEM

Informacije MIDEM je znanstveno-strokovno-društvena publikacija Strokovnega društva za mikroelektroniko, elektronske sestavne dele in materiale-MIDEM. Časopis objavlja prispevke domačih in tujih avtorjev, še posebej članov MIDEM, s področja mikroelektronike, elektronskih sestavnih delov in materialov, ki so lahko:

izvirni znanstveni članki, predhodna sporočila, pregledni članki, razprave z znanstvenih in strokovnih posvetovanj in strokovni članki.

Članki bodo recenzirani.

Časopis objavlja tudi novice iz stroke, vesti iz delovnih organizacij, inštitutov in fakultet, obvestila o akcijah društva MIDEM in njegovih članov ter druge relevantne prispevke.

Strokovni prispevki morajo biti pripravljeni na naslednji način

- 1. Naslov dela, imena in priimki avtorjev brez titul.
- 2. Ključne besede in povzetek (največ 250 besed).
- 3. Naslov dela v angleščini.
- 4. Ključne besede v angleščini (Key words) in podaljšani povzetek (Extended Abstract) v angleščini.
- 5. Uvod, glavni del, zaključek, zahvale, dodatki in literatura.
- 6. Imena in priimki avtorjev, titule in naslovi delovnih organizacij, v katerih so zaposleni.

Ostala splošna navodila

1. V članku je potrebno uporabljati SI sistem enot oz. v oklepaju navesti alternativne enote.

2. Risbe je potrebno izdelati s tušem na pavs ali belem papirju. Širina risb naj bo do 7.5 oz. 15 cm. Vsaka risba, tabela ali fotografija naj ima številko in podnapis, ki označuje njeno vsebino. Risb, tabel in fotografij ni potrebno lepiti med tekst, ampak jih je potrebno ločeno priložiti članku. V tekstu je potrebno označiti mesto, kjer jih je potrebno vstaviti.

3. Delo je lahko napisano in bo objavljeno v kateremkoli jugoslovanskem jeziku v latinici in v angleščini.

Uredniški odbor ne bo sprejel strokovnih člankov, ki ne bodo poslani v dveh izvodih.

Avtorji, ki pripravljajo besedilo v urejevalnikih besedil, lahko pošljejo zapis datoteke na disketi (1.2 ali 1.44) v formatih ASCII, wordstar (3.4, 4.0), wordperfect, word, ker bo besedilo oblikovano v programu Ventura 2.0. Grafične datoteke so lahko v formatu HPL, SLD (AutoCAD), PCX ali IMG/GEM.

Avtorji so v celoti odgovorni za vsebino objavljenega sestavka. Rokopisov ne vračamo.

Rokopise pošljite na naslov

Uredništvo Informacije MIDEM
Elektrotehniška zveza Slovenije
Dunajska 10, 61000 Ljubljana

UPUTE AUTORIMA

Informacije MIDEM je znanstveno-stručno-društvena publikacija Stručnog društva za mikroelektroniku, elektronske sestavne dijelove i materijale - MIDEM. Časopis objavljuje priloge domaćih i stranih autora, naročito članova MIDEM, s područja mikroelektronike, elektronskih sastavnih dijelova in materijala koji mogu biti:

izvorni znanstveni članci, predhodna priopćenja, pregledni članci, izlaganja sa znanstvenih i stručnih skupova i stručni članci.

Članci će biti recenzirani.

Časopis također objavljuje novosti iz struke, obavijesti iz radnih organizacija, instituta i fakulteta, obavijesti o akcijama društva MIDEM i njegovih članova i druge relevantne obavijesti.

Stručni članci moraju biti pripremljeni kako slijedi

- 1. Naslov članka, imena i prezimena autora bez titula.
- 2. Ključne riječi i sažetak (najviše 250 riječi).
- 3. Naslov članka na engleskom jeziku.
- 4. Ključne riječi na engleskom jeziku (3Key Words) i produženi sažetak (Extended Abstract) na engleskom jeziku.
- 5. Uvod, glavni dio, zaključni dio, zahvale, dodaci i literatura.
- 6. Imena i prezimena autora, titule i naslovi institucija u kojima su zaposleni.

Ostale opšte upute

1. U prilogu treba upotrebljavati SI sistem jedinica od. u zagradi navesti alternativne jedinice.

2. Crteže treba izraditi tušem na pausu ili bijelom papiru. Širina crteža neka bude do 7.5 odnosno 15 cm. Svaki crtež, tablica ili fotografija treba imati broj i naziv koji označuje njen sadržaj. Crteže, tabele i fotografije nije potrebno lijepiti u tekst, već ih priložiti odvojeno, a u tekstu samo naznačiti mjesto gdje dolaze.

3. Rad može biti pisan i biti će objavljen na bilo kojem od jugoslavenskih jezika u latinici i na engleskom jeziku.

Autori mogu poslati radove na disketama (1.2 ili 1.44) u formatima tekst procesora ASCII, wordstar (3.4. i 4.0), word, wordperfect pošto će biti tekst dalje obraden u Venturi 2.0. Grafičke datoteke mogu biti u formatu HPL, SLD (AutoCAD), PCX ili IMG/GEM.

Urednički odbor će odbiti sve radove koji neće biti poslani u dva primjerka.

Za sadržaj članaka autori odgovaraju u potpunosti. Rukopisi se na vraćaju.

Rukopise šaljite na adresu:

Uredništvo Informacije MIDEM
Elektrotehnična zveza Slovenije
Dunajska 10, 61000 Ljubljana
Slovenija

INFORMATION FOR CONTRIBUTORS

Informacije MIDEM is professional-scientific-social publication of Professional Society for Microelectronics, Electronic Components and Materials. In the Journal contributions of domestic and foreign authors, especially members of MIDEM, are published covering field of microelectronics, electronic components and materials. These contributions may be:

original scientific papers, preliminary communications, reviews, conference papers and professional papers.

All manuscripts are subject to reviews.

Scientific news, news from the companies, institutes and universities, reports on actions of MIDEM Society and its members as well as other relevant contributions are also welcome.

Each contribution should include the following specific components:

- 1. Title of the paper and authors' names.
- 2. Key Words and Abstract (not more than 250 words).
- 3. Introduction, main text, conclusion, acknowledgements, appendix and references.
- 4. Authors' names, titles and complete company or institution adress.

General information

1. Authors should use SI units and provide alternative units in parentheses wherever necessary.

2. Illustrations should be in black on white or tracing paper. Their width should be up to 7.5 or 15 cm. Each illustration, table or photograph should be numbered and with legend added. Illustrations, tables and photografphs are not to be placed into the text but added separatelly. Hower, their position in the text should be clearly marked.

3. Contributions may be written and will be published in any Yugoslav language and in english.

Authors may send their files on formatted diskettes (1.2 or 1.44) in ASCII, wordstar (3.4 or 4.0), word, wordperfect as text will be formated in Ventura 2.0. Graphics may be in HPL, SLD (AutoCAD), PCX or IMG/GEM formats.

Papers will not be accepted unless two copies are received.

Authors are fully responsible for the content of the paper. Manuscripts are not returned.

Contributions are to be sent to the address:

Uredništvo Informacije MIDEM
Elektrotehniška zveza Slovenije
Dunajska 10, 61000 Ljubljana,
Slovenia

TERMINOLOŠKI STANDARDI

V

Virtual temperature 2.5.4
Voltage, avalanche 2.1.17
Voltage, breakdown 2.4.3
Voltage, floating 2.4.2
Voltage reference diode 2.2.3
Voltage regulator diode 2.2.4
Voltage, reverse 2.4.1
Voltage, Zener 2.1.20

Z

Zener breakdown (of a semiconductor PN junction) 2.1.19
Zener voltage 2.1.20

4.2 Abecedni seznam izrazov v francoskem jeziku

A

Action tunnel (dans une jonction PN) 2.1.22

B

Bloc de redressement à semiconducteurs, 2.2.6
Borne (d'un dispositif à semiconducteurs) 2.3.1

C

Capacité thermique (d'un dispositif à semiconducteurs) 2.4.5
Capacité thermique d' un réseau thermique équivalent 2.4.7
Cellule à effet photovoltaique 2.2.20
Cellule photoconductrice 2.2.19
Claguage (d'une jonction PN polarisée en inverse) 2.1.15
Claguage par avalanche (d'une jonction PN semiconductrice) 2.1.16
Claguage par effet thermique (d'une jonction PN semiconductrice) 2.1.18
Claquage par effet Zener (d'une jonction PN semiconductrice) 2.1.19
Coefficient de Hall (d'un semiconducteur) 2.1.24
Constante de Hall 2.1.24
Couche diélectrique 2.1.14

D

Diode à semiconducteurs 2.2.2
Diode de redressement à avalanche 2.2.11
Diode de redressement à avalanche controlée 2.2.12
Diode de redressement à semiconducteurs 2.2.5
Diode de signal 2.2.9
Diode de tension de référence 2.2.3
Diode régulatrice de tension 2.2.4
Diode tunnel 2.2.7
Diode unitunnel 2.2.10
Dispositif à semiconducteurs 2.2.1

E

Effet Hall 2.1.23
Effet photoélectrique 2.1.25
Effet photovoltaique 2.1.26
Effet tunnel 2.1.21
Electrode (d'un dispositif à semiconducteurs) 2.3.2

F

Facteur de réduction avec la température 2.5.3
Fréquence de coupure 2.6.1

I

Impédance thermique en régime d'impulsions 2.4.10
Impédance thermique transitoire 2.4.9

J

Jonction 2.1.6
Jonction par alliage 2.1.8
Jonction par diffusion 2.1.9
Jonction par tirage 2.1.10
Jonction PN 2.1.7

L

Limiteur de surtensions transitoires au sélénium 2.2.21

TERMINOLOŠKI STANDARDI

P

Photo-diode 2.2.8
Photo-transistor 2.2.17
Porteur 2.1.11
Porteur de charge (abreviation: porteur) 2.1.11
Porteur majoritaire (dans un région semiconductrice) 2.1.12
Porteur minoritaire (dans une region semiconductrice) 2.1.13

R

Réseau thermique équivalent 2.4.6
Résistance thermique (d'un dispositif à semiconducteurs) 2.4.4
Résistance thermique (d'un réseau thermique equivalent) 2.4.8

S

Semiconducteur 2.1.1
Semiconducteur extrinséque 2.1.2
Semiconducteur type I (intrinséque) 2.1.5
Semiconducteur type N 2.1.3
Semiconducteur type P 2.1.4
Sens direct (d'une jonction PN) 2.3.3
Sens inverse (d'une jonction PN) 2.3.4

T

Température de stockage 2.5.2
Température du boîtier 2.5.1
Température équivalente interne 2.5.4
Température virtuelle 2.5.4
Tension d'avalanche 2.1.17
Tension de claquage 2.4.3
Tension de Zener 2.1.20
Tension flottante, 2.4.2
Tension inverse 2.4.1
Thyristor 2.2.18
Transistor 2.2.13
Transistor à effet de champ 2.2.16
Transistor bipolaire 2.2.14
Transistor unipolaire 2.2.15

TERMINOLOŠKI STANDARDI

Zveza z drugimi standardi

JUS N.R1.321 – Polprevodniški elementi. Diode. Izrazi in definicije
JUS N.R1.322 – Polprevodniški elementi. Tiristorji. Izrazi in definicije
JUS N.R1.323 – Polprevodniški elementi. Bipolarni in poljski transistorji. Izrazi in definicije

Na podlagi mnenja Republiškega sekretariata za kulturo SR Srbije št. 413-81/74-02 z dne 4.11.1974, se ne plača prometni davek